Spontaneous Symmetry Breaking in the Mesophase of an Achiral Flexible Liquid Crystal Trimer

March 2018

Haruna Sasaki

Spontaneous Symmetry Breaking in the Mesophase of an Achiral Flexible Liquid Crystal Trimer

A Thesis Submitted to

the Graduate School of Materials Science and Technology

Hirosaki University

for the Degree of Doctor of Engineering

by

March 2018

Haruna Sasaki

TABLE OF CONTENTS

GENERAL INTRODUCTION

§1. Mirror symmetry breaking[1]

Spontaneous symmetry breaking is a spontaneous process, during which a system in an initially symmetric state ends up in an asymmetric state, even though the underlying dynamic equations are still invariant under a symmetry transformation. Spontaneous mirror symmetry breaking is an efficient way to obtain homogeneously chiral agents, pharmaceutical ingredients and materials. The origin of homochirality of the molecules of life is still an unsolved problem[2-6]. Thus, spontaneous mirror symmetry breaking is also in the focus of the discussion around the emergence of uniform chirality in biological systems. It was observed in Pasteur's first resolution experiments, i.e. , crystallization of conglomerates of enantiomorphic crystals from supersaturated solution or supercooled melts formation[7]. Homochiral interactions are favoured over heterochiral. Conglomerate formation can be found for racemic mixtures of permanently chiral molecules.

According to Tschierske and Ungar, molecular chiral systems are categorized as follows[1]. Molecules could be distinguished by the height of the enantiomerisation barrier separating the enantiomeric pairs (Fig.I-1). For permanently chiral molecules (A) this barrier is sufficiently high compared to kT that they are stable over the long term. By reducing this barrier the molecule becomes transiently chiral and transitions between the enantiomers take place (B). There is another type of achiral molecules for which achiral conformers represent the energetic minimum (C). Triphenylene could be considered as such a case. These molecules belong to the group of prochiral molecules which have an achiral ground-state conformation, but by a slight twist can easily adopt chiral conformations representing only a local but not global minimum. The spontaneous mirror symmetry breaking results from (1) chiral discrimination of permanently chiral molecules, (2) chiral synchronization of transiently chiral molecules capable of adopting chiral conformations representing energy minima, and (3) chiral synchronization of prochiral molecules which have an achiral ground-state conformation, but can easily adopt a chiral conformation.[1] Tremendous progress has been made by mirror symmetry breaking during crystallisation from super cooled melts or supersaturates solutions, and by self-assembly on solid surfaces and in other highly ordered

structures[8, 9]. However, recent observations of spontaneous mirror symmetry breaking in liquids[10] and liquid crystals[10, 11-16] indicate that it is not limited to the well-ordered solid state[1]. In liquid crystalline phases, there are explicit symmetry breaking phenomena such as chiral nematic phases and chiral smectic phases, which are formed from chiral molecules, on the other hand, there are spontaneous symmetry breaking phenomena such as chiral conglomerate phases, which are formed from achiral molecules.

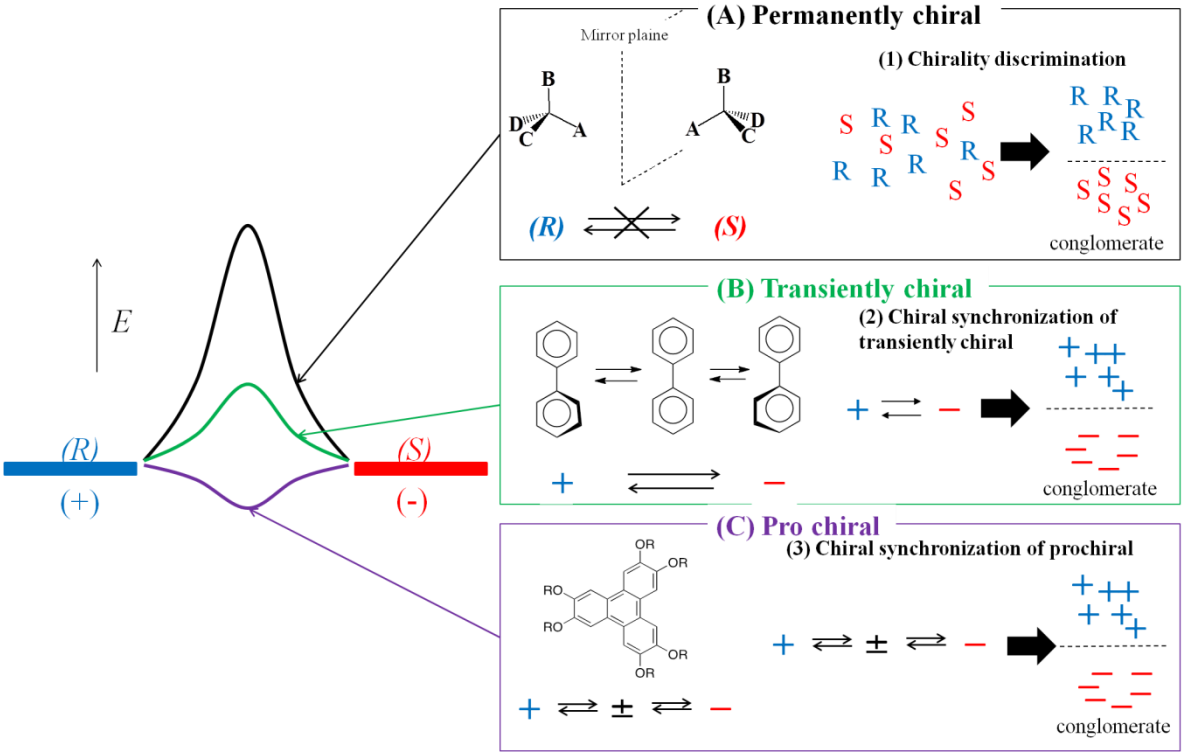

Fig. I– 1 Category of mirror symmetry breaking.

§2. Symmetry breaking in liquid crystals

Liquid crystals are matter in state which has both fluidity of liquids and optical anisotropy of solid crystals.[17-20] Liquid crystalline phases are classified by orientational order and positional order. In a nematic (N) phase, the orientational order of molecules is maintained, but the positional long range order of those is completely lost. On the other hand, in smectic phases, the orientational order of molecules is maintained, and the positional order of those is maintained in one dimension. That is, the smectic phases have a layered structure. In smectic A (SmA) and smectic C (SmC) phases, the positional order of molecules within each layer is

lost and random. In the SmA phase, molecules are arranged with their long axes perpendicular to the planes of the layers, whereas in the SmC phase their long axes are tiled with respect to the layer normal[21,22].

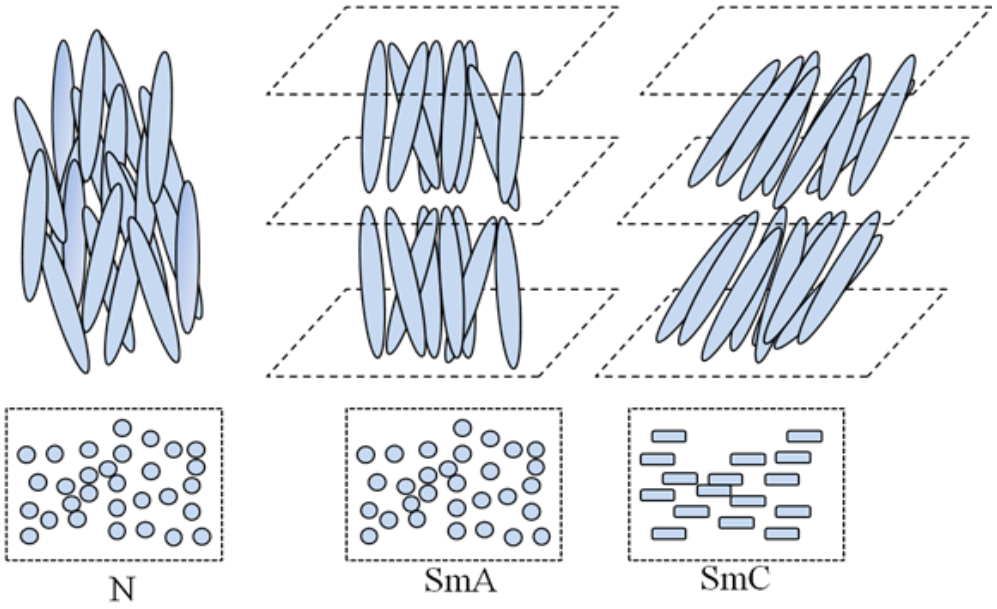

Fig. I– 2 Main types of namatic and smectic phases formed by calamitic molecules.

Introduction of chirality to those liquid crystal phases leads to a variety of helical structures. Furthermore, the reduced symmetry driven by chirality can produce interesting physical properties, such as ferroelectricity and nonliner optics. The chiral liquid crystalline phases are formed by chiral molecules or by an achiral host doped with a chiral material. Furthermore, chiral conglomerates have been observed for achiral liquid crystals via spontaneous mirror symmetry breaking.

2.1 Mirror symmetry breaking in chiral liquid crystals[23, 24]

2.1.1. Chiral nematic phase

In the chiral nematic (N*), the molecules pack together to form a helical macrostructure, as shown in Fig. I-3. In the N* phase formed by rod-like molecules, the helical axis is perpendicular to molecular long axis.

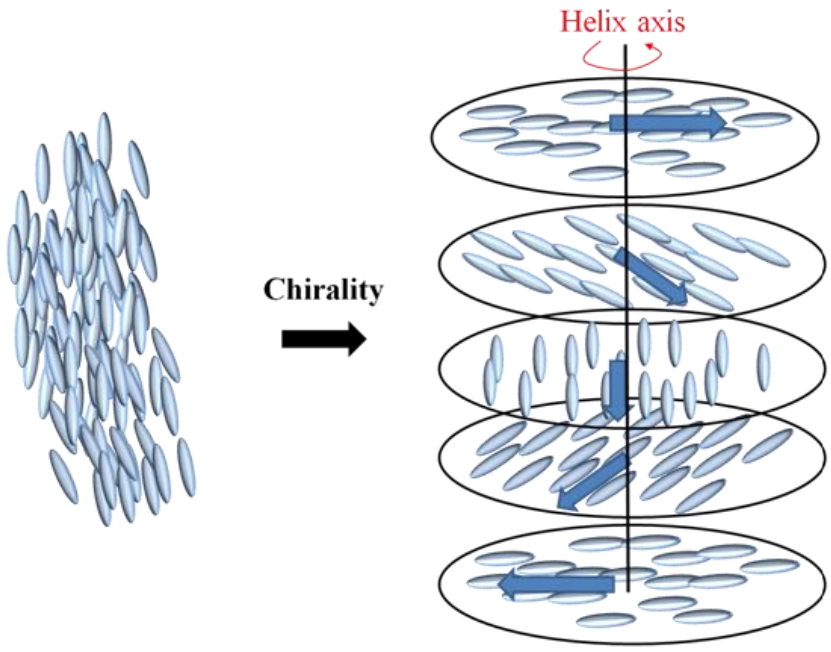

Fig. I– 3 Schematic representation of the transformation from a nematic phase to chiral nematic phase.

2.1.2 Chiral smectic phases

Smectic phases formed by chiral molecules, or by achiral host material doped with a chiral material, can also exhibit a helical structure. In this case, the situation is somewhat complex because the molecules are arranged in a diffuse-layered structure. Consequently, a helical macrostructure cannot propagate in a direction perpendicular to the molecular long axis as in case of the N* phase. Thus, if a helical structure is formed, the helix axis must be parallel with respect to the layer normal. Helical macrostructures are, therefore, only observed in smectic phase modifications in which the molecules are tilted with respect to the layer normal. In the chiral smectic C (SmC*) phase, the consituent molecules are arranged in diffuse layers where the molecules are tilted by an angle with resoect to the layer normal, as shown in Fig. I-4

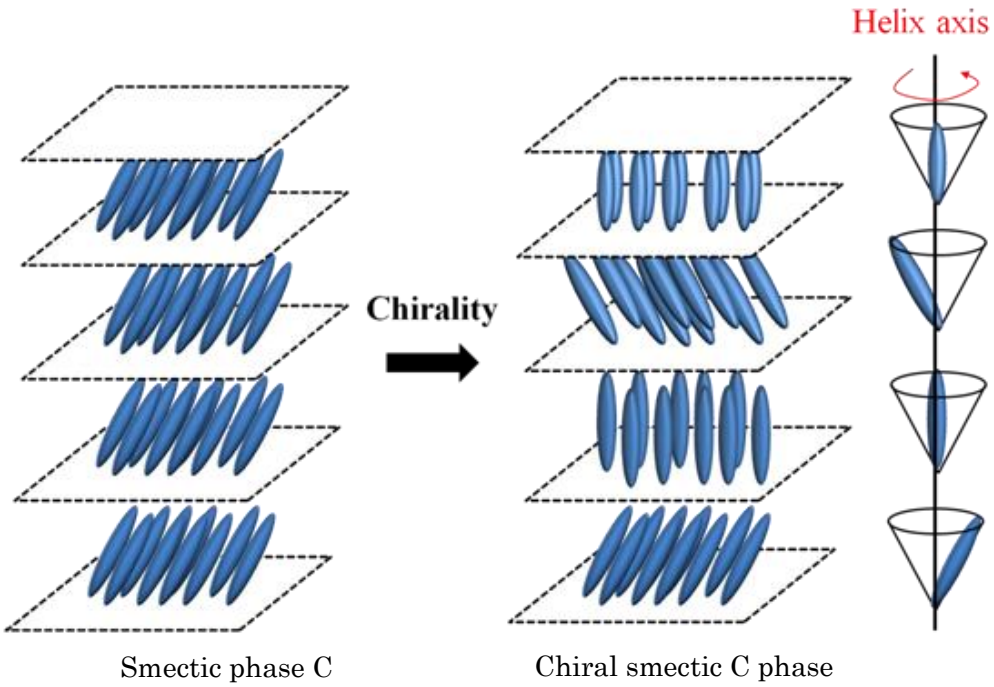

Fig. I– 4 Schematic representation of the transformation from a smectic C phase to the chiral smectic phase.

The chirality causes a smectic layer to exhibit a permanent spontaneous polarization with perpendicular to the tilt plane, producing ferroelectricity. The spontaneous polarization of the SmC* layer interacts with the electric field applied to the electrodes. Depending on the direction of the electric field the molecules are tilted either to the left or the right side of the layer normal (Fig.I-5). The molecular long axis is tilted by θ from the smectic layer normal. In opposite electric field of polarization director, switching corresponding polarization reverse. The SmC* liquid crystals are classified as ferroelectric liquid crystals.

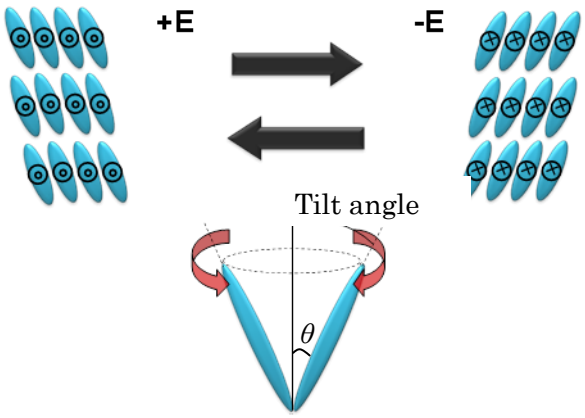

Fig. I– 5 Switching model in the SmC* phase.

2.1.3. Twist grain boundary phase[26, 27]

Twist grain boundary (TGB) phases were formed by resulting of the competition between the desire for the molecules to form a helical structure, duo to their chiral packing requirements, and the desire for the phase to form a layered structure. Typically, therefore, TGB phases are observed at the phase transition from the isotropic liquid or chiral namatic states to the smectic state. At a normal chiral nematic to SmA* transition, the helical ordering of chiral nematic phase collapses to give the layered structure of SmA* phase. However, for a transition mediated by a TGB phase, there is the desire for the molecules to form a helical structure and the desire for the phase to form a layered structure. Therefore, the system attempts to relieve this frustration by trying to form a helical structure, where the axis of the helix is perpendicular to the long axes of the molecules yet same time, they also try to form a lamellar structure. These two structures are incompatible with one another and cannot coexist. The matter is resolved via the formation of a periodic arrangement of screw dislocations, which enables a quasi-helical structure coexisting with a smectic molecular arrangement. This is achieved by having small blocks of molecules, which have a local smectic structure, being rotated with respect to one another by the screw dislocations, thereby forming a helical structure, as shown in Fig. I-6.

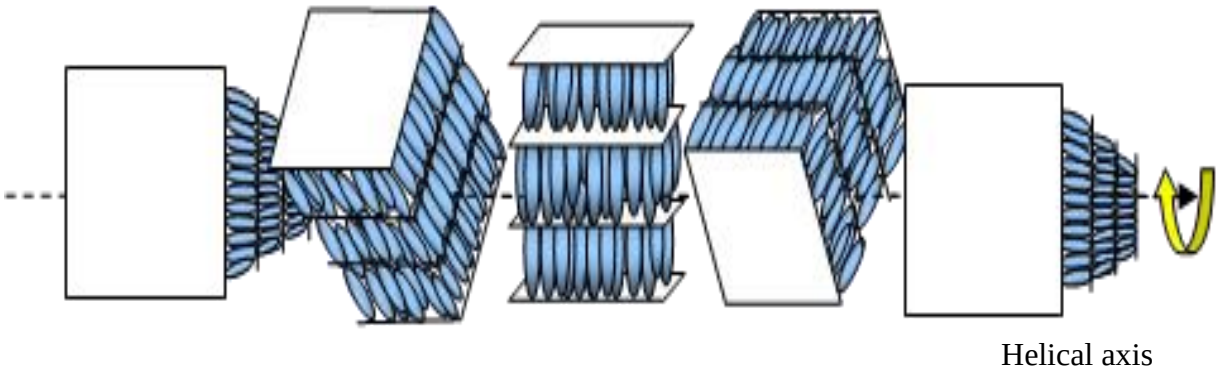

Fig. I– 6 Schematic representation of the TGB phase.

2.2. Spontaneous mirror symmetry breaking in achiral liquid crystals

2.2.1. Bent core liquid crystals[28]

Bent-core liquid crystals have attracted special attention in the field of liquid crystal research because of its intriguing novel features as compared to conventional liquid crystals formed by rod-like or disk-like molecules. Niori et al. discovered ferroelectric switching[29], and then, Sekine et al. suggested chirality in a fluid smectic phase of bent-core molecule P-n-O-PIMB (Fig. I-7) despite the molecules being achiral[13]. These findings opened new avenues for the study of polar order and chiral superstructures of liquid crystals[28, 30]. Bent-core liquid crystal phases are classified into B1~B7 phases depending on the local structure. The B2 phase which has a smectic (lamellar) structure is the most extensively studied bent-core phase. A bent-core molecule is tilted with respect to the layer normal in the B2 phase. Link et al. proposed how the chirality can arise in the smectic phase of achiral bent-core molecules[31]. As shown in Fig. I-8, a polar direction, tilt direction and layer normal define either a right- and left-handed Cartesian coordinate system, providing a chiral configuration of the individual layers. Therefore, opposite chirality is introduced by tilting an achiral bent-core molecule in the opposite direction in a smectic layer[32].

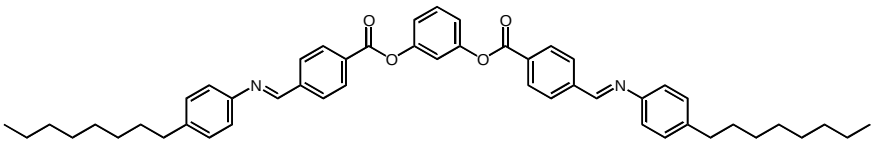

P-8-O-PIMB : Cr 72 B3 140 B2 158 Iso

Fig. I– 7 A molecular structure and phase transition temperature (°C) of P-8-O-PIMB.

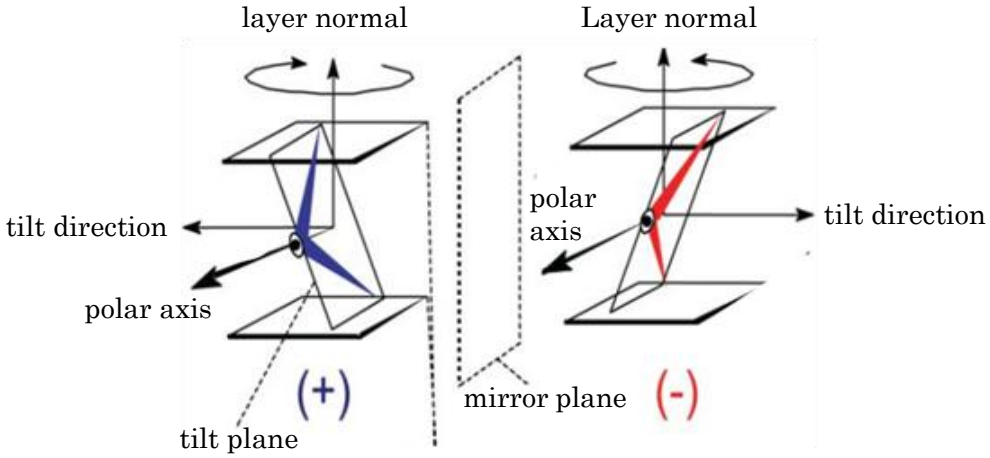

Fig. I– 8 Definition of chirality in tilted smectic phase of bent-core molecules.

On the other hand, Watanabe et al. suggest that the chiral origin in achiral bent-core liquid crystals is conformational chirality[33]. They measured solid-state ^{13}C NMR measurements in the B2 and B4 phases of the achiral banana-shaped molecule[34]. In both phases, an NMR resonance signal assigned to carbonyl carbons of the ester linkages appears as doublet peaks, showing that the two carbonyl carbons are circumstanced in different electronic environments on the NMR time scale. This distinct splitting of the carbonyl carbon signal indicate that the individual molecule claims the twisted conformation, where the two carbonyl carbons of the ester moieties are twisted away from each other by rotating out of the molecular core plane with different dihedral angles. They concluded that the origin of the chirality of the B2 and B4 phases in the achiral banana-shaped molecular system is attributable to the twisted conformation.

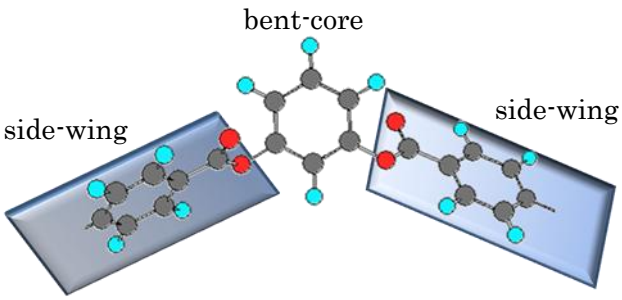

Fig. I– 9 Molecular model of an achiral bent-core molecule in the B2 and B4 phases.

2.2.2 Chiral conglomerate phases

The chiral conglomerates consisting of domains with opposite handedness have been observed recently in achiral liquid crystalline phases[10, 12-17]. They have attracted much attention not only for the spontaneous mirror symmetry breaking but also for their nanostructures. Some of them are optically isotropic. [35-38]. Fig. I-10 shows category of chiral conglomerate phases. They are classified into three categories, depending on the local structure : a liquid-crystalline sponge phase formed by strongly deformed fluid layers[28], helical nanocrystalline phases (HNC phases)[30] and herical nanofilament phases (HNF phases, also assigned B4 phases)[29]. In this report I denote the chiral conglomerate phase which exhibits the dark texture under crossed polarizers as dark conglomerate (DC) phases.

The DC phase exhibiting a sponge structure, which is usually formed during cooling of the

isotropic liquid, have little or no birefringence. The texture under crossed polarizers is nearly dark. Such phases are macroscopically isotropic sponge-like liquid crystals. They show globally disordered focal conic domains[35, 39, 40]. The application of high voltage transforms some of such phases to the B2 phase[35, 41]. The HNF phases have usually weak birefringence between crossed polarozers as shown in Fig. I-10. It is apparently a solid phase[36]. No electro-optical switching can be found in the HNF phases.

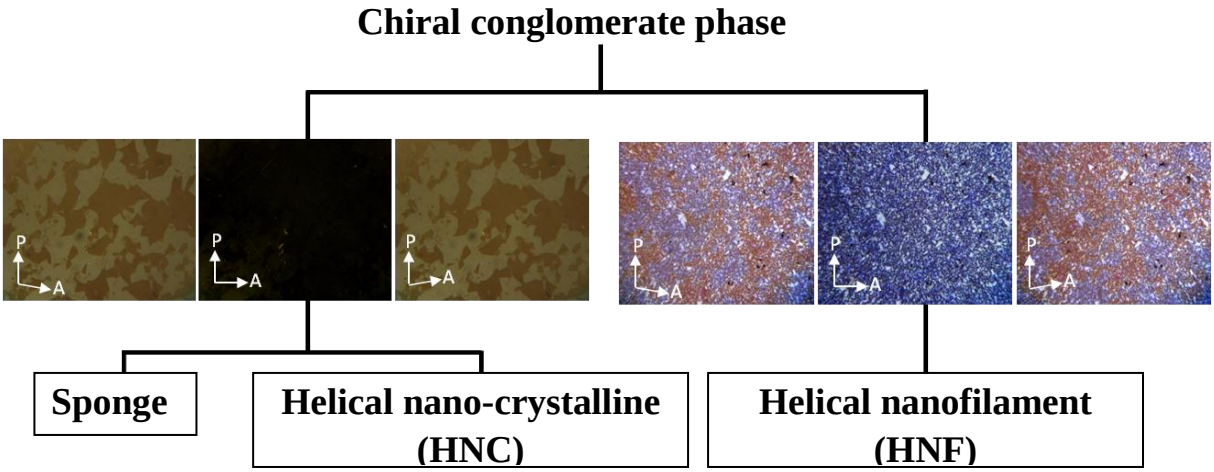

Fig. I– 10 Category of chiral conglomerate phases.

X-ray diffraction measurements were studied in the frastrated phases of achiral bent-core liquid crystals. There are layer-oriented reflections was found in the B2 phase of P-8-OPIMB, when the phase transition to HNF occurred, the layer reflections at small angles appeared as ring patterns for both incident directions (Fig.I-11, right)[42], indicating that the layers are deformed in the HNF phase. According to the high-resolution XRD of P-9-OPIMB at the B2–HNF phase transition, where the B2 and HNF phases coexist, the transition to the HNF phase is marked by the vanishing of the peak of the long-range lamellar smectic order existing in the B2 phase (Fig.I-12 (a), left), together with the appearance of a diffuse peak owing to the short-range local layer ordering in the HNF phase (Fig.I-12 (b), left) over scales of less than 40 nm (≈8 layers). In addition, at a wide-angle region, the broad peak of the liquid-like in-plane order of the B2 phase (Fig. I-12 (a), right) is also replaced by multiple diffuse peaks (Fig. I-12 (b), right), indicating the in-plane crystalline positional order, which was assigned as hexatic by XRD in the HNF phase[36]. In similar to the HNF phase, XRD data also showed a small-angle diffuse peak together with multiple wide-angle peaks in the sponge phaser ,

indicating the short-range order of smectic layers and crystalline intralayer ordering, respectively[35].

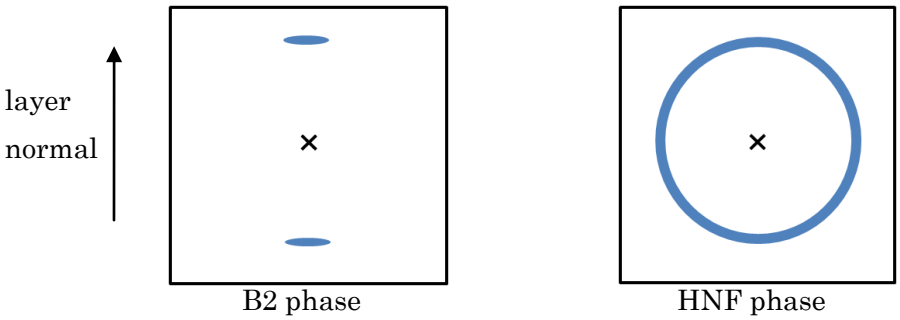

Fig. I– 11 2D X-ray patterns in the B2 and HNF phases in a small-angle range.

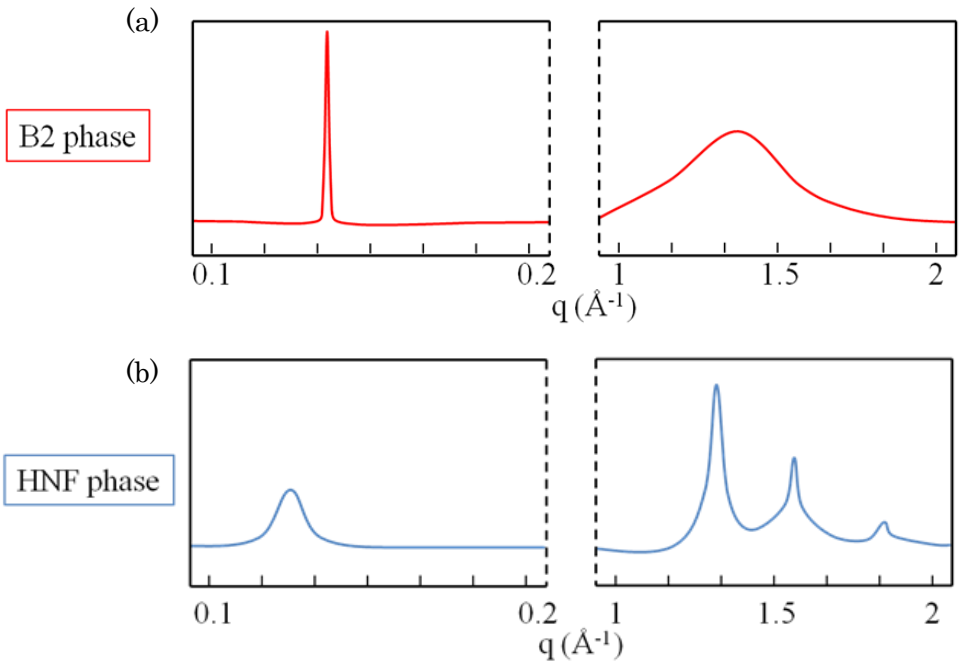

Fig. I– 12 High-resolution powder X-ray diffractions in the B2 and HNF phases of P-9-OPIMB[36].

The difference in nanostructure between the sponge phase and the HNF phase was demonstrated by observation of surface structure using scanning electron microscope (SEM) and freeze-fracture transmission electron microscope (FFTEM). Fig.I-13 depicts the FFTEM images of a sponge phase and HNF phase. With respect to the sponge phase, the bulk shows disordered focal conic domains organized in the disordered plumber's nightmare structure[40].

The HNF phase is one of the most complex hierarchical self-assemblies[31, 41]. Layer topology of the HNF phase observed for bent-core molecules has been extensively investigated[43-45]. The diverse topology of the HNF phase on the glass surface was reported by Chen et al.[43] The twisted layer structure of the bulk is suppressed near the glass substrate. Furthermore, the helical nanofilaments form a network which acts as a porous nanoconfinement medium of a large internal area, with the guest material confined to nanoscale interstitial volumes between the filaments[46-48]. For that reason, it can produce nanostructured composites.

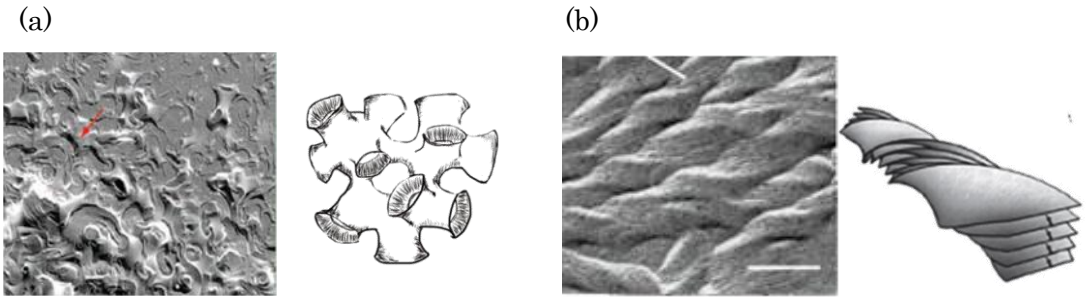

Fig. I– 13 FFTEM images of the sponge[35] and HNF phases with their models[36].

Fig. I-14 depicts a forming model of the HNF phase and that of the sponge phase[35, 36]. Results of earlier studies have demonstrated that the smectic layers of both the sponge and HNF phases of bent-core liquid crystals tend to have saddle-splay curvature. The optical activity in both phases is attributable to the layer chirality[31] or the coupling of molecular conformational chirality to the layer chirality[33].

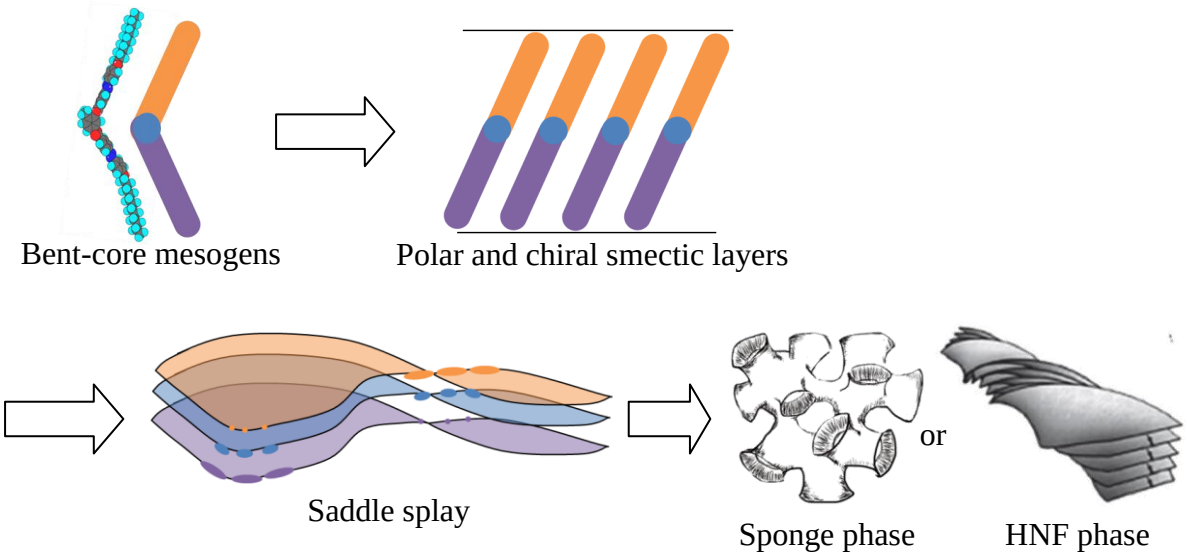

Fig. I– 14 Forming model of the HNF phase and that of the sponge phase[35, 36].

2.2.3. Twist-bend nematic phase

The spontaneous mirror symmetry breaking was also observed in a nematic phase of achiral bent-shaped molecules. This was predicted by Meyer[49] and by Dozov[50] who proposed that certain mesogenic molecules might have a tendency to pack into bent structures. Pure uniform bend in space is impossible, by the spontaneous bend must be accompanied by other deformations of the local director, either twist or splay, giving rise to the so-called twist-bend nematic or splay-bend nematic, respectively. In the twist-bend nematic (N_{TB}) phase, the molecules pack together in a continuous bend in the same direction, thus the local director is circular. In order to minimize the free energy, the bend is expelled into the third dimension via twist(Fig.I-15(b)). The N_{TB} phase was first identified for a liquid crystal dimer with a flexible odd-numbered spacer, 1,7-bis-{4-(4'-cyanophenyl)phenyl}heptane (CB7CB) as shown in Fig.I-15(a)[14, 15] and the assignment confirmed using FETEM[51]. Not only bent-shaped dimers but also bent-core compounds have been reported to exhibit the N_{TB} phase.

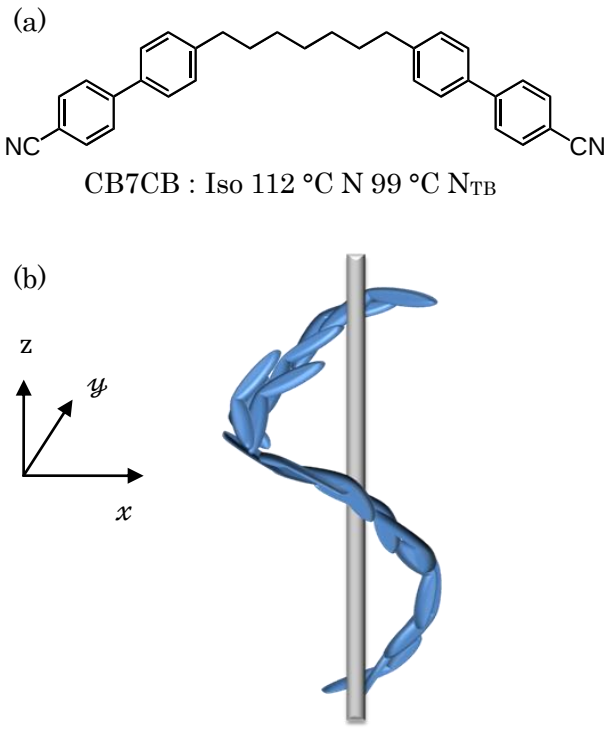

Fig. I– 15 (a) Molecular structure and phase transition temperature of CB7CB and (b) molecular model of the N_{TB} phase.

§3. Supermolecular liquid crystals stabilizing the frustrated phase

Recently, molecular topologies and microsegregation have attracted much attention as the origins for producing novel self-organizing systems. Fig. I-16 shows various molecular topologies for the design of large discrete supermolecules. Supramolecular assemblies composed of supermolecules, i.e. dimeric, trimeric, oligomeric and dendritic liquid crystals, are of current interest in the design of new liquid crystal materials. The supermolecue describes a large molecule in which smaller identifiable components are covalently bound[52-54]. Dimeric liquid crystals, which are the simplest architectural form of supermolecular liquid crystals, are attractive because they exhibit different properties from those of conventional low molar mass liquid crystals and serve as model compounds for main chain liquid crystal polymers. For example, the transition properties of dimeric liquid crystals are known to depend on the length and parity of the flexible spacer. Furthermore, liquid crystal trimers[55, 56] and tetramers[57] have been reported. Pronounced odd-even effects were observed for transition properties of linear liquid crystal oligomers on varying the physical properties of spacer length.

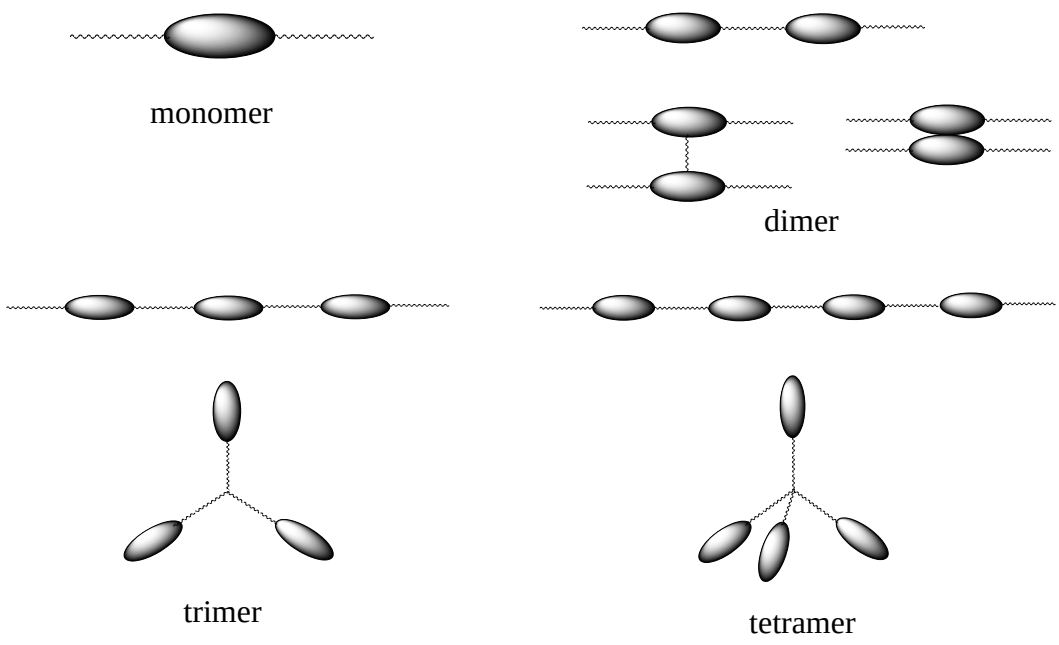

Fig. I– 16 Various molecular topologies for the design of large discrete supermolecules.

Liquid crystal trimers which are three mesogenic units connected via alkyl spacers have been investigated by several research groups. They are know the show transition properties depending in the parity of the spacer as same as liquid crystal dimer[53-55]. Supermolecular assemblies of liquid crystal trimers have been reported to exhibit hiearchical structures via coupling of core-core interactions and molecular shape[58-62]. Imrie et al. reported that non-symmetric trimers exhibit a triply intercalated alternating smectic C (SmC) phase [63, 64]. Yoshizawa et al. reported that the SmC phase of trimers partly showed defect lines that were similar to the chiral SmC phase[61] and a chiral LC trimer showed a de Vries-like smectic phases[65].

§4. Aim of this study

Spontaneous symmetry breaking has been of great importance in the study of science. Layer chirality or conformation chirality is thought to be the origin producing the chiral conglomerates possessing layer structure. Almost molecules exhibing chiral conglomerates are rigid bent-core molecules. With respect to the N_{TB} phase, bent-shaped dimers and bent-core molecules show N_{TB} phases. The bent shapes can produce a local bent director. Inherent bent shape of a liquid crystal molecule producing those chiral conglomerate phenomena of achiral liquid crystals.

Recently, Yoshizawa reported that LC oligomers in which several mesogemic units are connected via flexible spacers exhibited frustrated phases with hierarchical structures[66]. LC oligomers are thought to have an order within a molecules. They were found to exhibit various molecular packing structures in the liquid-crystalline phases as follows, U-shaped and λ-shaped oligomers form a cybotactic nematic phase[67] and incomensurated smectic phases[68], respectively. Chiral T-shaped compounds show blue phases with wide temperature ranges[69]. A liquid crystal trimer is a supermolecule in which three mesogneic units are organized. Intermolecular interactions can be designed between adjacent trimers depending on the spacer parity. Furthermore, designed core-core intermolecular interactions between zigzag trimers with odd-membered spacers is expected to induce a twist conformation in the trimer. A novel spontaneous mirror symmetry breaking can be observed for desiged liquid crystal trimers. Not only observation of spontaneous mirror symmetry breaking but also new nanostructures will be presented in this thesis.

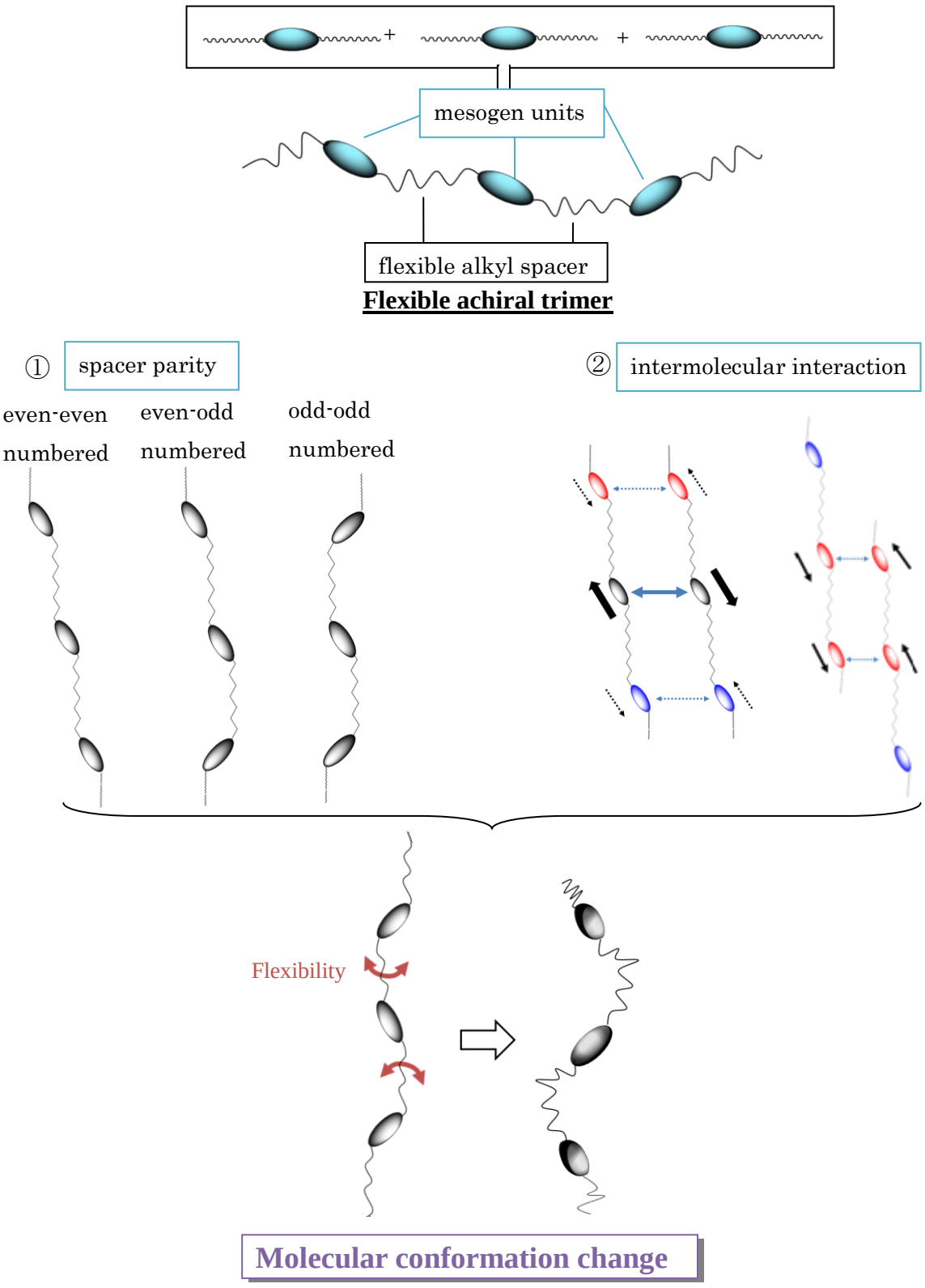

Fig. I– 17 Molecuar design concept for novel trimer liquid crystal systems.

§5. Reference

[1] C. Tschierske and G. Ungar, *ChemPhysChem*, 2016, **17**, 9.

[2] A. Guijarro and M. Yus, The Origin of Chirality in the Molecules of Life, *RSC Publishing, Cambridge,* 2009; L. D. Barron, *Space Sci. Rev.* 2008, **135**, 187.

[3] J. Podlech, *Cell. Mol. Life Sci*., 2001, **58**, 44.

[4] J. E. Hein, D. Gherase, D. G. Blackond, *Top. Curr. Chem*. 2012, **333**, 83.

[5] M. Valos, R. Babiano, P. Cintas, J. L. Jimnez, J. C. Palacios, *Tetrahedron: Asymmetry*, 2010, **21**, 1030.

[6] K. R. Mirazo, C. Briones, A. L. Escosura, *Chem. Rev*., 2014, **114**, 285.

[7] J. L. Pasteur, *Ann. Chim. Phys*., 1848, **24**, 442.

[8] D. K. Kondepudi and G. W. Nelson, *Phys. Rev. Lett*., 1983, **50**, 1023.

[9] D. K. Kundepurdi, R. J. Kaufmann, N. Singh, *Science*, 1990, **250**, 875.

[10] C. Dressel, F. Liu, M. Prehm, X. Zeng, G. Ungar, C. Tschierske, *Angew. Chem. Int. Ed*. 2014, **53**, 13115.

[11] C. Dressel, T. Reppe, M. Prehm, M. Brautzsch, C. Tschierske, *Nat. Chem.*, 2014, **6**, 971.

[12] T. Sekine, T. Niori, M. Sone, J. Watanabe, S. Choi, Y. Takanishi, H. Takezoe, *Jpn. J. Appl. Phys*., 1997, **36**, 6455.

[13] V. Görtz and J. W. Goodby, *Chem. Commun*., 2005, 3262.

[14] V. P. Panov, M. Nagaraj, J. K. Vij, Y. P. Panarin, A. Kohlmeier, M. G. Tamba, R. A. Lewis, G. H. Mehl, *Phys. Rev. Lett*., 2010, **105**, 167801.

[15] V. Borshch, Y.-K. Kim, J. Xiang, M. Gao, A. Jàkli, V. P. Panov, J. K. Vij, C. T. Imrie, M. G. Tamba, G. H. Mehl, O. D. Lavrentovich, *Nat. Commun.*, 2013, **4**, 2635.

[16] H. Takezoe, *Top. Curr. Chem*., 2012, **318**, 303.

[17] T. Tachibana, K. Kobayashi, S. Kusabayashi, H. Suzuki, K. Honda, M. Sukigara, *Liquid Crystals (Ekisyou)*, Kyouritsu Syuppan, 1972 [in Japanese].

[18] K. Okano and S. Kobayashi, *Liquid Crystals (Ekisyou)* Basics, Baihukan, 1985 [in Japanese].

[19] G. W. Gray, Introduction**,** Historical Development, in the *Handbook of Liquid Crystals Vol 1* : *Fundamentals*, ed. D. Demus, J. W. Gray, H.- W. Spiess**,** V. Vill, Wiley-VCH, Weinheim, 1998, ch. I, pp. 1-14.

[20] *Handbook of Liquid Crystals(Ekisyou Binran)*, ed. Editorial board of Handbook of Liquid

Crystals, 2000 [in Japanese].

[21] (a) C. Tschierske, *J. Mater. Chem*. 1998, **8**, 1485. (b) C. Tschierske, *J. Mater. Chem*. 2001, **11**, 2647.

[22] (a) J. W. Goodby, G. H. Mehl, I.M. Saez, R. P. Tuffin, G. Machenzie, R. Auzely-Velty, T. Benvegnu, D. Plusquellec, *Chem. Commun.* 1998, 2057. (b) I. Saez and J. W. Goodby, *J. Mater. Chem*. 2005, **15**, 26.

[23] *Handbook of Liquid Crystals(Ekisyou Binran),* ed. Editorial board of Handbook of Liquid Crystals, 2000, pp280 [in Japanese].

[24] G. Ungar, F. Liu and X. Zeng, *in Handbook of Liquid Crystals*, ed. J. W. Goodby, P. J. Collings, H. Gleeson, P. Raynes, C. Tschierske, T. Kato, Wiley-VCH Verlag, Weinheim, 2014, vol. 1, ch. 7, pp. 197–229.

[25] R. B. Meyer, *Mol Cryst. Liq. Cryst*., 1976, **40**, 74.

[26] J. W. Goodby, M. A. Waugh, S. M. Stein, E. Chin, R. Pindak, J. S. Patel, *J. Am. Chem. Soc*., 1989, **111**, 8119.

[27] J. W. Goodby, *Struct. Bonding*, 1999, **95**, 83.

[28] H. Takezoe and Y. Takanishi, *Jpn. J. Appl. Phys.*, 2006, **45**, 597.

[29] T. Niori, T. Sekine, J. Watanabe, H. Takezoe, *J. Mater. Chem.,* 1996, **6**, 1231.

[30] A. Eremin and A. Jàkli, *Soft matter*, 2013, **9**, 615.

[31] D. R. Link, G. Natale, R. Shao, J. E. Maclennan, N. A. Clark, E. Körblova, D. M. Walba, *Science*, 1997, **278**, 1924.

[32] D. M. Walba, E. Körblova, R. Shao, J. E. Maclennan, D. R. Link, M. A. Glaser, N. A. Clark, *Science*, 2000, **288**, 2181.

[33] J. Thisayukta, H. Takezoe, J. Watanabe, *Jpn. J. Appl. Phys*., 2001, **40**, 3277.

[34] H Kurosu, M. Kawasaki, M. Hirose, M. Yamada S. Kang, J. Thisayukta, M. Sone, H. Takezoe, J. Watanabe, *Phys. Chem. A*, 2004, **108**, 4674.

[35] L. E. Hough, M. Spannuth, M. Nakata, D. A. Coleman, C. D. Jones, G. Dantlgraber, C. Tschierske, J. Watanabe, E. Körblova, D. M. Walba, J. E. Maclennan, M. A. Glaser , N. A. Clark, *Science*, 2009, **325**, 452.

[36] L. E. Hough, H. T. Jung, D. Krüerke, M. S. Heberling, M. Nakata, C. D. Jones, D. Chen, D. R. Link, J. Zasadzinski, G. Heppke, J. P. Rabe, W. Stocker, E. Körblova, D. M. Walba, M. A. Glaser, N. A. Clark, *Science*, 2009, **325**, 456.

[37] M. Alaasar, M. Prehem, C. Tschierske, *Chem. – Eur. J*., 2016, **22**, 6583.

[38] M. Nagaraj, *Liq. Cryst*., 2016, **43**, 2244.

[39] D. Chen, Y. Shen, C. Zhu, L. E. Hough, N. Gimeno, M. A. Glaser, J. E. Maclennan, M. B. Ros, N. A. Clark, *Soft Matter*, 2011, **7**, 1879.

[40] D. Chen, R. Shao, J. E. Maclennan, M. A. Glaser, E. Körblova, D. M. Walba, N. Gimeno, M. B. Ros, N. A. Clark, *Liq. Cryst*., 2013, **40**, 1730.

[41] M. Nagaraj, K. Usami, Z. Zhang, V. Görtz, J. W. Goodby, H. F. Gleeson, *Liq. Cryst*., 2014, **41**, 800.

[42] J. Thisayukta, H. Takezoe, J. Watanabe, *Jpn. J. Appl. Phys*., 2001, **40**, 3277.

[43] D. Chen, M.-S. Heberling, N. Nakata, L. E. Hough, J. E. Maclennan, M. A. Glaser, E. Körblova, D. M. Walba, J. Watanabe, N. A. Clark, *ChemPhysChem*, 2012, **13**, 155.

[44] H. Kim. S. Lee, T. J. Shin, Y. J. Cha, E. Körblova, D. M. Walba, N. A. Clark, S. B. Lee, N. A. Clark, D. K. Yoon, *Soft Matter*, 2013, **9**, 6185.

[45] S. H. Ryu, H. Kim, S. Lee, Y. J. Cha, T. J. Shin, H. Ahn, E. E. Körblova, D. M. Walba, N. A. Clark, S. B. Lee, D. K. Yoon, *Soft Matter*, 2015, **11**, 7778.

[46] H. Kim, S. Lee, T. J. Shin, E. Körblova, D. M. Walba, N. A. Clark, S. B. Lee, D. K. Yoon, *Proc. Natl. Acad. Sci. U. S. A*., 2014, **111**, 14342.

[47] D. Chen, C. Zhu, H. Wang, J. E. Maclennan, M. A. Glaser, E. Körblova, D. M. Walba, J. A. Rego, E. A. Soto-Bustamante, N. A. Clark, *Soft Matter*, 2013, **9**, 462.

[48] V. L. Khoa, H. Takezoe, F. Araoka, *Adv. Mater*., 2017, **29**, 1602737.

[49] R. B. Meyer, in *Les Houches Summer School in Theoretical Physics*, ed. R. G. Balian**,** G. Weil, Gordon, Breach, New York, 1976, pp. 273–373.

[50] I. Dozov, *Europhys. Lett*., 2001, **56**, 247.

[51] D. Chen, J. H. Porada, J. B. Hooper, A. Klittnick, Y. Shen, M. R. Tuchb,, E. Korblova, D. Bedrov, D. M. Walba, M. A. Glaser, J. E. Maclennan, N. A. Clark, *Proc. Natl. Acad. Sci. U. S. A.*, 2013, **110**, 15931.

[52] C.T. Imrie, G.R. Luckhurst. In the *Handbook of Liquid Crystals*, *Vol 2B*, D. Demus, J.W. Goodby, G.W. Gray, H.-W. Spiess, V. Vill (Eds.), pp. 801-833, Wiley-VCH, Weinheim (1998).

[53] C.T. Imrie, P.A. Hendrson. *Curr. Opin. Colloid Iinterface Sci.*, 2002, **7**, 298.

[54] C.T. Imrie. *Struct. Bond.*, 1999, **96**, 149.

[55] P.A. Henderson, A.G. Cook, C.T. Imrie. *Liq. Cryst.*, 2004, **31** 1427.

[56] A. Yoshizawa, N. Uehara, M. Kurauchi, A. Yamaguchi, *Liq. Cryst.*, 2007, **34** 1121.

[57] P.A. Henderson, C.T. Imrie. *Liq. Cryst.*, 2005, **32**, 1531.

[58] P. Keller, *Mol. Cryst. liq. Cryst*., 1985,**123**, 247.

[59] G. S. Attard, C. T. Imrie, *Liq. Cryst*., 1989, **6**, 387.

[60] N. V. Tsvetkov, V. V. Zuev, V. N. Tsvetkov, *Liq. Cryst.*, 1997, **22**, 245.

[61] C. T. Imrie and G. R. Luckhurst, *J. Mater. Chem.*, 1998, **8**, 1339.

[62] B. Q. Chen, A. Kameyama, T. Nishikubo, *Macromolecules*, 1999, **32**, 6485.

[63] C.T. Imrie, P.A. Henderson, J.M. Seddon. *J. Mater. Chem.*, 2004, **14**, 2486.

[64] P.A. Henderson, C.T. Imrie, *Liq. Cryst.*, 2005, **32**, 673.

[65] D. Tsuji, Y. Takanishi, J. Yamamoto, A. Yoshizawa, *J. Phys. Chem. C*., 2012, **116**, 8678.

[66] A. Yoshizawa, *J. Mater. Chem*., 2008, **18**, 2877.

[67] W. Nishiya, Y Takanishi, J Yamamoto, A. Yoshizawa, *J. Mater. Chem. C*, 2014, **2**, 3677.

[68] A.Yamaguchi, M. Watanabe, A. Yoshizawa, *Liq. Cryst.*,2007, **34**, 633.

[69] A. Yoshizawa, M. Sato, J. Rokunohe, *J. Mater. Chem*., 2005, **15**, 3285.

CHAPTER 1

Supermolecular bent configuration composed of achiral flexible liquid crystal trimers exhibiting chiral domains with opposite handeness

1.1. Introduction

Chirality's effects on the physical properties of materials and how chirality arises have attracted great interest in chemistry studies. Chirality in liquid crystals is recognized as influencing phase structures and electro-optical properties[1]. For the discovery of a liquid-crystalline phase in cholesterol derivatives, molecular chirality has been necessary to produce a chiral liquid-crystalline phase.

Chiral synchronization in lamellar liquid-crystalline phases engenders DC phases and HNF phase that have been observed in some achiral bent-shaped molecules. Results of earlier studies have demonstrated that the smectic layers of both the DC and HNF phases of bent-core liquid crystals tend to have saddle splay curvature. [2,3] Whereas the DC phase comprises disordered focal conic domains, the HNF phase forms helical nanofilaments. The optical activity in the DC and HNF phases has been investigated extensively, revealing that it is attributable to the layer chirality[4] or the coupling of molecular conformational chirality to the layer chirality[5]. Furthermore, new modifications of HNF phases have been reported[6.7]. Almost all molecules exhibiting these chiral phases have a rigid bent-core structure, except in a few cases in which the HNF phase of an achiral dimer possessing a flexible odd-numbered spacer was reported recently[8-10]. The inherent conformation of the rigid molecule influences the origin of the chirality. Such bent-core molecules tend to form layer structures. Therefore, they do not show a nematic phase. Mixtures of the HNF bent core materials with rod-like nematic liquid crystals as 5CB have been designed[8]. The bulk HNF phase is porous [11.12]. For that reason, it can produce nanostructured composites. [13,14] Furthermore, Gorecka et al. reported physical gels of the HNF phase consisting of achiral dimesogenic molecules. [10] Fundamental interest in the unusual phenomena of the HNF phase does exist. Its potential applications have attracted much attention. Material design for the HNF phase is an attractive issue. Not only bent-core compounds but also liquid crystal oligomers exhibit frustrated chirality-dependent properties. Recently, the twist-bend nematic phase (N_{tb}) showing domains of opposite handedness was observed for members of achiral α,ω-bis-4-(4'-cyanobiphenyl)alkanes with flexible odd-numbered methylene spacers[15]. The molecules form a helix. The director is tilted with respect to the helical axis in the Ntb phase. [16,17] Dozov proposed that inducing some twist can produce a spontaneous bend. Moreover, he predicted that the Ntb phase can exist for bent molecules[18,19]. The Ntb phase has been

observed for liquid crystal dimers with an odd-numbered methylene spacer[20,21] and a bent-core liquid crystal[22,23]. Most recently, an Ntb phase driven by hydrogen bonding has been observed for 4-[6-(4'-cyanobiphenyl-4-yl)pentyloxy]benzoic acid[24]. That evidence reinforces the notion that shape is a key factor stabilizing the Ntb phase. The formation of hydrogen bonded dimeric complexes between pairs of acid moieties yields a supramolecular liquid crystal trimer in which three mesogenic units are mutually inclined to one another. Imrie et al. suggested that intercalation of the molecules stabilizes the helical arrangement of the Ntb phase[25]. Ivsic et al. prepared some cyanobiphenyl dimers with an imino linkage group exhibiting the Ntb phase[26]. They suggested that not only the geometry of the molecule but also the twist conformation contributes to the formation of the Ntb phase. Recently, symmetry breaking has been reported to occur in nonpolar SmC phases of a 4-cyanoresorcinol bent-core[27] and in liquid phases of polycatenar molecules [28].

In this chapter, I prepared a homologous series of achiral liquid crystal trimers in which three mesognic units are connected via heptamethylene spacers. Systematically structural modifications of the flexible achiral trimers in which phenylpyrimidine units orientate for relative of within each trimer were performed (Fig.1-1). I report here that an equimolecular mixture of some of the trimers exhibits N and DC phases.

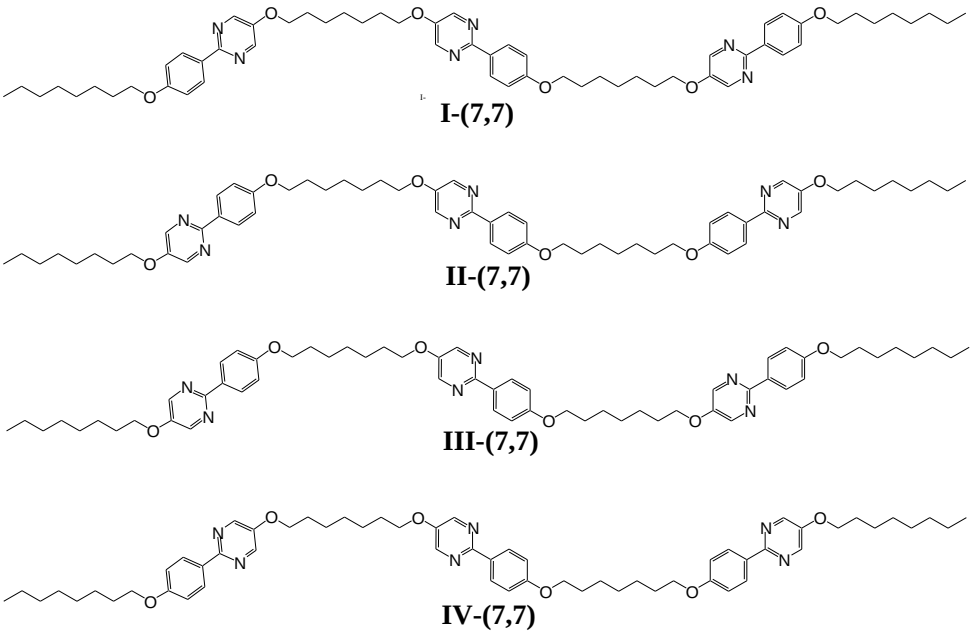

Fig.1– 1 Modifications of liquid crystal trimers under investigation.

1.2. Experimental

1.2.1. Preparation of materials

For use in this study, 5-hydroxy-2-(4-hydroxyphenyl)pyrimidine was purchased from Midori Kagaku Co. Ltd. The purity of each trimer compound was checked elemental analysis (EA 1110; CE Instruments Ltd).Confirmation of the structures of intermediates and products was obtained by infrared (IR) spectroscopy (BIO RAD FTS-30) and proton nuclear magnetic resonance (^{1}H NMR) spectroscopy (JEOL JNM-ECA500).

In the reporting of IR data, the following abbreviations have been used.

str. stretching

In the reporting of ^{1}H NMR data, the following abbreviations have been used.

s. singlet
d. doublet
t. triplet
q. quartet
m. multiplet

The analyses of the structures of the products by means of spectroscopic methods were found to be consistent with the predicted structures.

1.2.1.1.

2-{4-[7-(2-(4-octyloxyphenyl)pyrimidin-5-yloxy)heptyloxy]phenyl}-5-{7-[2-(4-octyloxyphenyl)pyrimidin-5-yloxy]heptyloxy}pyrimidine [I-(7,7)]

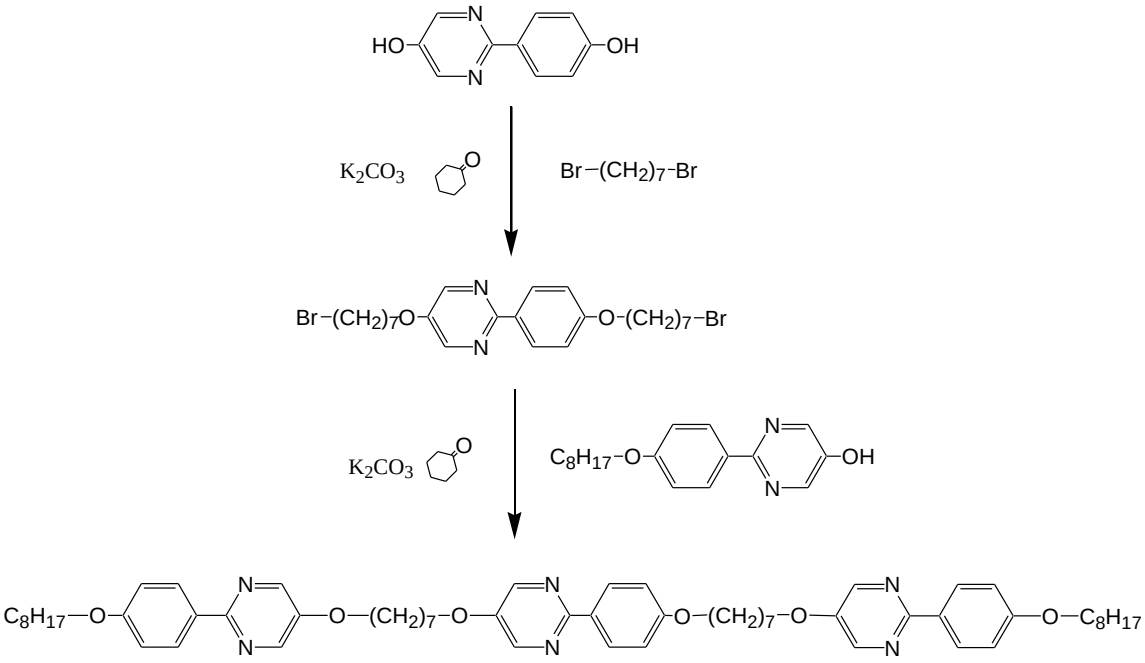

I-(7,7)

Scheme1– 1 Preparation of **I–(7,7)**.

Potassium carbonate (2.20 mmol,305 mg) was added to a solution of 2-(4-hyrdroxyphenyl)-5-pyrimidinol (1.00 mmol,188 mg) and 1,7-dibromohexane (3.00 mmol, 730 mg) in cyclohexanone (20 ml). The reaction mixture was stirred at 95 °C for 7 h. After filtration of the precipitate, the solvent was removed by evaporation. Then, the residue was purified using column chromatography on silica gel with a toluene : ethyl acetate (15 : 1) mixture as an eluent. The obtained white solid was washed from hexane to give 2-[4-(7-bromo-heptyloxy)phenyl]-5-(7-bromo-heptyloxy)pyrimidine. Yield 187 mg (35 %).

Potassium carbonate (0.50 mmol,69.5 mg) was added to a solution of 2-(4'-octyloxy phenyl)-5-pyrimidinol (0.50 mmol, 150 mg) and 2-[4-(7-bromo-heptyloxy)phenyl]-5-(7-bromo-heptyloxy)pyrimidine (0.25 mmol,135.6 mg) in cyclohexanone (10 ml). The reaction mixture was stirred at 120 °C for 8 h. After filtration

of the precipitate, the solvent was removed by evaporation. Then, the residue was washed with hot ethanol and was recrystallized from toluene to give the desired compound. Yield 177 mg (72 %).

^{1}HNMR (500 MHz, $CDCl_3$, TMS): δ=8.40 (s, 6H, Ar-**H**), 8.26 (d, 6H, Ar-**H**, *J* = 7.4 Hz), 7.0 (d, 6H, Ar-**H**, *J* = 8.6 Hz), 4.09 (t, 4H, -OC**H$_2$**-, *J* = 6.3 Hz), 4.08 (t, 2H, -OC**H$_2$**-, *J* = 6.3 Hz), 4.03 (m, 2H, -OC**H$_2$**-, *J* = 6.6 Hz), 4.01 (m, 4H, -OC**H$_2$**-, *J* = 6.6 Hz), 1.87–1.77 (m, 12H, aliphatic-**H**), 1.54–1.44 (m, 16H, aliphatic-**H**), 1.34–1.29 (m, 16H, aliphatic-**H**), 0.89 (t, 6H, -C**H$_3$**, *J* = 6.9 Hz)

IR (KBr):ν cm^{-1}: 2938, 2854 (C-H str), 1607, 1581, 1544, 1515, 1433 (C=C, C=N str), 1250 (C-O str)

Elemental analysis calc. for $C_{60}H_{80}N_6O_6$: C,73.44; H, 8.22; N, 8.56. Found C, 73.80; H, 8.16; N, 8.52.

1.2.1.2.

2-{4-[7-(4-(5-Octyloxypyrimidin-2-yl)phenyloxy)heptyloxy]phenyl}-5-{7-[4-(5-octyloxy-pyrimidin-2-yl)phenyloxy]heptyloxy}pyrimidine [II-(7,7)]

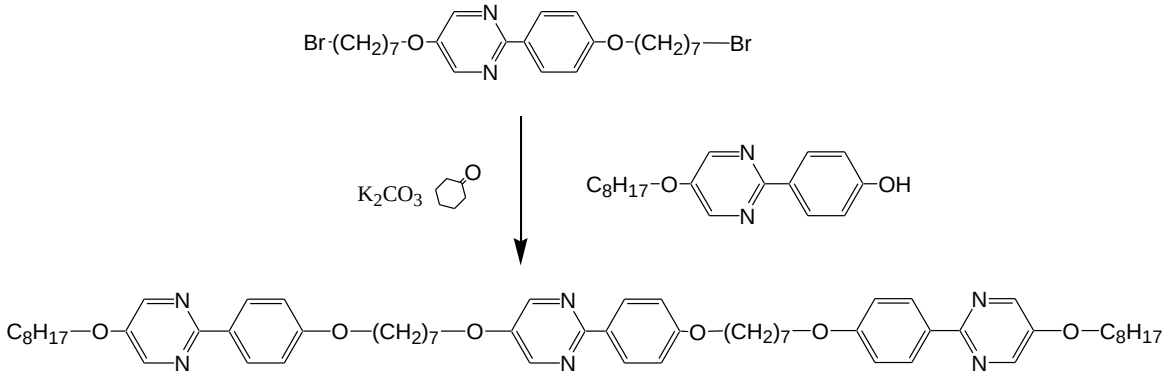

II-(7,7)

Scheme1– 2 Preparation of **II–(7,7)**

Potassium carbonate (0.5 mmol, 69.1 mg) was added to a solution of 2-[4-(7-bromo-heptyloxy)phenyl]-5-(7-bromo-heptyloxy)pyrimidine (0.25 mmol,135.6 mg) and 2-(4-hydroxyphenyl)-5-octyloxy-pyrimidine (0.5 mmol,150.2 g) in cyclohexanone (20 ml). The reaction mixture was stirred at 125 °C for 7 h. After filtration of the precipitate, the

solvent was removed by evaporation. Then, the residue was washzed from hot ethanol and recrystallized from toluene to give the desired compound. Yield 169.9 mg (69 %).

^{1}HNMR (500 MHz, $CDCl_3$, TMS): δ=8.40 (s, 6H, Ar-**H**), 8.25 (d, 6H, Ar-**H**, *J* = 9.2 Hz), 6.96 (d, 6H, Ar-**H**, *J* = 8.6 Hz), 4.08 (t, 2H, -OC**H$_2$**-, *J* = 6.3 Hz), 4.07 (t, 4H, -OC**H$_2$**-, *J* = 6.3 Hz), 4.03 (t, 2H, -OC**H$_2$**-, *J* = 6.3 Hz), 4.02 (t, 4H, -OC**H$_2$**-, *J* = 6.3 Hz), 1.84–1.79 (m, 12H, aliphatic-**H**), 1.53–1.44 (m, 16H, aliphatic-**H**), 1.35–1.29 (m, 16H, aliphatic-**H**), 0.89 (t, 6H, -C**H$_3$**, *J* = 6.9 Hz)

IR (KBr):ν cm^{-1}: 2936, 2854 (C-H str), 1607, 1581, 1544, 1515, 1433 (C=C, C=N str), 1250 (C-O str)

Elemental analysis calc. for $C_{60}H_{80}N_6O_6$: C,73.44; H, 8.22; N, 8.56. Found C, 73.36; H, 7.96; N, 8.62.

1.2.1.3.

2-{4-{7-[2-(4-Octyloxyphen-2-yl)pyrimidin-5-oxy]heptyloxy}phenyl}-5-{7-[4-(5-octyloxy-pyrimidin-2-yl)phenoxy]heptyloxy}pyrimidine [III-(7,7)]

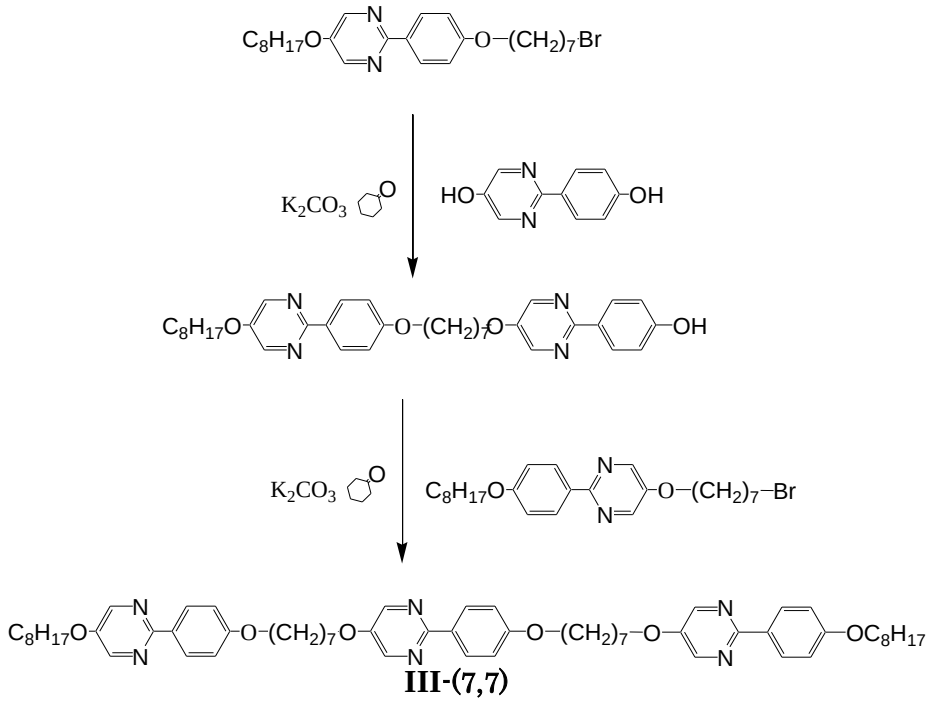

III-(7,7)

Scheme1– 3 Preparation of **III–(7,7)**

Potassium carbonate (1.25 mmol, 138 mg was added to a solution of

2-(4-hyrdroxyphenyl)-5-pyrimidinol (1.25 mmo, 235 mg) and 5-Octyloxy-2-(4-(7-bromo-heptyloxy)-phenyl)pyrimidine (1.00 mmol, 478 mg) in cyclohexanone (20 ml). The reaction mixture was stirred at 95 °C for 6 h. After filtration of the precipitate, the solvent was removed by evaporation. Then, the residue was purified using column chromatography on silica gel with a dichloromethane : ethyl acetate (8 : 1) mixture as an eluent. The obtained white solid was recrystallized from ethanol to give 2-(4-hyrdroxyphenyl)-5-{7-[4-(5-octyloxypyrimidin-2-yl)phenoxy]heptyloxy}pyrimidine.
Yield 367 mg (63 %).

Potassium carbonate (0.55 mmol, 76.0 mg) was added to a solution of 2-(4-Octyloxyphenyl)-5-(7-bromo-heptyloxy)pyrimidine (0.55 mmol, 263 mg) and 2-(4-hyrdroxyphenyl)-5-{7-[4-(5-octyloxypyrimidin-2-yl)phenoxy]heptyloxy}pyrimidine (0.55 mmol, 322 mg) in cyclohexanone (20 ml). The reaction mixture was stirred at 130 °C for 9 h. After filtration of the precipitate, the solvent was removed by evaporation. Then, the residue was washzed from hot ethanol and recrystallized from toluene to give the desired compound. Yield 446.6 mg (83 %).

^{1}HNMR (500 MHz, $CDCl_3$, TMS): δ=8.40 (s, 6H, Ar-**H**), 8.26 (d, 6H, Ar-**H**, *J* = 9.2 Hz), 6.96 (d, 6H, Ar-**H**, *J* = 9.2 Hz), 4.08 (t, 4H, -OC**H$_2$**-, *J* = 6.6 Hz), 4.07 (t, 2H, -OC**H$_2$**-, *J* = 6.6 Hz), 4.03 (t, 4H, -OC**H$_2$**-, *J* = 6.3 Hz), 4.00 (t, 2H, -OC**H$_2$**-, *J* = 6.6 Hz), 1.88–1.77 (m, 12H, aliphatic-**H**), 1.55–1.45 (m, 16H, aliphatic-**H**), 1.34–1.29 (m, 16H, aliphatic-**H**), 0.89 (t, 6H, -C**H$_3$**, *J* = 6.4 Hz)

IR (KBr):ν cm^{-1}: 2933, 2854 (C-H str), 1607, 1582, 1545, 1515, 1435 (C=C, C=N str), 1249 (C-O str)

Elemental analysis calc. for $C_{60}H_{80}N_6O_6$: C,73.44; H, 8.22; N, 8.56. Found C, 73.77; H, 7.99; N, 8.44.

1.2.1.4.

2-(4-(7-(4-(5-octyloxypyrimidin-2-yl)phenoxy)heptyloxy)phenyl)-5-(7-(2-(4-octyloxy-phen-1-yl)pyrimidin-5-oxy)heptyloxy)pyrimidine [IV -(7,7)]

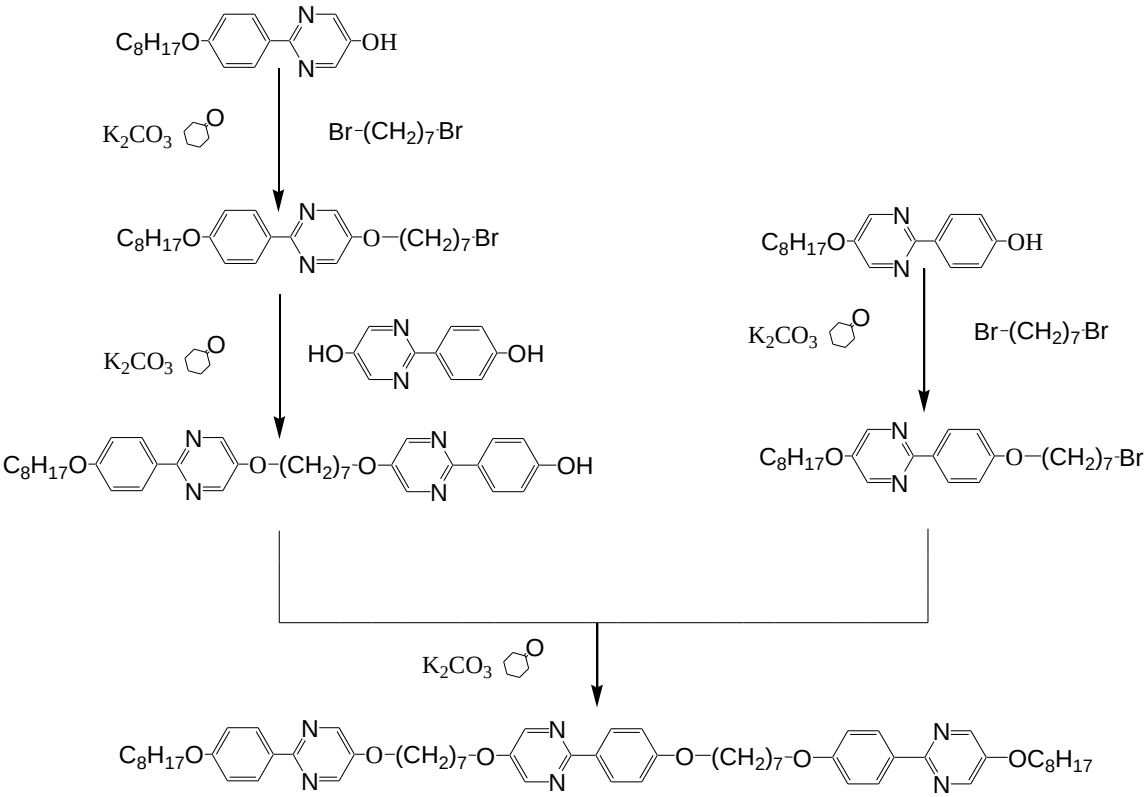

IV-(7,7)

Scheme1– 4 Preparation of **IV–(7, 7)**

Potassium carbonate (1.50 mmol, 207 mg) was added to a solution of 2-(4'-hyrdroxyphenyl)-5-octyloxy-pyrimidine(1.50 mmol,451 mg) and 1,7-Dibromoheptane (2.25 mmol, 0.60 g) in cyclohexanone (20 ml). The reaction mixture was stirred at 95 °C for 8 h. After filtration of the precipitate, the solvent was removed by evaporation. Then, the residue was purified using column chromatography on silica gel with a hexane : ethyl acetate (4 : 1) mixture as an eluent. The obtained white solid was recrystallized from hexane to give 5-Octyloxy-2-(4-(7-bromo-heptyloxy)-phenyl)pyrimidine. Yield 381 mg (50 %).

Potassium carbonate (1.00 mmol, 138 mg) was added to a solution of 2-(4-hydroxyphenyl)-5-pyrimidinol (1.25 mmol, 235 mg) and

2-(4-Octyloxyphenyl)-5-(7-bromo-octyloxy)pyrimidine (1.00 mmol, 478 mg) in cyclohexanone (20 ml). The reaction mixture was stirred at 95 °C for 8 h. After filtration of the precipitate, the solvent was removed by evaporation. Then, the residue was purified using column chromatography on silica gel with a toluene : ethyl acetate (2 : 1) mixture as an eluent. The obtained white solid was washed from hexane to give 2-(4-hyrdroxyphenyl)-5-{7-[2-(4-octyloxyphenyl)pyrimidin-5-oxy]heptyloxy}pyrimidine. Yield 374 mg (64 %).

Potassium carbonate （4.00 mmol, 0.55 g) was added to a solution of 2-(4'-Octyloxy phenyl)-5-pyrimidinol (4.00 mmol, 1.20 mg) and 1,7-Dibromoheptane (6.00 mmol, 1.55 g) in cyclohexanone (20 ml). The reaction mixture was stirred at 95 °C for 4 h. After filtration of the precipitate, the solvent was removed by evaporation. Then, the residue was purified using column chromatography on silica gel with a hexane : ethyl acetate (3 : 1) mixture as an eluent. The obtained white solid was recrystallized from hexane to give 2-(4-octyloxyphenyl)-5-(7-bromo-heptyloxy)pyrimidine. Yield 1.04 g (55 ％).

Potassium carbonate (0.55 mmol, 76.0 mg) was added to a solution of 5-octyloxy-2-(4-(7-bromo-heptyloxy)-phenyl)pyrimidine (0.55 mmol, 263 mg) and 2-(4-hyrdroxyphenyl)-5-{7-[2-(4-Octyloxyphenyl)pyrimidin-5-oxy]heptyloxy}pyrimidine (0.55 mmol, 322 mg)in cyclohexanone (20 ml). The reaction mixture was stirred at 130 °C for 8 h. After filtration of the precipitate, the solvent was removed by evaporation. Then, the residue was washzed from hot ethanol and recrystallized from toluene to give the desired compound. Yield 388 mg (72 ％).

^{1}HNMR (500 MHz, $CDCl_3$, TMS): δ=8.41 (s, 6H, Ar-**H**), 8.26 (d, 6H, Ar-**H**, *J* = 8.6 Hz), 6.96 (d, 6H, Ar-**H**, *J* = 8.6 Hz), 4.09 (t, 4H, -OC**H$_2$**-, *J* = 6.6 Hz), 4.07 (t, 2H, -OC**H$_2$**-, *J* = 6.6 Hz), 4.02 (t, 4H, -OC**H$_2$**-, *J* = 6.6 Hz), 3.99 (t, 2H, -OC**H$_2$**-, *J* = 6.6 Hz), 1.87–1.77 (m, 12H, aliphatic-**H**), 1.54–1.47 (m, 16H, aliphatic-**H**), 1.34–1.29 (m, 16H, aliphatic-**H**), 0.89 (t, 6H, -C**H$_3$**, *J* = 6.7 Hz)

IR (KBr):ν cm^{-1}: 2940, 2854 (C-H str), 1607, 1581, 1544, 1515, 1433 (C=C, C=N str), 1251 (C-O str)

Elemental analysis calc. for $C_{60}H_{80}N_6O_6$: C,73.44; H, 8.22; N, 8.56.Found C, 73.67; H, 7.80; N, 8.54.

1.2.2. Liquid-crystalline and physical properties

The initial phase assignments and corresponding transition temperatures for each final compound were determined using thermal optical microscopy using a polarizing microscope (BX-51; Olympus Optical Co. Ltd.) equipped with a temperature control unit (LK-600PM; Japan High Tech). The temperatures and enthalpies of transition were investigated using differential scanning calorimetry (DSC, DSC 6200; Seiko Instruments Inc.). The XRD patterns of the homeotropically aligned sample during a cooling process were obtained using a real-time X-ray diffractometer (MicroMax−007HF; Rigaku Corp.) equipped with a hot stage and a temperature-control processor. A sample was put on a convex lens, which was then placed in a custommade temperature-stabilized holder (stability within ±0.1 °C). The phase transition of the sample under the X-ray beam was monitored by observing the texture using polarized light microscopy with a CCD camera. The X-ray apparatus was equipped with a platform arrangement and a two-dimensional detector (Image intensifier and CCD C9299−01; Hamamatsu Photonics KK). Then, X-rays were generated at 40 kV and 20 mA; the sample was irradiated with a Cu Kα X-ray beam, with confocal mirrors to correlate the incident X-ray beam and to increase its intensity. Each diffraction pattern was obtained using the detector at a camera distance of ca. 730 mm. The correlation length along the layer normal (ξ) was determined using the Ornstein−Zernicke expression as follows. First, the X-ray profile as a function of 2θ is converted to a scattering function of q according to

$$q = (4\pi/\lambda) \sin \theta \qquad (1)$$

By fitting the X-ray profiles using the following Lorentzian equation, the correlation length ξ is determined.

$$I(q) = \frac{I_0}{1+(q-q_0)^2\xi^2} + \text{background} \qquad (2)$$

Therein, I0 and q0 respectively signify the peak height and the peak position of q.

Electro-optical properties were measured using standard lectro-optical techniques. The ITO-coated glass sandwich cells purchased from EHC Corp. were constructed with 2 μm pacers. The unidirectionally buffed inner surfaces had been coated with a polyimide aligning agent.

1.3. Results and Discussion

1.3.1. Liquid crystalline properties of liquid crystal trimers

After preparing a homologous series of achiral liquid crystal trimers, I investigated phase transition behavior using polarized optical microscopy (POM) and differential scanning calorimetry (DSC). Their molecular structures and phase transition properties of a homologous series of achiral liquid crystal trimers are presented in Fig.1-2. The difference in phase transition behavior among these trimers is attributable to the relative orientation of phenylpyrimidine units within each trimer. Compounds **I-(7,7)**, **III-(7,7)**, and **IV-(7,7)** show SmA and SmC phases, whereas compound **II-(7,7)** shows only an N phase. No chirality dependent phenomenon was observed for any trimer.

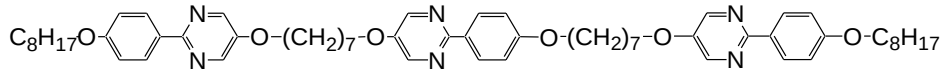

I-(7,7)

Iso 165.5 SmA 148.2 SmC 139.0 Cr

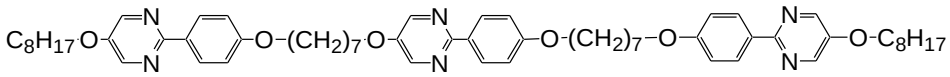

II-(7,7)

Iso 157.2 N 140.0 Cr

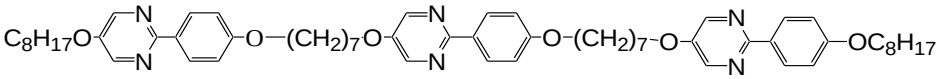

III-(7,7)

Iso 169.6 SmA 167.5 SmC 165.0 Cr

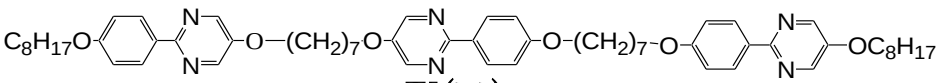

IV-(7,7)

Iso 166.5 SmA 164.0 SmC 149.0 SmB 130.0 Cr

Fig.1– 2 Molecular structures and phase transition temperatures/°C.

I investigated the phase transition behaviors of mixtures existing between these trimers. Fig. 1-3 portrays a phase diagram of cooling between trimer **II-(7,7)** and **IV-(7,7)**. A chiral phase, which is shown later to be the HNF phase, was found to be induced for binary mixtures of **II-(7,7)** and **IV-(7,7)** containing 50–70 mol% of **IV-(7,7)**. No other binary mixture among compounds **I~IV-(7,7)** exhibits such a chiral phase.

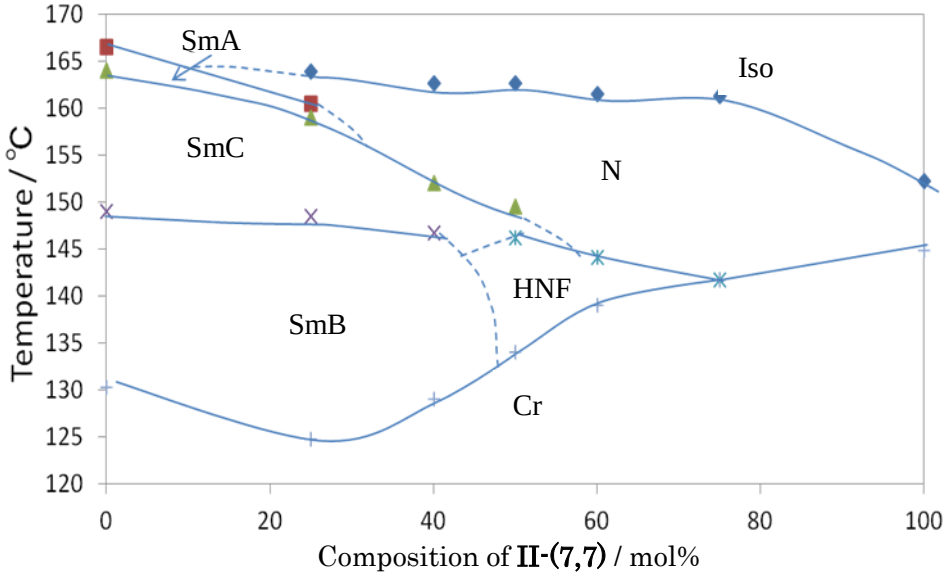

Fig.1– 3 Phase diagram of II-(7,7) and IV-(7,7).

On cooling the binary mixture of **II-(7,7)** and **IV-(7,7)**, an N phase and then a SmC phase appeared. On further cooling, birefringence of the sample in the homeotropic alignment started to decrease at 146.2 °C. Temperature-dependent polarized optical textures of the mixture are listed in Fig.1-4. It decreased concomitantly with decreasing temperature. The texture became nearly dark at 143 °C. By observing the sample under slightly uncrossed polarizers, the texture splits into darker and brighter domains, as shown in Fig.1-4(d). By uncrossing the polarizers in opposite directions by the same angle (10°), the darker and brighter domains exchange. The brightness of the domains does not change by rotation of the sample between the polarizers. These results indicate that they have optical activity with opposite senses and exclude that distinct tilt orientations are responsible for this effect [27]. Such optical activity was not detected in the N, SmC or Cry phase.

(a) N phase at 160 °C

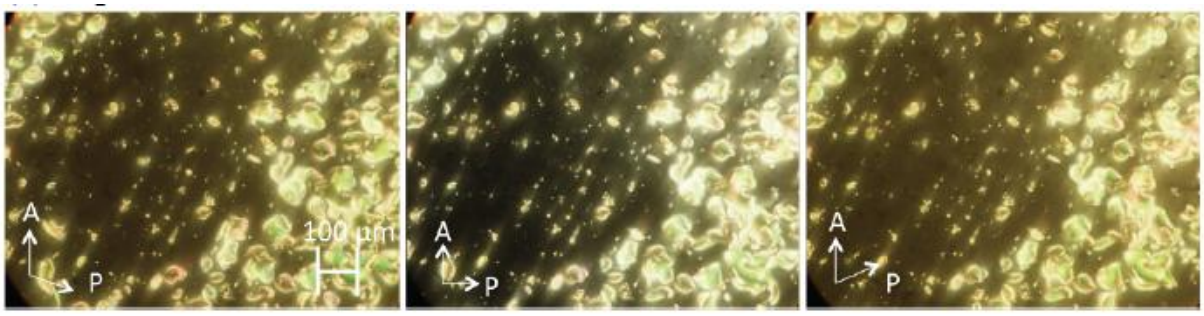

(b) SmC phase at 147 °C

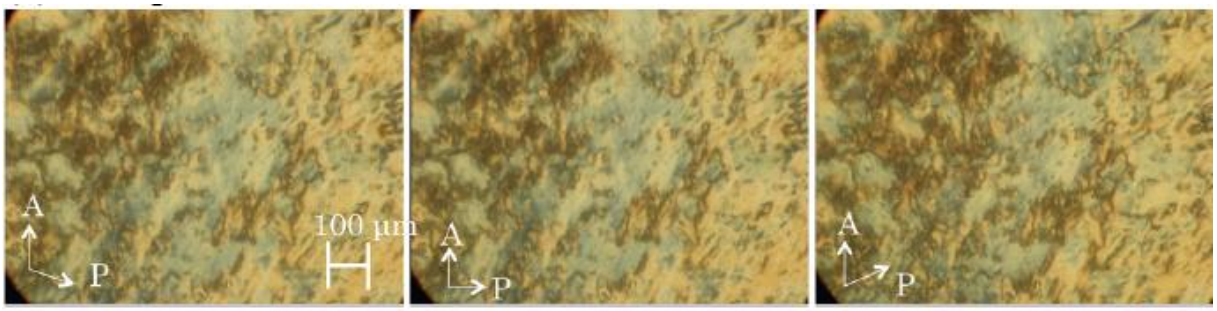

(c) HNF phase at 145 °C

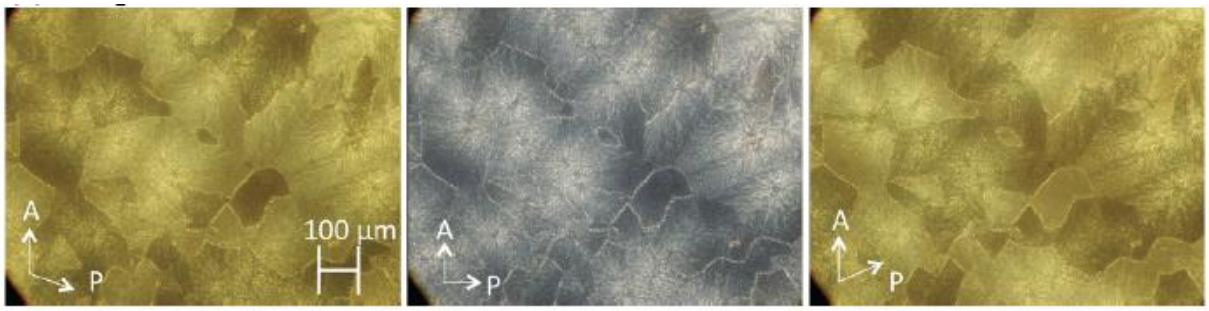

(d) HNF phase at 138 °C

Fig.1– 4 Polarized optical textures of an equimolecular mixture of compounds **II-(7,7)** and **IV-(7,7)** on a glass slide with a cover glass with uncrossed and crossed polarizers.

A cooling DSC thermogram of the equimolecular mixture between the trimers is portrayed in Fig.1-5. Phase transition temperatures (°C) and Δ*S*/*R* in parentheses of the equimolecular mixture on cooling were the following: isotropic liquid 163.6 (1.74) N 149.5 (0.04) SmC 146.2 (9.66) chiral phase. The melting temperature was 146.2 °C.

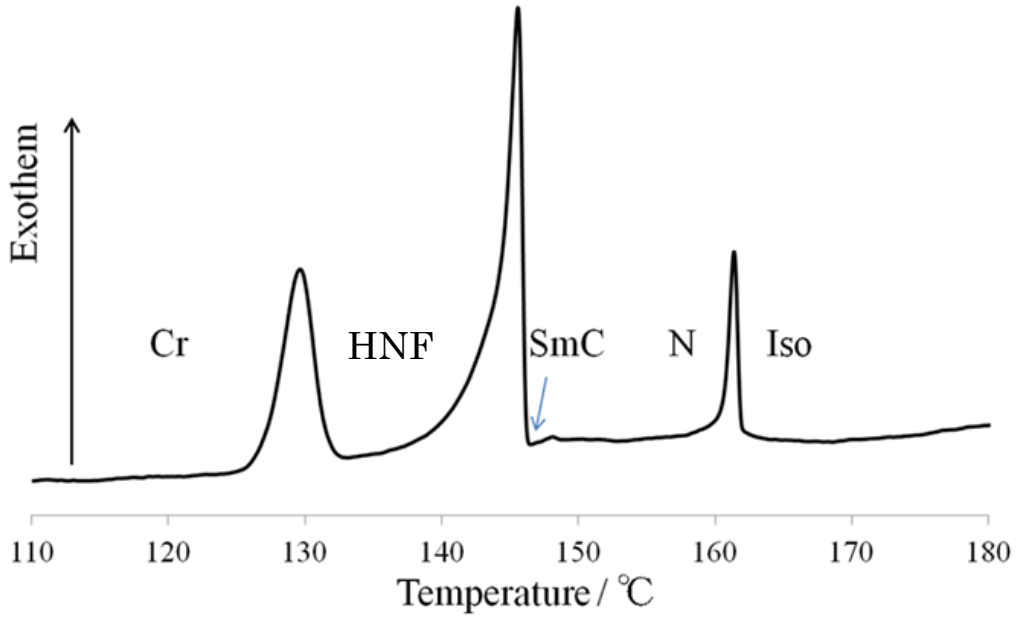

Fig.1– 5 DSC thermogram of an equimolecular mixture of compounds II-(7,7) and IV-(7,7) on cooling. The cooling rate was 2 °C min^{-1}.

I investigated the electro-optical response in the chiral phase by application of an AC field to the sample in a homogeneously aligned cell with a gap of 2 μm using a sine wave with an AC field at a frequency of 10 Hz. Despite increasing of the electric field up to ±30 V μm^{-1}, electro-optical switching was not detected in this phase. These results support that the solid chiral phase is the HNF phase. It is noteworthy that the mixture exhibited both N and HNF phases. Although 1,7-naphthalene central-core molecules[29] and dimesogenic molecules with an odd-numbered spacer show N and HNF phases[9,10], almost all bent-core compounds exhibiting a HNF phase do not show an N phase.

Fig.1-6 portrays the temperature dependence of the texture under uncrossed polarizers in the HNF phase. Contrast between darker and brighter domains was low in the HNF phase in the vicinity of the SmC− HNF transition. Then, it was enhanced with decreasing temperature until 143 °C. The contrast did not change at temperatures below 143 °C.

(a) 146.2 °C (b) 146.0 °C (c) 145.5 °C

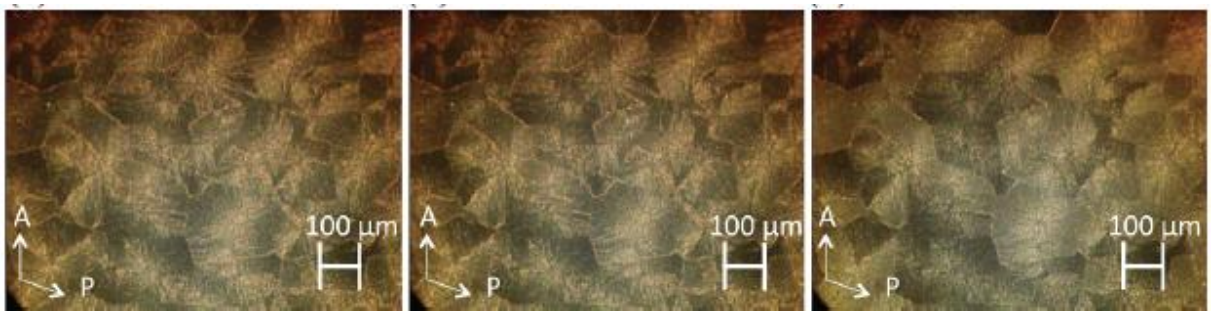

(d) 145.0 °C (e) 144.5 °C (f) 144.0 °C

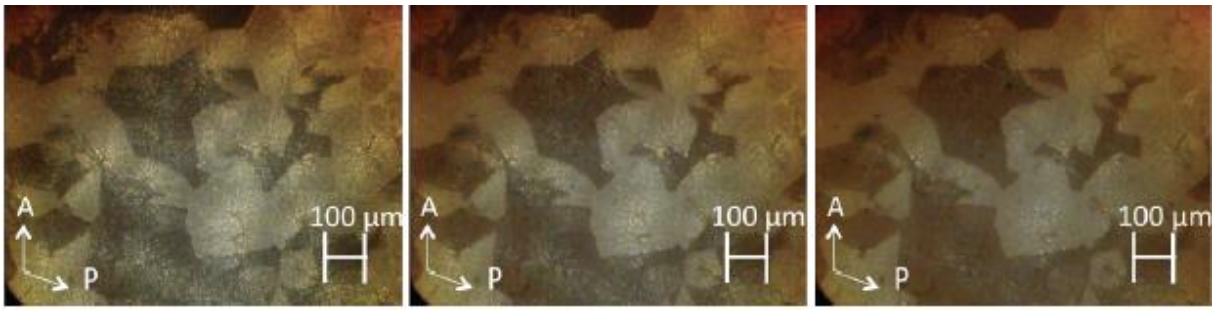

(g) 143.0 °C (h) 140.0 °C (i) 135.0 °C

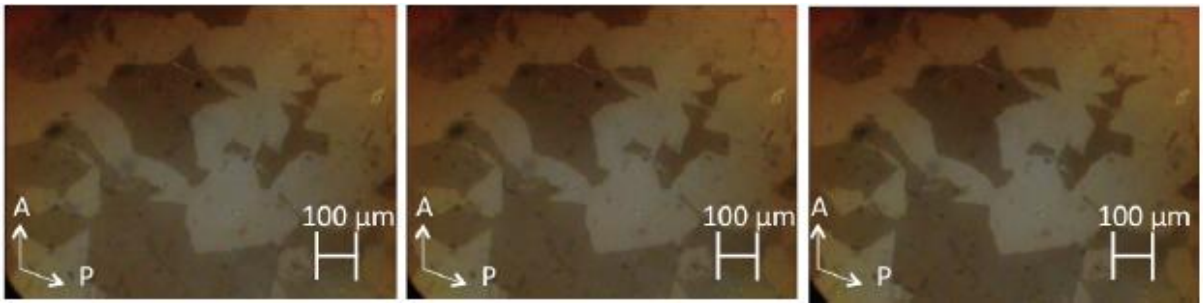

Fig.1– 6 Polarized optical textures of the HNF phase under uncrossed polarizers as a function of temperature.

1.3.2. X-ray Diffraction

To elucidate the phase structures, X-ray measurements were conducted. Fig.1-7 portrays X-ray diffraction patterns in the small-angle region of the mixture in the SmC and HNF phases. Alignment was performed by the slow cooling of a small drop of the sample on a convex lens. On cooling the sample, a sharp scattering appeared beside the equator in the SmC phase (Fig.1-7(a)). In the HNF phase, in addition to the sharp scattering, weak and broad scattering appeared in a circle (Fig.1-7(b)). Upon further cooling in the HNF phase, all diffractions were smeared out to form closed rings (Fig.1-7(c)). No sharp scattering appeared in the N phase, revealing that the N phase is not a cybotactic N phase, which is often seen in a bent core liquid crystal, but a conventional N phase[30,31].

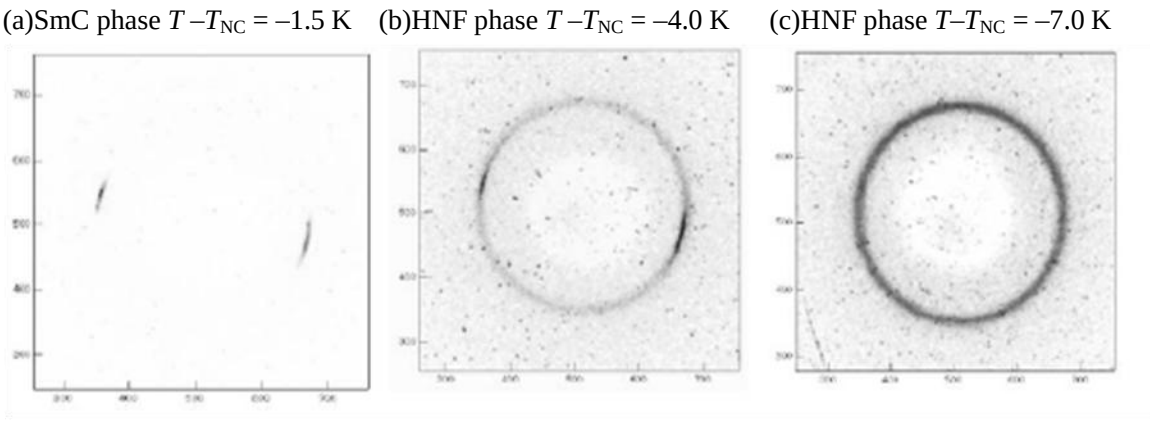

Fig.1– 7 X-ray diffraction patterns in the small-angle region of an equimolecular mixture of compounds **II-(7,7)** and **IV-(7,7)**: (a) SmC phase at $T - T_{NC} = -1.5$ K, (b) HNF phase at $T - T_{NC} = -4.0$ K, and (c) HNF phase at $T - T_{NC} = -7.0$ K.

Fig.1-8 depicts X-ray diffraction profiles in the small angle region in the SmC and HNF phases of the mixture. The X-ray diffraction peak in the small-angle region of the mixture in SmC was sharp with strong intensity. However, the peak in the HNF phase became broad. Correlation lengths for the periodicity in the small-angle region in the SmC and HNF phases are, respectively, 3800 Å at $T - T_{NC} = -1.5$ K and 410 Å at $T - T_{NC} = -7.0$ K (T_{NC}: the N−SmC transition temperature). With respect to the wide-angle region in the HNF phase, several sharp peaks were observed as portrayed in Fig.1-9 indicating that it has positional

order within the layer. The shape of the diffraction pattern in the small- and wide-angle range is similar to that in the HNF phase of P-9-O-PIMB. [4] According to analysis of shapes of peaks in the wide-angle region of P-8-O-PIMB by Folcia et al., the HNF phase has an antiferroelectric in-layer arrangement of the moleucles. [32]

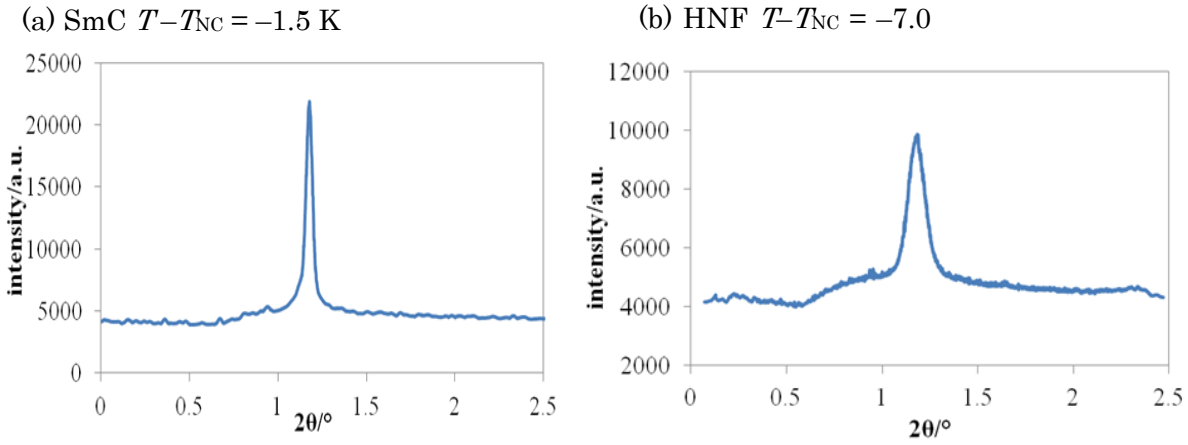

Fig.1– 8 X-ray diffraction profiles in the small-angle region of an equimolecular mixture of compounds **II-(7,7)** and **IV-(7,7)**: (a) SmC phase at $T - T_{NC} = -1.5$ K and (b) HNF phase at $T - T_{NC} = -7.0$ K.

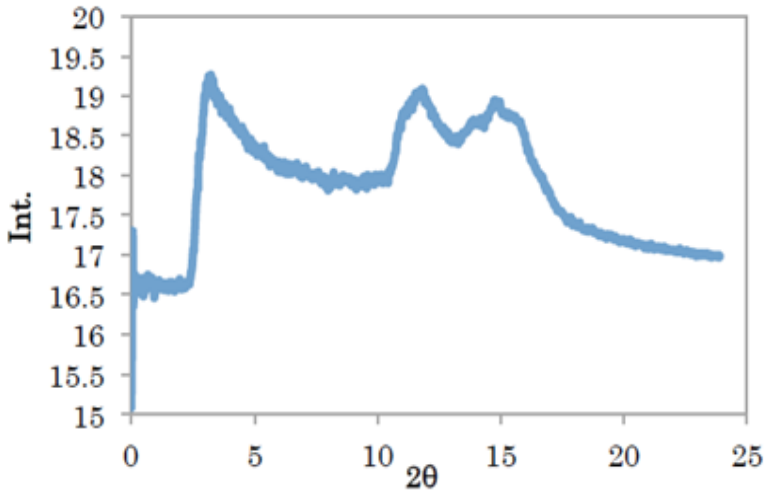

Fig.1– 9 X-ray diffraction profile in the wide-angle region of an equimolecular mixture of compounds **II-(7,7)** and **IV-(7,7)** in the HNF phase at $T - T_{NC} = -9.0$ K.

Fig.1-10 portrays the temperature dependence of the periodicity length in the SmC and HNF phases of the mixture. The layer spacing in the SmC phase at $T - T_{NC} = -1.5$ K is 76 Å. The layer spacing decreases with decreasing temperature in the SmC phase. When cooling to the HNF phase, the layer spacing maintains a constant value of 75.7 Å. Then, it decreases with decreasing temperature. It reaches a saturated value of 74.7 Å at $T - T_{NC} = -5.5$ K. Extended molecular lengths for compounds **II-(7,7)** and **IV-(7,7)** with all trans conformation of the spacers are estimated using MOPAC to be 67 Å. Their conformations are shown in Fig.1-11. Both SmC and HNF phases were found to have an interdigitated structure. However, the layer spacing in the SmC phase of compound **IV-(7,7)** was 62 Å. Therefore, interaction between compounds **II-(7,7)** and **IV-(7,7)** produces an interdigitated molecular organization. The layer spacing in the HNF phase below $T - T_{NC} = -5.5$ K is almost constant. It is consistent with the fact that the contrast between darker and brighter domains in the HNF phase did not change at temperatures below 143 °C, as shown in Fig.1- 6. The correlation length of along the layer normal (410 Å at $T - T_{NC} = -7.0$ K) corresponds to about 5−6 layers.

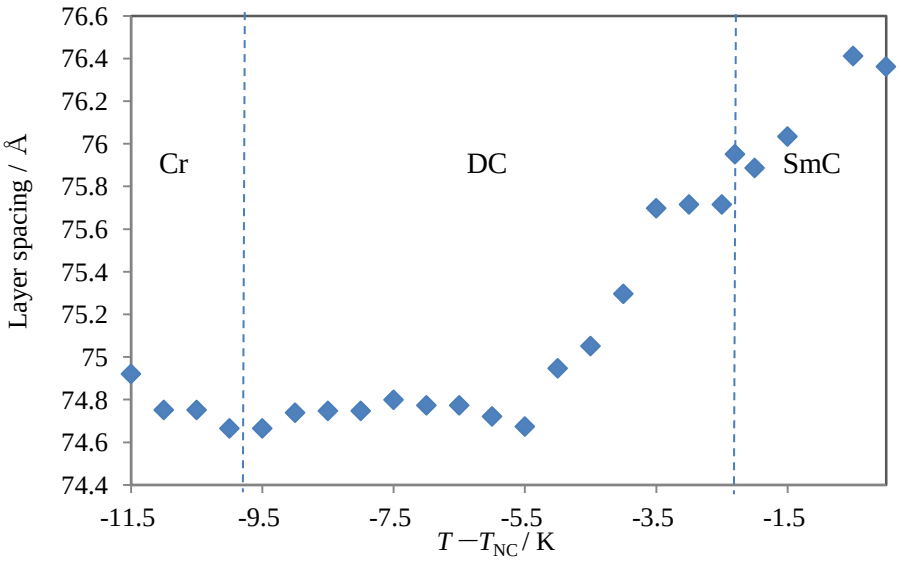

Fig.1– 10 Temperature dependence of the periodicity length in the SmC, HNF, and Cry phases of an equimolecular mixture of compounds **II-(7,7)** and **IV-(7,7)**.

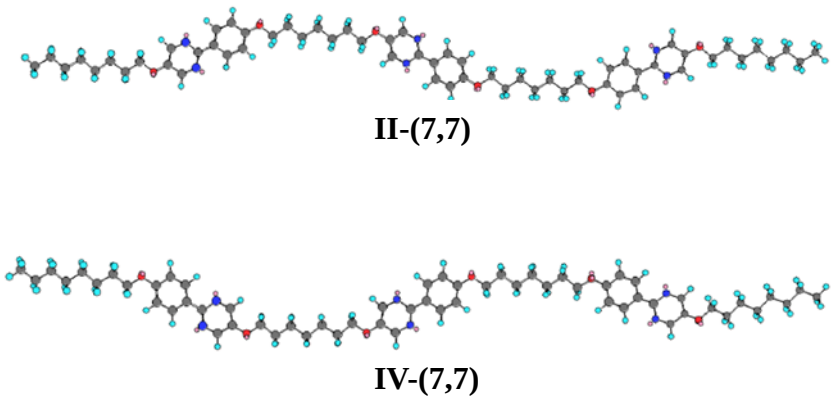

Fig.1– 11 MOPAC models for compounds **II-(7,7)** and **IV-(7,7)**.

With respect to the tilt angle in the SmC phase of the mixture, I have not obtained it by POM because of the difficulty to get a well-aligned domain. I estimated it by XRD. I adopt a packing model for the interdigitated structure in the SmC phase, as shown in Fig.1-12. Dipole−dipole interactions between phenylpyrimidine units in adjacent molecules can form the molecular packing. The tilt angle is estimated to be 25° at $T - T_{NC} = -1.5$ K by XRD based on the fact that the interdigitated molecular length is 84 Å. The large tilt angle results from the first order N−SmC phase transition. The packing model seems to be realistic. On the other hand, the tilt angle in the SmC phase of compound **IV-(7,7)** at $T - T_{NC} = -15$ K is 10° by POM and it is 9° by XRD. The small tilt angle results from the second order SmA−SmC phase transition.

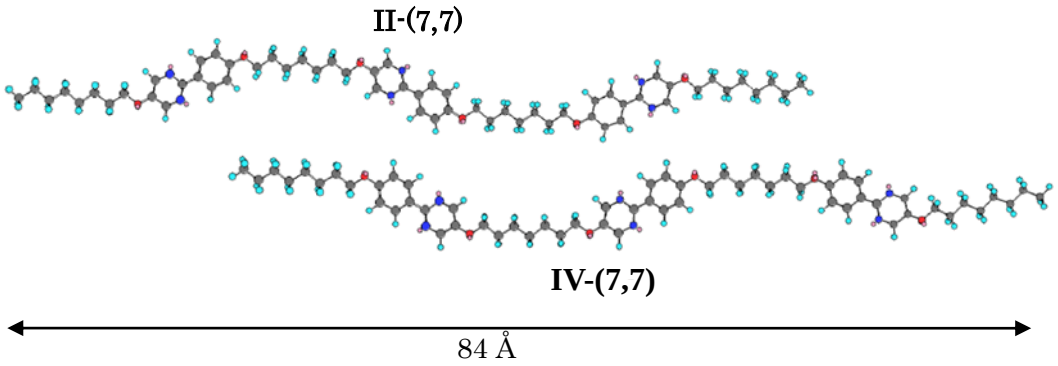

Fig.1– 12 Packing model for the interdigitated structure in the SmC phase of the mixture.

1.3.3. Model for Origin of the Chirality

As described above, spontaneous symmetry breaking in soft matter has previously mainly been observed for bent-core mesogens and dimesogens with an odd-numbered spacer. To the best of our knowledge, this is the first report of an achiral trimesogen forming a chiral conglomerate. I discuss how the chirality arises in the HNF phase of the mixture. Compounds **II-(7,7)** and **IV-(7,7)** have flexible spacers. Therefore, they do not form an inherent twist structure such as a propeller conformer to produce conformational chirality. The 2-phenylpyrimidine units also do not provide a twist between the aromatics. They have no rigid bent structure that tends to form smectic layers. Therefore, the mixture shows the conventional nematic phase. Not a polar B2 but a nonpolar SmC phase was observed. In the N and SmC phases, the molecular organization has no chiral origin. The present HNF phase appears below the SmC phase in the equimolecular mixture, indicating that intermolecular interaction between compounds **II-(7,7)** and **IV-(7,7)** in the HNF phase produces the chiral nature. The phase sequence of N−SmC−HNF was reported to occur in only a dimesogenic compound with a heptamethylenespacer[9]. Gorecka et al. reported that dimesogenic compounds containing azo units exhibit a strong odd−even effect regarding mesophase sequence as a function of carbon number in the spacer[9]. Bent shape and distance between mesognic units of the dimer are thought to contribute to the appearance of the phase sequence. Fig.1-13 presents a molecular organization model for the origin of the chirality. Since both compounds **II-(7,7)** and **IV-(7,7)** have odd-numbered spacers, I assume that the phenylpyrimidine units in each trimer are assumed to be mutually inclined with respect to one other. In an equimolecular mixture of compounds **II-(7,7)** and **IV-(7,7)**, dipole−dipole interactions between phenylpyrimidine units in adjacent molecules might produce the interdigitated SmC phase. I assume a molecular packing model for the interdigitated arrangements, as shown in Fig.1-12 The molecules tilt along the (−) y-axis with respect to the layer normal (z-axis). The birefringence decreases at the SmC−HNF transition, and it decreases concomitantly with decreasing temperature in a hightemperature region in the HNF phase. In the same temperature region, the layer spacing decreases. The decrease in the layer spacing cannot be explained by the further molecular tilt along the (−) y-axis. It can be attributed to the tilt of the adjacent two molecules to opposite directions along the (±) x-axis.

The temperature dependence of the optical textures shown in Fig.1-6 is attributed to the molecular tilt to opposite directions. The tilt to opposite directions is also consistent with an antiferroelectric in-layer arrangement suggested by Folcia et al. [32] Viewed along the y-axis, the two molecules can be seen to form a bent structure. The appearance of the B4 phase is explained as follows according to Clark et al. [4] The supermolecules with a bent structure form well-defined smectic layers with in-plane crystal or hexatic order. The half-molecular tilt directions on either side of the layer midplane are nearly orthogonal. The projections onto the layer midplane of the lattices formed by the arms (blue and red) do not match, resulting in a local preference for saddle splay curvature characteristic, thereby driving the HNF phase. It should be noticed that flexible spacers of the trimers become more rigid in the crystalline mesophase HNF than in the SmC phase and that a helical molecular conformation induced by the dipole−dipole interaction could be possibly stabilized. I cannot exclude a possibility that the intermolecular interaction between compounds **II-(7,7)** and **IV-(7,7)** might induce a twist conformation in each trimer, which produces chiral characteristics of the binary mixture consisting of achiral molecules.

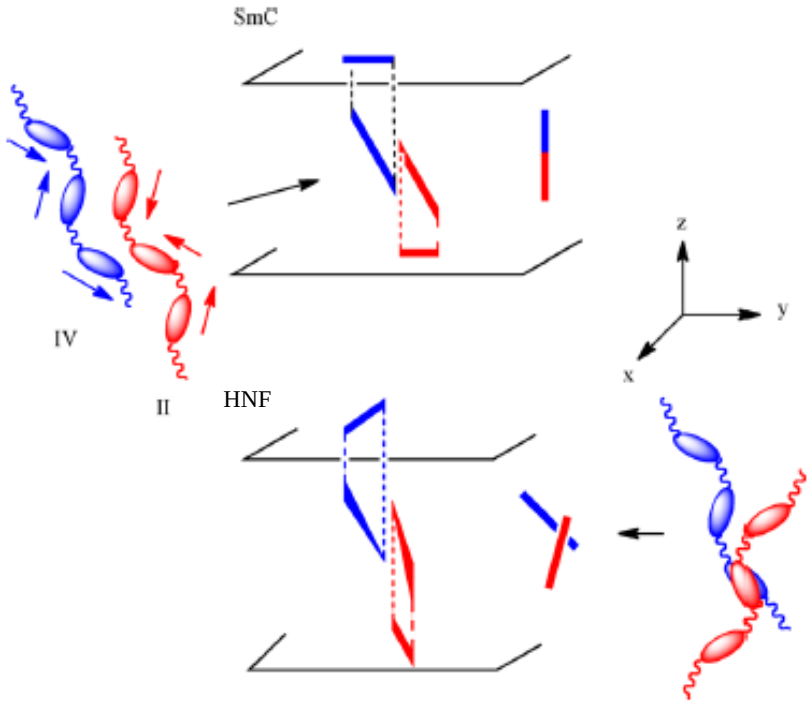

Fig.1– 13 Molecular organization model for the origin of chirality for the binary mixture consisting of achiral flexible trimers.

1. 4. Conclusion

I prepared a homologous series of achiral liquid crystal trimers in which three phenylpyrimidine units are connected via flexible heptamethylene spacers. An equimolecular mixture of compound **II-(7,7)** with an N phase and compound **IV-(7,7)** showing SmA, SmC, and SmB phases was found to exhibit N, SmC, and HNF phases. It is the first report of an achiral trimesogen forming a chiral conglomerate. The interdigitation of the zigzag trimers driven by the dipole−dipole interaction might form a supermolecular bent configuration, which induces a local preference for the saddle splay curvature to drive the HNF phase. The present approach might be an important new molecular design for production of the helical nanofilament HNF phase.

1. 5.Reference

[1] J. W. Goodby, *Symmetry and Chirality in Liquid Crystals in Handbook of Liquid Crystals*; D. Demus, J. W. Goodby, G. W. Gray, H. W.Spiess, V. Vill, Eds.; Wiley-VCH: Weinheim, Germany, 1998; Vol. 1, Chapter V, pp 115−132.

[2] R. A. Reddy and C.Tschierske, *J. Mater. Chem*., 2006, **16**, 907.

[3] E. Hough, H. T. Jung, D.Kruerke, M. S. Heberling, M. Nakata, C. D. Jones, D. Chen, D. R. Link, J. Zasadzinski, G. Heppke, J. P. Rabe, W. Stocker, E. Körblova, D. M. Walba, M. A. Glaser, N. A. Clark, *Science*, 2009, **325**, 456.

[4] G. D. Heppke, D. Parghi, D. Sawade, *Liq. Cryst*., 2000, **27**, 313.

[5] J. Thisayukta, H. Takezoe, J. Watanabe, *Jpn. J. Appl. Phys*., 2001, **40**, 3277.

[6] M. Alaasar, M. Prehm, M. Brautzsch, C. Tschierske, *Soft Matter*, 2014, **10**, 7285.

[7] M. Alaasar,, M. Prehm,, M. Brautzsch, C. Tschierske, *J. Mater. Chem.* C, 2014, **2**, 5487.

[8] T. Uda, S. Masuko, F. Araoka, K. ishikawa, H. Takezoe, *Angew. Chem., Int. Ed.,* 2013, **52**, 6863.

[9] A. Zep, K. Sitkowska, D. Pociecha, E. Gorecka, *J. Mater. Chem*. C, 2014, **2**, 2323.

[10] A. Zep, M. Salamonczyk, N. Vaupotic D. Pociecha, E. Gorecka, *Chem. Commun.*, 2013, **49**, 3119.

[11] J. Thisayukta, H. Takezoe, J. Watanabe, *Jpn. J. Appl. Phys*., 2001, **40**, 277.

[12] E. A. Matsumoto, G. P. Alexander, R. D. Kamien, *Phys. Rev. Lett*., 2009, **103**, 257804.

[13] D. Chen, J. E. Maclennan, R. Shao, D. K. Yoon, H. Wang, E. Ko.rblova, D. M. Walba, M. A. Glaser, N. A. Clark,. *J. Am. Chem. Soc*., 2011, **133**, 12656.

[14] D. Chen, Y.Shen, C. Zhu, L. E. Hough, N. Gimeno, M. A. Glaser, J. Maclennan, M. B. Ros, N. A. Clark, *Soft Matter*, 2011, **7**, 1879.

[15] M. Cestari, S. Diez-Berart, D. A. Dunmur, A. Ferrarini, M. R. de la Fuente, D. J. B. Jackson, D. O. Lopez, G. R. Luckhurst, M. A. Perez- Jubindo, R. M. Richardson, J. Salud, B. A. Timimi, H. Zimmermann,. *Phys. Rev. E*, 2011, **84**, 031704.

[16] V. Borshch, Y.-K. Kim, J. Xiang, M. Gao, A. Jakli, V. P. Panov, J. K. Vij, C. T. Imrie, M. G. Tamba, G. H. Mehl, O. D. Lavrentovich, *Nat. Commun.*, 2013, **4**, 2635.

[17] D. Chen, J. H. Porada, J. B. Hooper, A. Klittnick, Y. Shen, M. R. Tuchband, E. Korblova, D. Bedrov, D. M. Walba, M. A. Glaser, J. E. Maclennan, N. A. Clark, *Proc. Natl. Acad. Sci. U.S.A.*, 2013, **110**, 15931.

[18] I. Dozov, *Europhys. Lett.*, 2001, **56**, 247.

[19] C. Meyer, G. R. Luckhurst, I. Dozov, *Phys. Rev. Lett.*, 2013, **111**, 067801.

[20] V. P. Panov, M. Nagaraj, J. K. Vij, Y. P. Panarin, A. Kohlmeier, M. G. Tamba, R. A. Lewis, G. H. Mehl, *Phys. Rev. Lett.*, 2010, **105**, 167801.

[21] P. A. Henderson and C. T. Imrie, *Liq. Cryst.*, 2011, **38**, 1407.

[22] R. Mandle, E. J. Davis, C. T. Archbold, S. J. Cowling, J. W. Goodby, *J. Mater. Chem*. C, 2014, **2**, 556.

[23] Schröder, M. W. Diele, S. Pelzl, G. Dunemann, U. Kresse, H. Weissflog, W. Different Nematic Phases, a Switchable SmCP Phase Formed By Homologues of a New Class of Asymmetric Bent-Core Mesogens. *J. Mater. Chem*. 2003, **13**, 1877−1882.

[24] D. Chen, M. Nakata, R. Shao, M. R. Tuchband, M. Shuai, U. Baumeister, W. Weissflog, D. M. Walba, M. A. Glaser, J. E. Maclennan, N. A. Clark, *Phys. Rev. E: Stat. Phys., Plasmas, Fluids, Relat. Interdiscip. Top.* 2014, **89**, 022506.

[25] S. M. Jansze, A. Martinez-Felipe, J. M. D. Storey, A. T. M. Marcelis, C. T. Imrie, *Angew. Chem., Int. Ed.* 2015, **54**, 643.

[26] T. Ivsic, M. Vinkovic, U. Baumeister, A. Mikleusevic, A. Lesac, *Soft Matter,* 2014, **10**, 9334.

[27] M. Alaasar, M. Prehem, M. Nagaraj, J. K. Vij, C. Tschierske, *Adv. Mater*., 2013, **25**, 2186.

[28] C. Dressel, T. Reppe, M. Prehm, M. Brautzsch, C. Tschierske, *Nat. Chem*., 2014, **6**, 971.

[29] S. K. Lee, X. Li, S. Kang, J. Watanabe, *J. Mater. Chem*., 2009, **19**, 4517.

[30] E. T. Samulski, *Liq. Cryst*., 2010, **37**, 669.

[31] C. Tschierske and D. J. Photions, *J. Mater. Chem*., 2010, **20,** 4263.

[32] J. Martinez-Perdiguero, I. Alonso, C. L. Folcia, J. Etxebarria, J. Ortega, *J. Mater. Chem*., 2009, **19**, 5161.

CHAPTER 2

Achiral flexible liquid crystal trimers exhibiting chiral conglomerates

2.1. Introduction

The smectic layers in both the sponge and HNF phases of bent-core liquid crystals tend to have a saddle splay curvature[1,2]. The optical activity in the DC phases has been investigated extensively, revealing that it is attributable to the layer chirality[3] or to the coupling of molecular conformational chirality to the layer chirality[4]. Furthermore, DC phases of new types including modifications of the HNF phase have been observed[5–8]. Almost all molecules exhibiting the DC phases have a rigid bent-core structure, except in a few cases in which the HNF phase of an achiral dimer possessing an odd-numbered spacer was reported[9–12]. The ground-state conformation of rigid molecules influences the origin of the chirality. Such bent-core molecules tend to form layered structures, and they do not often exhibit a nematic phase. Chiral conglomerate formation is thought to be due to chirality synchronization of the transiently chiral bent-shaped molecules[13-16]. Fundamental interest persists in the unusual phenomena related to the DC phases. Materials exhibiting DC phases can support important applications such as organic semiconductors and organic photovoltaics[17]. Actually, the material design for DC phases is an attractive subject.

In chapter 1, We found an equimolecular mixture of achiral liquid crystal trimers exhibiting the DC phase, suggesting that dipole–dipole interactions between adjacent cores play an important role in the appearance of the DC phase[18].

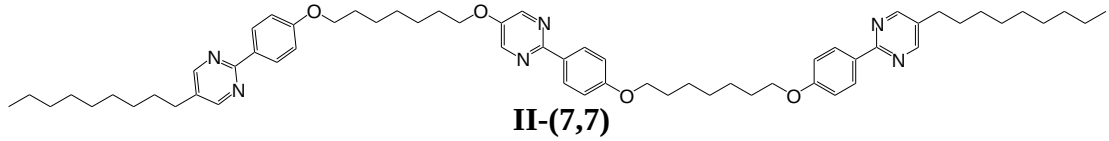

II-(7,7)

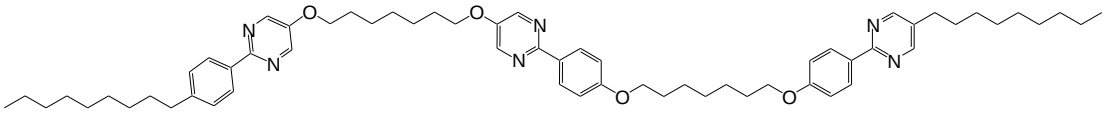

IV-(7,7)

Fig.2– 1 Molecular structure of **II-(7,7)** and **IV-(7,7)**.

Furthermore, the DC phase was induced in binary mixtures of achiral nematic liquid crystal trimers (trimer-(7,7), Fig.2-2) possessing a central biphenyl unit and

4'-hexyloxy-4-cyanobiphenyl (6OCB). The interaction between a phenylpyrimidine unit of trimer-(7,7) and a cyanobiphenyl unit of 6OCB can produce a twisted conformation of the central biphenyl of the trimer, which induces chiral segregation and layer deformation to drive the chiral conglomerate[19].

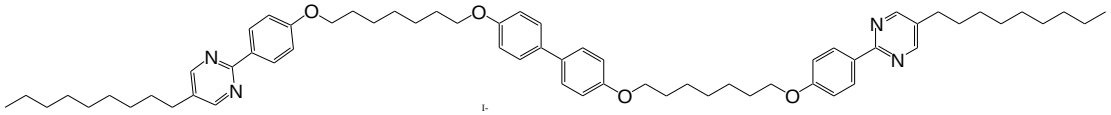

Symmetric trimer-(7,7)

Fig.2– 2 The molecular structure of trimer-(7,7).

In this chapter, I prepared a homologous series of achiral liquid crystal trimers in which two phenylpyrimidine units and one biphenyl unit were connected via flexible methylene spacers. Some achiral liquid crystal trimers possessing odd-numbered spacers were found to exhibit a DC phase. I discuss how the molecular structures affect the spontaneous mirror symmetry breaking.

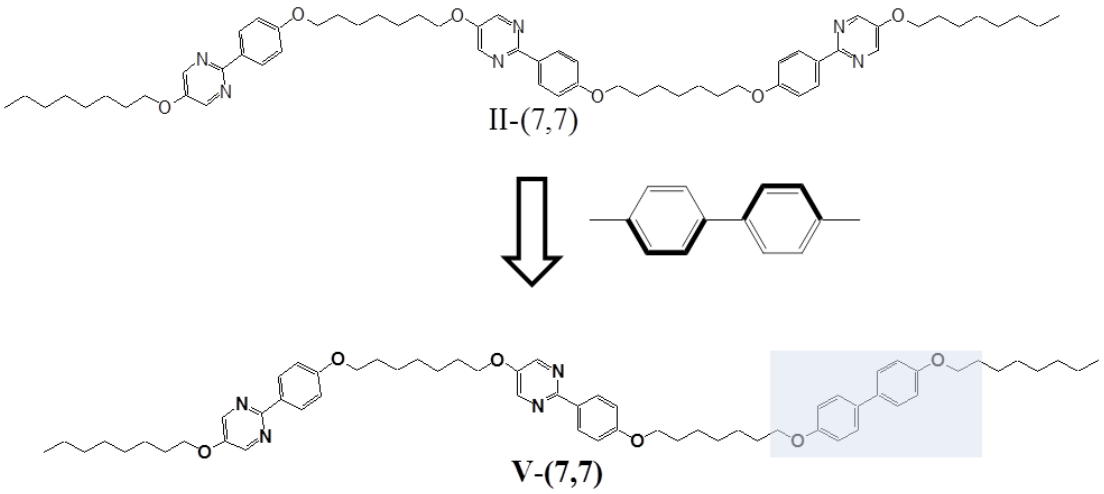

Fig.2– 3 Molecular design of trimer investigated.

2.2. Experimental

2.2.1. Preparation of materials

For use in this study, 5-hydroxy-2-(4-hydroxyphenyl)pyrimidine was purchased from Midori Kagaku Co. Ltd. The purity of each final compound was confirmed using elemental analysis (EA 1110; CE Instruments Ltd). Confirmation of the structures of intermediates and products was obtained by infrared (IR) spectroscopy (BIO RAD FTS-30) and proton nuclear magnetic resonance (^{1}H NMR) spectroscopy (JEOL JNM-ECA500).

In the reporting of IR data, the following abbreviations have been used.

str. stretching

In the reporting of ^{1}H NMR data, the following abbreviations have been used.

s. singlet
d. doublet
t. triplet
q. quartet
m. multiplet

The analyses of the structures of the products by means of spectroscopic methods were found to be consistent with the predicted structures.

2.2.1.1.

2-{4-[ω-(4-(4-Octyloxyphenyl)phenyloxy)alkyloxy]phenyl}-5-{ω-[4-(5-octyloxy-pyrimidin-2-yl)phenyloxy] alkyloxy}pyrimidine (V–(n,m)) and 2-{4-[7-(4-(4-octyloxyphenyl)phenyloxy)heptyloxy]phenyl}-5-{7-[2-(4-octyloxy-phenyl)pyrimidin-5-yloxy]heptyloxy}pyrimidine (VI–(7,7)).

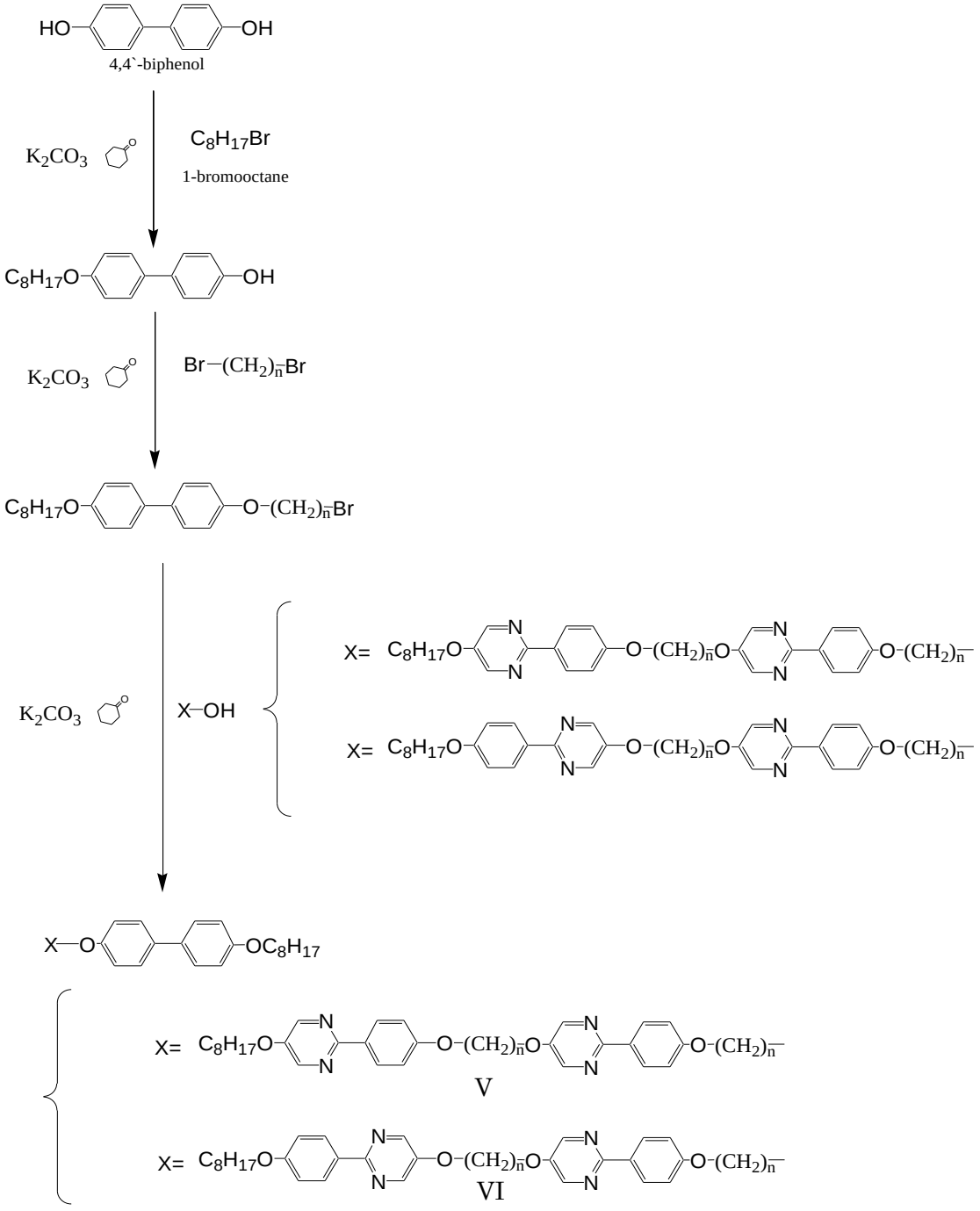

Scheme2– 1 Preparation of V–(n,m) and VI-(n,m)

2-{4-[5-(4-(4-Octyloxyphenyl)phenyloxy)pentyloxy]phenyl}-5-{5-[4-(5-octyloxypyrimidin-2-yl)phenyloxy]pentyloxy}pyrimidine (V–(5,5)).

Potassium carbonate (2.0 mmol, 276 mg) was added to a solution of 4,4'-biphenol (2.50 mmol, 466 mg) and 1-bromooctane (2.00 mmol, 386 mg) in cyclohexanone (10 ml). Thereaction mixture was stirred at 95 °C for 6 h. After filtration of the precipitate, the solvent was removed by evaporation. Then, the residue was purified using column chromatography on silica gel with a toluene : ethyl acetate (10 : 1) mixture as an eluent. The obtained white solid was washed with hexane to give 4-(4-octyloxyphenyl)phenol. Yield 243 mg (41%).

Potassium carbonate (2.0 mmol, 276 mg) was added to a solution of 4-(4-octyloxyphenyl)phenol (2.0 mmol, 597 mg) and 1,5-dibromopentane (2.5 mmol, 575 mg) in cyclohexanone (10 ml). The reaction mixture was stirred at 95 °C for 9 h. After filtration of the precipitate, the solvent was removed by evaporation. Then, the residue was purified using column chromatography on silica gel with a hexane : ethyl acetate (5 : 1) mixture as an eluent. The obtained white solid was recrystallized from ethanol to give 1-(4-octyloxyphenyl)-4-(5-bromopentyloxy)-benzene. Yield 476 mg (53.2%).

Potassium carbonate (0.3 mmol, 42 mg) was added to a solution of 1-(4-octyloxyphenyl)-4-(5-bromopentyloxy)benzene (0.3 mmol, 134 mg) and 2-(4-hydroxyphenyl)-5-{5-[4-(5-octyloxypyrimidin-2-yl)phenyloxy]pentyloxy}pyrimidine (0.3 mmol, 167 mg) in cyclohexanone (10 ml). The reaction mixture was stirred at 130 °C for 9 h. After filtration of the precipitate, the solvent was removed by evaporation. Then, the residue was washed with hot ethanol and was recrystallized from toluene to give the desired compound. Yield 198 mg (71%).

^{1}HNMR (500 MHz, $CDCl_3$, TMS): δ=8.40 (s, 2H, Ar-**H**), 8.41 (s, 2H, Ar-**H**), 8.26 (d, 4H, Ar-**H**, *J* = 8.0 Hz), 7.45 (d, 2H, Ar-**H**, *J* = 9.2 Hz), 7.45 (d, 2H, Ar-**H**, *J* = 8.6 Hz), 6.97 (d, 4H, Ar-**H**, *J* = 9.2 Hz), 6.94 (d, 2H, Ar-**H**, *J* = 9.2 Hz), 6.92 (d, 2H, Ar-**H**, *J* = 9.2 Hz), 4.12 (t, 2H, -OC**H**$_2$-, *J* = 6.3 Hz), 4.07 (t, 4H, -OC**H**$_2$-, *J* = 6.3 Hz), 4.06 (t, 2H, -OC**H**$_2$-, *J* = 6.3 Hz), 4.03 (t, 2H, -OC**H**$_2$-, *J* = 6.9 Hz), 3.98 (t, 2H, -OC**H**$_2$-, *J* = 6.9 Hz), 1.96–1.68 (m, 16H, aliphatic-**H**), 1.49–1.29 (m, 20H, aliphatic-**H**), 0.89 (t, 6H, -C**H**$_3$, *J* = 6.9 Hz).

IR (KBr): ν cm^{-1}: 2925, 2868 (C-H str), 1607, 1581, 1542, 1499, 1434 (C=C, C=N str), 1256 (C-O str).

Elemental Analysis Calcd. for C,75.45; H, 8.08; N, 6.07. Found C, 75.45; H, 7.68; N, 6.06.

2-{4-[6-(4-(4-Octyloxyphenyl)phenyloxy)hexyloxy]phenyl}-5-{6-[4-(5-octyloxypyrimidin-2-yl)phenyloxy] hexyloxy }pyrimidine (V–(6, 6)).

Potassium carbonate (3.0 mmol, 417 mg) was added to a solution of 4-(4-octyloxyphenyl)phenol (3.0 mmol, 895 g) and 1,6-dibromohexane (4.5 mmol, 1.10 g) in cyclohexanone (10 ml). The reaction mixture was stirred at 95 °C for 12 h. After filtration of the precipitate, the solvent was removed by evaporation. Then, the residue was purified using column chromatography on silica gel with a hexane : ethyl acetate (5 : 1) mixture as an eluent. The obtained white solid was recrystallized from ethanol to give 1-(4-octyloxyphenyl)-4-(6-bromohexyloxy)-benzene. Yield 878 mg (63%).

Potassium carbonate (0.35 mmol, 48 mg) was added to a solution of 1-(4-octyloxyphenyl)-4-(6-bromohexyloxy)benzene (0.35 mmol, 162 mg) and 2-(4-hydroxyphenyl)-5-{6-[4-(5-octyloxypyrimidin-2-yl)phenyloxy]hexyloxy}pyrimidine (0.35 mmol, 200 mg) in cyclohexanone (10 ml). The reaction mixture was stirred at 130 °C for 12 h. After filtration of the precipitate, the solvent was removed by evaporation. Then, the residue was washed with hot ethanol and was recrystallized from toluene to give the desired compound. Yield 197 mg (69%).

^{1}HNMR (500 MHz, $CDCl_3$, TMS): δ=8.40 (s, 4H, Ar-**H**), 8.27 (d, 4H, Ar-**H**, *J* = 8.6 Hz), 7.44 (d, 4H, Ar-**H**, *J* = 8.6 Hz), 6.96 (d, 4H, Ar-**H**, *J* = 9.2 Hz), 6.93 (d, 2H, Ar-**H**, *J* = 9.2 Hz), 4.10 (t, 2H, -OC**H**$_2$-, *J* = 6.3 Hz), 4.08 (t, 2H, -OC**H**$_2$-, *J* = 6.3 Hz), 4.05 (t, 4H, -OC**H**$_2$-, *J* = 6.3 Hz), 4.01 (t, 2H, -OC**H**$_2$-, *J* = 6.9 Hz), 3.98 (t, 2H, -OC**H**$_2$-, *J* = 6.9 Hz), 1.86–1.78 (m, 12H, aliphatic-**H**), 1.59–1.30 (m, 28H, aliphatic-**H**), 0.89 (t, 6H, - C**H**$_3$, *J* = 6.9 Hz).

IR (KBr): ν cm^{-1}: 2941, 2867 (C-H str), 1608, 1482, 1499, 1435 (C=C, C=N str), 1249 (C-O str).

Elemental Analysis Calcd. for C,75.75; H, 8.26; N, 5.89. Found C, 76.05; H, 7.93; N, 5.93.

2-{4-[7-(4-(4-Octyloxyphenyl)phenyloxy)heptyloxy]phenyl}-5-{7-[4-(5-octyloxypyrimidin-2-yl)phenyloxy]heptyloxy}pyrimidine (V-(7,7))

Potassium carbonate (0.74 mmol, 102 mg) was added to a solution of 4-(4-octyloxyphenyl)phenol (0.74 mmol, 220 mg) and 1,7-dibromohexane (0.93 mmol, 239

mg) in cyclohexanone (10 ml). The reaction mixture was stirred at 95 °C for 10 h. After filtration of the precipitate, the solvent was removed by evaporation. Then, the residue was purified using column chromatography on silica gel with a hexane : ethyl acetate (5 : 1) mixture as an eluent. The obtained white solid was recrystallized
from ethanol to give 1-(4-octyloxyphenyl)-4-(7-bromoheptyloxy)-benzene. Yield 181 mg (51%).

Potassium carbonate (0.15 mmol, 21 mg) was added to a solution of 1-(4-octyloxyphenyl)-4-(7-bromoheptyloxy)benzene (0.15 mmol, 71 mg) and 2-(4-hydroxyphenyl)-5-{7-[4-(5-octyloxypyrimidin-2-yl)phenyloxy]heptyloxy}pyrimidine (0.15 mmol, 90mg) in cyclohexanone (10 ml). The reaction mixture was stirred at 130 °C for 10 h. After filtration of the precipitate, the solvent was removed by evaporation. Then, the residue was washed with hot ethanol and was recrystallized from toluene to give the desired compound. Yield 112 mg (76%).

^{1}H NMR (500 MHz, $CDCl_3$, TMS): δ = 8.40 (s, 4H, Ar–**H**), 8.26 (d, 4H, Ar–**H**, *J* = 9.2 Hz), 7.44 (d, 4H, Ar–**H**, *J* = 6.9 Hz), 6.96 (d, 4H, Ar–**H**, *J* = 8.6 Hz), 6.93 (d, 4H, Ar–**H**, *J* = 8.6 Hz), 4.08 (t, 2H, –OC**H**$_2$–), 4.07 (t, 2H, –OC**H**$_2$–), 4.03 (t, 2H, –OC**H**$_2$–), 4.02 (t, 2H, –OC**H**$_2$–), 3.99 (t, 2H, –OC**H**$_2$–), 3.98 (t, 2H, –OC**H**$_2$–), 1.86–1.76 (m, 12H, aliphatic-**H**), 1.53–1.29 (m, 32H, aliphatic-**H**), 0.89 (t, 6H, –C**H**$_3$, *J* = 6.9 Hz).

IR(KBr): ν cm^{-1}: 2938, 2854 (C–H str), 1607, 1581, 1542, 1499, 1434 (C=C, C=N str), 1251 (C–O str).

Elemental analysis calc. for $C_{62}H_{82}N_4O_6$: C,76.04; H, 8.44; N, 5.72. Found C, 76.41; H, 8.00; N, 5.64.

2-{4-[9-(4-(4-Octyloxyphenyl)phenyloxy)nonyloxy]phenyl}-5-{9-[4-(5-octyloxypyrimidin-2-yl)phenyloxy]nonyloxy}pyrimidine (V–(9,9)).

Potassium carbonate (1.5 mmol, 207 mg) was added to a solution of 4-(4-octyloxyphenyl)phenol (1.5 mmol, 448 mg) and 1,9-dibromononane (2.3 mmol, 644 mg) in cyclohexanone (10 ml). The reaction mixture was stirred at 95 °C for 9 h. After filtration of the precipitate, the solvent was removed by evaporation. Then, the residue was purified using column chromatography on silica gel with a hexane : ethyl acetate (4 : 1) mixture as an eluent. The obtained white solid was recrystallized from ethanol to give

1-(4-octyloxyphenyl)-4-(9-bromononyloxy)-benzene. Yield 381 mg (51%).

Potassium carbonate (0.19 mmol, 26 mg) was added to a solution of 1-(4-octyloxyphenyl)-4-(9-bromononyloxy)benzene (0.19 mmol, 96 mg) and 2-(4-hydroxyphenyl)-5-{9-[4-(5-octyloxypyrimidin-2-yl)phenyloxy]nonyloxy}pyrimidine (0.19 mmol, 118 mg) in cyclohexanone (10 ml). The reaction mixture was stirred at 130 °C for 3 h. After filtration of the precipitate, the solvent was removed by evaporation. Then, the residue was washed with hot ethanol and was recrystallized from toluene to give the desired compound. Yield 130 mg (66%).

^{1}HNMR (500 MHz, $CDCl_3$, TMS): δ=8.40 (s, 4H, Ar-**H**), 8.26 (d, 4H, Ar-**H**, *J* = 8.6 Hz), 6.96 (d, 4H, Ar-**H**, *J* = 8.3 Hz), 6.93 (d, 4H, Ar-**H**, *J* = 8.0 Hz), 4.07 (t, 4H, - OC**H$_2$**-, *J* = 6.3 Hz), 4.02 (t, 2H, -OC**H$_2$**-, *J* = 6.3 Hz), 4.05 (t, 2H, -OC**H$_2$**-, *J* = 6.3 Hz), 3.99 (t, 2H, -OC**H$_2$**-, *J* = 6.9 Hz), 3.97 (t, 2H, -OC**H$_2$**-, *J* = 6.9 Hz), 1.85–1.69 (m, 12H, aliphatic-**H**), 1.47–1.29 (m, 40H, aliphatic-**H**), 0.89 (t, 6H, -C**H$_3$**, *J* = 6.9 Hz).

IR (KBr): ν cm^{-1}: 2933, 2851 (C-H str), 1608, 1582, 1544, 1499, 1435 (C=C, C=N str), 1246 (C-O str).

Elemental Analysis Calcd. for C,76.56; H, 8.76; N, 5.43. Found C, 76.76; H, 8.40; N, 5.43.

2-{4-[5-(4-(4-Octyloxyphenyl)phenyloxy)pentyloxy]phenyl}-5-{7-[4-(5-octyloxypyrimidin-2-yl)phenyloxy]heptyloxy}pyrimidine (V–(7,5)).

Potassium carbonate (0.3 mmol, 42 mg) was added to a solution of 1-(4-octyloxyphenyl)-4-(5-bromopentyloxy)benzene (0.3 mmol, 134 mg) and 2-(4-hydroxyphenyl)-5-{7-[4-(5-octyloxypyrimidin-2-yl)phenyloxy]heptyloxy}pyrimidine (0.3 mmol, 175 mg) in cyclohexanone (10 ml). The reaction mixture was stirred at 130 °C for 6 h. After filtration of the precipitate, the solvent was removed by evaporation. Then, the residue was washed with hot ethanol and was recrystallized from toluene to give the desired compound. Yield 225 mg (79%).

^{1}HNMR (500 MHz, $CDCl_3$, TMS): δ=8.40 (s, 4H, Ar-**H**), 8.26 (d, 4H, Ar-**H**, *J* = 9.2 Hz), 7.45 (d, 4H, Ar-**H**, *J* = 8.6 Hz), 6.96 (d, 4H, Ar-**H**, *J* = 8.6 Hz), 6.93 (d, 4H, Ar-**H**, *J* = 9.2 Hz), 4.08 (t, 2H, -OC**H$_2$**-, *J* = 6.3 Hz), 4.07 (t, 2H, -OC**H$_2$**-, *J* = 6.3 Hz), 4.05 (t, 2H, -OC**H$_2$**-, *J* = 6.3 Hz), 4.03 (t, 2H, -OC**H$_2$**-, *J* = 6.9 Hz), 4.02 (t, 2H, -OC**H$_2$**-, *J* = 6.3 Hz), 3.98 (t, 2H, -OC**H$_2$**-, *J* = 6.9 Hz), 1.92–1.76 (m, 12H, aliphatic-**H**), 1.72–1.29 (m, 28H, aliphatic-**H**), 0.89 (t, 6H,

-C**H**$_3$, *J* = 6.9 Hz).

IR (KBr): ν cm^{-1}: 2936, 2867 (C-H str), 1608, 1544, 1499, 1434 (C=C, C=N str), 1252 (C-O str).

Elemental Analysis Calcd. for C,75.75; H, 8.26; N, 5.89. Found C, 76.85; H, 7.75; N, 5.96.

2-{4-[9-(4-(4-Octyloxyphenyl)phenyloxy)nonyloxy]phenyl}-5-{7-[4-(5-octyloxypyrimidin-2-yl)phenyloxy]heptyloxy}pyrimidine (V–(7,9)).

Potassium carbonate (0.3 mmol, 42 mg) was added to a solution of 1-(4-octyloxyphenyl)-4-(9-bromononyloxy)benzene (0.3 mmol, 134 mg) and 2-(4-hydroxyphenyl)-5-{7-[4-(5-octyloxypyrimidin-2-yl)phenyloxy]heptyloxy}pyrimidine (0.3 mmol, 175 mg) in cyclohexanone (10 ml). The reaction mixture was stirred at 130 °C for 6 h. After filtration of the precipitate, the solvent was removed by evaporation. Then, the residue was washed with hot ethanol and was recrystallized from toluene to give the desired compound. Yield 239 mg (79%).

^{1}HNMR (500 MHz, $CDCl_3$, TMS): δ=8.40 (s, 4H, Ar-**H**), 8.26 (d, 4H, Ar-**H**, *J* = 9.2 Hz), 7.44 (d, 4H, Ar-**H**, *J* = 6.9 Hz), 6.96 (d, 4H, Ar-**H**, *J* = 9.2 Hz), 6.93 (d, 4H, Ar-**H**, *J* = 8.6 Hz), 4.08 (t, 2H, -OC**H**$_2$-, *J* = 6.3 Hz), 4.07 (t, 2H, -OC**H**$_2$-, *J* = 6.3 Hz), 4.03 (t, 2H, -OC**H**$_2$-, *J* = 6.3 Hz), 4.01 (t, 2H, -OC**H**$_2$-, *J* = 6.9 Hz), 3.98 (t, 4H, -OC**H**$_2$-, *J* = 6.9 Hz), 1.86–1.76 (m, 12H, aliphatic-**H**), 1.53–1.29 (m, 36H, aliphatic-**H**), 0.89 (t, 6H, -C**H**$_3$, *J* = 6.9 Hz).

IR (KBr): ν cm^{-1}: 2933, 2853 (C-H str), 1608, 1583, 1544, 1499, 1435 (C=C, C=N str), 1246 (C-O str).

Elemental Anal Calcd. for C,76.30; H, 8.60; N, 5.56. Found C, 76.55; H, 7.96; N, 5.60.

2-{4-[7-(4-(4-octyloxyphenyl)phenyloxy)heptyloxy]phenyl}-5-{7-[2-(4-octyloxyphenyl)pyrimidin-5-yloxy]heptyloxy}pyrimidine (VI–(7,7)).

Potassium carbonate (0.3 mmol, 42 mg) was added to a solution of 1-(4-octyloxyphenyl)-4-(7-bromoheptyloxy)benzene (0.3 mmol, 143 mg) and 2-(4-Hydroxyphenyl)-5-{7-[2-(4-octyloxyphenyl)pyrimidin-5-oxy]hepyloxy}pyrimidine (0.3 mmol, 175 mg) in cyclohexanone (10 ml). The reaction mixture was stirred at 130 °C for 6 h. After filtration of the precipitate, the solvent was removed by evaporation. Then, the residue

was washed with hot ethanol and was recrystallized from toluene to give the desired compound. Yield 217 mg (74%).

^{1}HNMR (500 MHz, $CDCl_3$, TMS): δ=8.41 (s, 4H, Ar-**H**), 8.25 (d, 4H, Ar-**H**, *J* = 8.0 Hz), 7.45 (d, 4H, Ar-**H**, *J* = 8.6 Hz), 6.96 (d, 4H, Ar-**H**, *J* = 8.0 Hz), 6.93 (d, 4H, Ar-**H**, *J* = 8.6 Hz), 4.09 (t, 4H, -OC**H$_2$**-, *J* = 6.3 Hz), 4.02 (t, 2H, -OC**H$_2$**-, *J* = 6.3 Hz), 4.01 (t, 2H, -OC**H$_2$**-, *J* = 6.9 Hz), 3.99 (t, 2H, -OC**H$_2$**-, *J* = 6.3 Hz), 3.98 (t, 2H, -OC**H$_2$**-, *J* = 6.9 Hz), 1.87–1.77 (m, 12H, aliphatic-**H**), 1.56–1.29 (m, 32H, aliphatic-**H**), 0.89 (t, 6H, -C**H$_3$**, *J* = 6.9 Hz).

IR (KBr): ν cm^{-1}: 2938, 2854 (C-H str), 1607, 1581, 1542, 1499, 1434 (C=C, C=N str), 1251 (C-O str).

Elemental analysis Calcd for C,76.04; H, 8.44; N, 5.72. Found C, 77.0; H, 8.06; N, 5.71.

2.2.1.2.

2-{4-[7-(4-(5-Octyloxypyrimidin-2-yl)phenyloxy)heptyloxy]phenyl}-5-{7-[4-(4-octyloxyphenyl)phenyloxy]heptyloxy}pyrimidine (VII–(7,7)) and 2-{4-[7-(2-(4-Octyloxyphenyl)pyrimidin-5-yloxy)phenyloxy)heptyloxy]phenyl}-5-{7-[4-(4-octyloxyphenyl)phenyloxy]heptyloxy}pyrimidine (VIII–(7,7)).

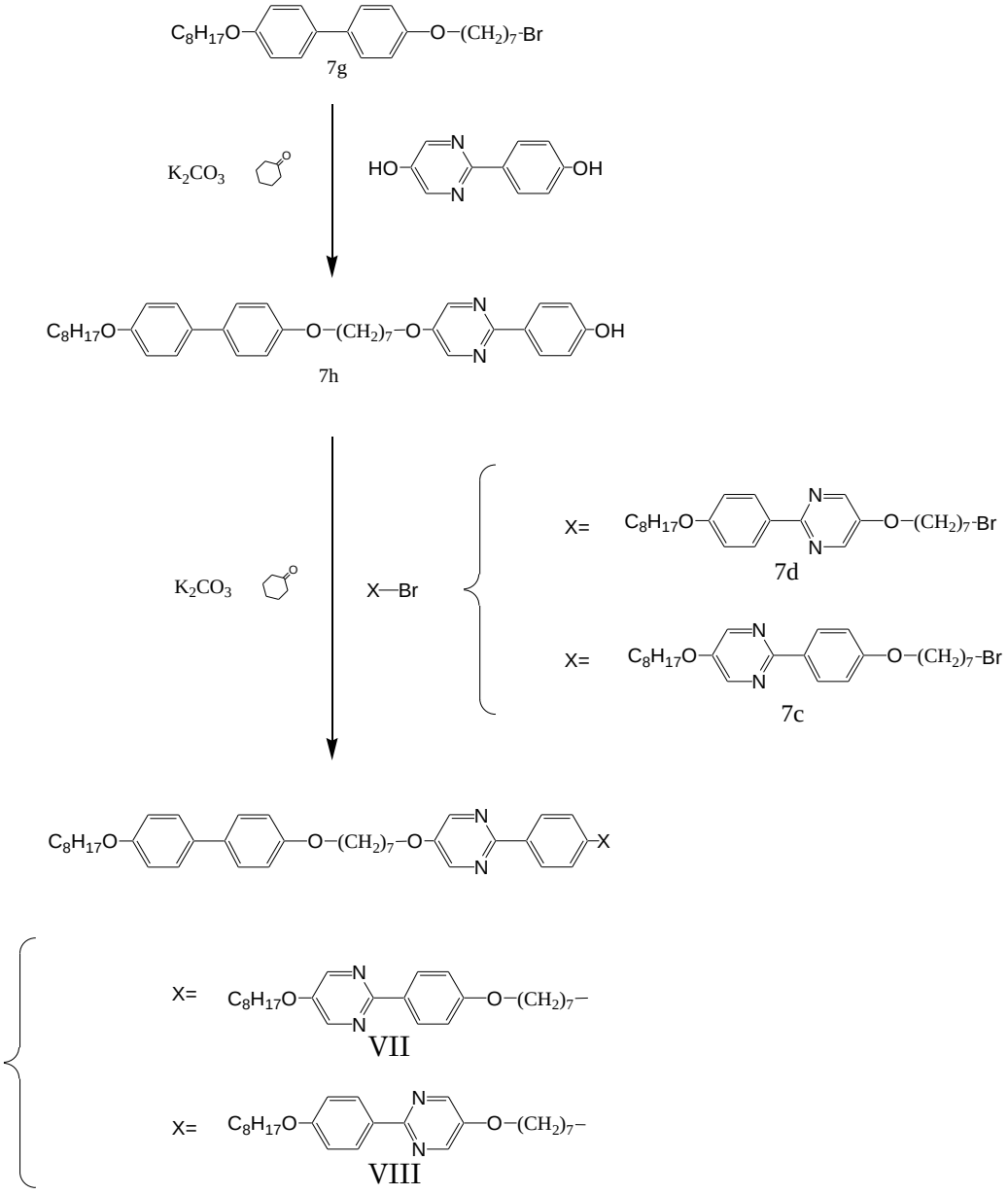

Scheme2– 2 Preparation of VII–(7,7) and VIII-(7,7)

2-{4-[7-(4-(5-Octyloxypyrimidin-2-yl)phenyloxy)heptyloxy]phenyl}-5-{7-[4-(4-octyloxyphenyl)phenyloxy]heptyloxy}pyrimidine (VII–(7,7)).

Potassium carbonate (1.5 mmol, 207 mg) was added to a solution of 1-(4-octyloxyphenyl)-4-(7-bromo-heptyloxy)benzene (1.5 mmol, 713 mg) and 2-(4'-hydroxyphenyl)-5-octyloxy-pyrimidine (2.0 mmol, 376 mg) in cyclohexanone (10 ml). The reaction mixture was stirred at 90 °C for 7 h. After filtration of the precipitate, the solvent was removed by evaporation. Then the residue was purified using column chromatography on silica gel with a toluene : ethyl acetate (5:1) mixture as the eluent. The obtained white solid was recrystallized from ethanol to give 2-(4-hydroxyphenyl)-5-{7-[4-(4-octyloxyphen-1-yl)phenoxy]heptyloxy}pyrimidine. Yield 491 mg (56.2 %)

Potassium carbonate (0.3 mmol, 42 mg) was added to a solution of 2-(4-hydroxyphenyl)-5-{7-[4-(4-octyloxyphen-1-yl)phenoxy]heptyloxy}pyrimidine (0.3 mmol, 175 mg) and 5-octyloxy-2-(4-(7-bromo-heptyloxy)-phenyl)pyrimidine (0.3 mmol, 143 mg) in cyclohexanone (10 ml). The reaction mixture was stirred at 135 °C for 8 h. After filtration of the precipitate, the solvent was removed by evaporation. Then the residue was washed with hot ethanol and recrystallized fom toluene to give the desired compound. Yield 175 mg (60 %)

^{1}HNMR (500 MHz, CDCl3, TMS): δ=8.40 (s, 4H, Ar-**H**), 8.26 (d, 4H, Ar-**H**, *J* = 8.6 Hz), 7.45 (d, 4H, Ar-**H**, *J* = 8.6 Hz), 7.44 (d, 4H, Ar-**H**, *J* = 9.2 Hz), 6.96 (d, 4H, Ar-**H**, *J* = 8.6 Hz), 6.93 (d, 4H, Ar-**H**, *J* = 8.6 Hz), 4.08 (t, 2H, -OC**H$_2$**-, *J* = 6.3 Hz), 4.07 (t, 2H, -OC**H$_2$**-, *J* = 6.3 Hz), 4.02 (t, 4H, -OC**H$_2$**-, *J* = 6.3 Hz), 3.99 (t, 2H, -OC**H$_2$**-, *J* = 6.3 Hz), 3.97 (t, 2H, -OC**H2**-, *J* = 6.3 Hz), 1.84–1.76 (m, 12H, aliphatic-**H**), 1.58–1.29 (m, 32H, aliphatic-**H**), 0.89 (t, 6H, -C**H$_3$**, *J* = 6.9 Hz). IR (KBr): ν cm^{-1}: 2933, 2854 (C-H str), 1607, 1582, 1544, 1499, 1434 (C=C, C=N str), 1247 (C-O str). Elemental Analysis Calcd. for C,76.04; H, 8.44; N, 5.72. Found C, 76.47; H, 8.19; N, 5.68.

2-{4-[7-(2-(4-Octyloxyphenyl)pyrimidin-5-yloxy)phenyloxy)heptyloxy]phenyl}-5-{7-[4-(4-octyloxyphenyl)phenyloxy]heptyloxy}pyrimidine (VIII–(7,7)).

Potassium carbonate (0.3 mmol, 42 mg) was added to a solution of 2-(4-hydroxyphenyl)-5-{7-[4-(4-octyloxyphen-1-yl)phenoxy]heptyloxy}pyrimidine (0.3 mmol, 175 mg) and 2-(4-Octyloxyphenyl)-5-(7-bromo-heptyloxy)pyrimidine (0.3 mmol, 143 mg) in cyclohexanone (10 ml). The reaction mixture was stirred at 135 °C for 8 h. After filtration of the precipitate, the solvent was removed by evaporation. Then the residue was washed with hot ethanol and recrystallized fom toluene to give the desired compound. Yield 249 mg (84.9 ％)

^{1}HNMR (500 MHz, CDCl3, TMS): δ=8.40 (s, 4H, Ar-**H**), 8.26 (d, 4H, Ar-**H**, *J* = 8.6 Hz), 7.45 (d, 2H, Ar-**H**, *J* = 8.6 Hz), 7.44 (d, 2H, Ar-**H**, *J* = 8.6 Hz), 6.96 (d, 2H, Ar-**H**, *J* = 8.6 Hz), 6.96 (d, 2H, Ar-**H**, *J* = 8.6 Hz), 6.93 (d, 4H, Ar-**H**, *J* = 8.6 Hz), 4.08 (t, 4H, -OC**H$_2$**-, *J* = 6.3 Hz), 4.03 (t, 2H, -OC**H$_2$**-, *J* = 6.3 Hz), 4.00 (t, 2H, -OC**H$_2$**-, *J* = 6.3 Hz), 3.99 (t, 2H, -OC**H$_2$**-, *J* = 6.3 Hz), 3.98 (t, 2H, -OC**H$_2$**-, *J* = 6.9 Hz), 1.88–1.76 (m, 12H, aliphatic-**H**), 1.56–1.29 (m, 32H, aliphatic-**H**), 0.89 (t, 6H, -C**H$_3$**, *J* = 6.9 Hz).

IR (KBr): ν cm-1: 2935, 2865 (C-H str), 1607, 1544, 1499, 1435 (C=C, C=N str), 1248 (C-O str).

Elemental analysis Calcd for C,76.04; H, 8.44; N, 5.72. Found C, 77.16; H, 7.92; N, 5.70.

2.2.2. Liquid-crystalline and physical properties

The initial phase assignments and the corresponding transition temperatures for each final compound were determined using a polarizing optical microscope (POM, BX-51; Olympus Optical Co. Ltd) equipped with a temperature control unit (LK-600PM; Japan High Tech Co. Ltd). The temperatures and enthalpies of transition were investigated using differential scanning calorimetry (DSC, DSC 6200; Seiko Instruments Inc.). The X-ray diffraction patterns of the homeotropically aligned samples during cooling were obtained using a real-time X-ray diffractometer (MicroMax-007HF; Rigaku Corp.) equipped with a hot stage and a temperature-control processor. The samples were put on a convex lens, which was then placed in a custommade temperature-stabilized holder (stability within -0.1 °C). The phase transition of the samples under the X-ray beam was monitored by observing the texture simultaneously using a polarized light microscope with a CCD camera. The X-ray apparatus was equipped with a platform arrangement and a two-dimensional detector (Image intensifier and CCD C9299-01; Hamamatsu Photonics KK) for small-angle X-ray scattering (SAXS), and an imaging plate (BAS-SR 127; Fujifilm) for wideangle X-ray scattering (WAXS). Then X-rays were generated at 40 kV and 20 mA. The samples were irradiated with a Cu-Ka X-ray beam, using confocal mirrors to correlate the incident X-ray beam and to increase its intensity. The camera distances from the samples to the detectors were ca. 730 mm for SAXS and 40 mm for WAXS. The correlation length along the layer normal (x) was determined using the Ornstein–Zernike expression as follows. First, the X-ray profile as a function of $2\theta$was converted to a scattering function of q according to the following equation:

$$q = (4\pi/\lambda)\sin\theta \qquad (1)$$

By fitting the X-ray profiles using the following Lorentzian equation, the correlation length$\xi$was determined.

$$I(q) = \frac{I_0}{1+(q-q_0)^2\xi^2} + \text{background} \qquad (2)$$

where I_0 and q_0, respectively, signify the peak height and the peak position of q. Electro-optical properties were measured using standard electro-optical techniques. The ITO-coated glass sandwich cells purchased from EHC Corp. were constructed using 2 μm spacers. The ITO electrodes were covered with a polymer alignment layer, rubbed unidirectionally.

2.3. Results and Discussion

2.3.1 Physical properties of V-(7,7)

I investigated its phase transition behaviour using polarized optical microscopy (POM) and differential scanning calorimetry (DSC). Fig.2-4 shows the A Molecular structure of **V-(7,7)**.

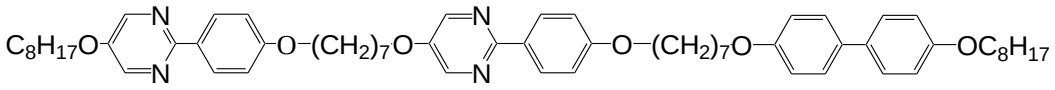

Fig.2– 4 A Molecular structure of **V-(7,7)**

The phase transition temperatures and Δ*S/R* of trimer **V-(7,7)** were as follows: Iso 155.8 °C (1.2) N 146.4 °C (10.4) DC. The DC phase did not change until 0 °C. On heating a virgin sample, the crystal (Cry1)–crystal (Cry2) transition was observed at 144.0 °C (5.5). Then, the Cry2 phase changed to the N phase at 135.2 °C and then to the Iso phase at 156.9 °C (8.8). In the Cry1 and Cry2 phases, no chiral nature was detected. The DSC thermogram is portrayed in Fig.2-5.

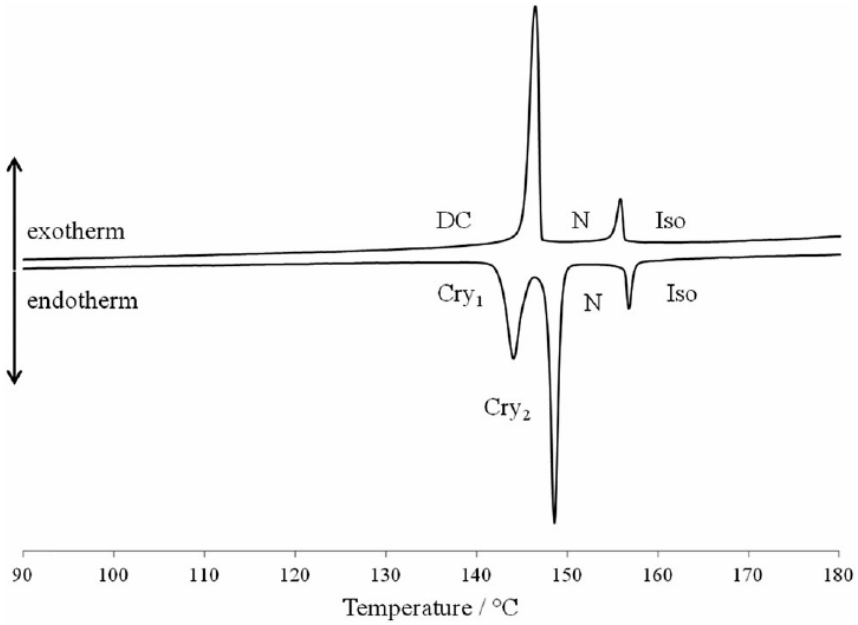

Fig.2– 5 DSC thermogram of trimer **V-(7,7)**. The rate of cooling and heating was 5 °Cmin^{-1}.

Fig.2-6 shows the optical textures of trimer **V-(7,7)**. the N phase with the schilieren textures was observed at 150 °C (Fig.2-6(a)), furthermore cooling, N-DC phase transition was observed at 147 °C, as shown in Fig.2-6(b). Fig.2-6(c) depicts optical textures in the DC phase at 130 °C under crossed and uncrossed polarizers. The texture of the DC phase under crossed polarizers was nearly dark, suggesting that it was optically isotropic. By observing the sample in the DC phase under slightly uncrossed polarizers (10°), the texture was split into darker and brighter domains. By uncrossing the polarizers in opposite directions by the same angle, the darker and brighter domains were exchanged. The domain brightness did not change by rotation of the sample between the polarizers. These results indicate that they have optical activity with opposite senses. With respect to the N phase above the DC phase, no chiral nature was detected. Chiral aggregation occurs at the N to DC phase transition.

I investigated the electro-optical response in the DC phase by application of an AC field to the sample in a homogeneously aligned cell with a gap of 2 μm using a triangle wave with an AC field of ±30 V μm^{-1} at a frequency of 10 Hz. Electro-optical switching was not observed in the DC phase.

(a)

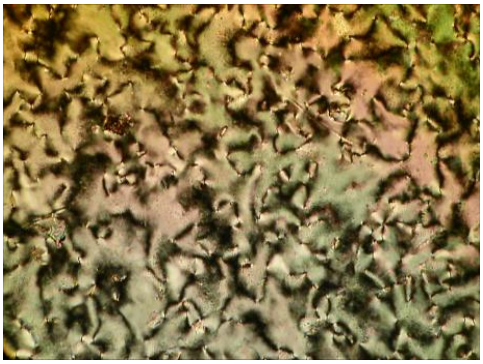

N phase (150 °C)

(b)

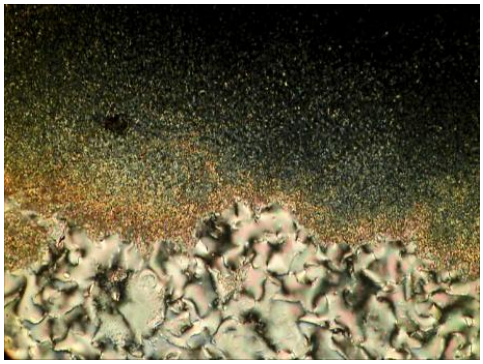

N-DC phase transition (147 °C)

(c)

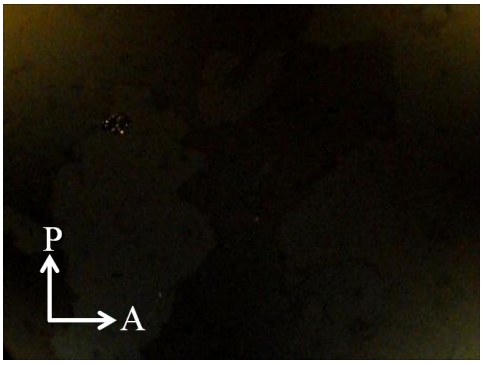

DC phase (130 °C) under crossed polarizers.

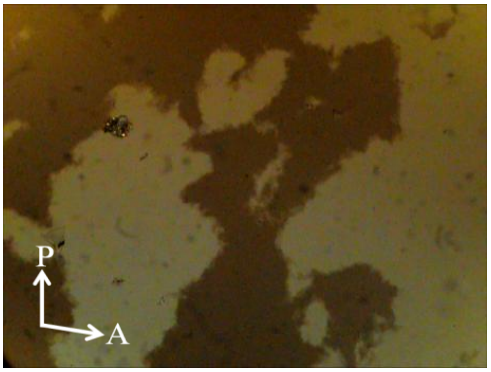

DC phase (130 °C) under uncrossed polarizers (10 °)

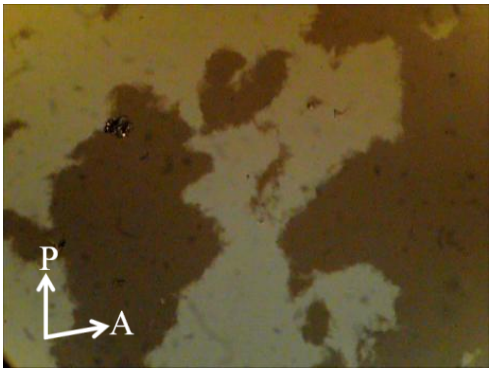

DC phase (130 ℃) under uncrossed polarizers (-10 °)

Fig.2– 6 Polarized optical textures of trimer **V-(7,7)** on a glass slide with a cover glass.

To elucidate the phase structure, X-ray measurements were conducted. Alignment was performed by the slow cooling of a small drop of the sample on a convex lens. The N to DC phase transition was confirmed by the texture change. Fig.2-7(a) portrays an X-ray diffraction pattern in the small-angle region of trimer **V-(7,7)** in the DC phase at $T-T_{NDC}$ = −13.0 K (T_{NDC}: N–DC transition temperature). In the DC phase, weak and broad scattering appeared in a circle. Fig.2-7(b) depicts the X-ray diffraction profiles in the small-angle region of trimer **V-(7,7)** in the N and DC phases. A diffuse scattering at around 2θ = 1.41° can be seen in the N phase at $T-T_{NDC}$ = 10.0 K, suggesting that a short-range order with a periodicity length of about 62 A exists in the N phase. Therefore, the N phase is not a cybotactic N phase,35,36 which is often seen in a bent-core liquid crystal, but a conventional N phase. A peak at 2θ= 1.56° was observed in the DC phase, revealing that the DC phase has a layer structure with a periodicity length of 56.5 A. The correlation length for the periodicity in the small-angle region in the DC phase is 350 A at $T-T_{NDC}$ = −13.0 K, which corresponds to about six layers. Fig.2-8(a) showsan X-ray diffraction pattern in the wide-angle region of trimer **V-(7,7)** in the DC phase. Fig.2-8(b) shows profiles in the wide-angle region of trimer **V-(7,7)** in the N and DC phases. Four peaks 2θ= 14.8°, 19.4°, 23.5°, and 27.5° were observed in the DC phase, as portrayed in Fig.2-8(b), indicating that it has positional order within the layer. No other peak was detected in the middle-angle and wide-angle regions. These results reveal that the DC phase is a crystalline structure.

(a) (b)

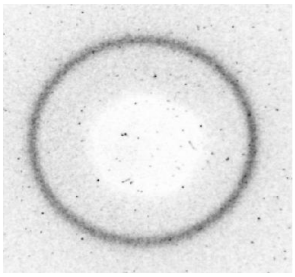

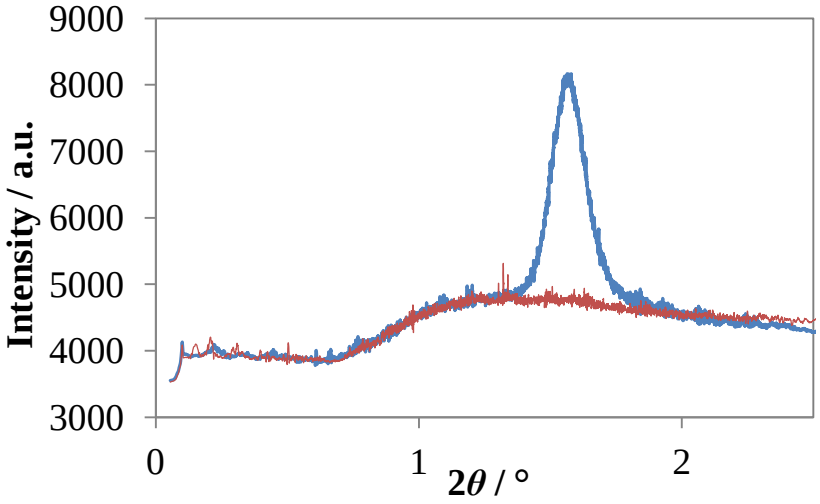

Fig.2– 7 (a) X-ray diffraction pattern of trimer V-(7,7) in the DC phase at $T-T_{NDC}$ = −13.0 K in the small-angle region. (b) X-ray diffraction profiles of trimer V-(7,7) in the N phase at $T-T_{NDC}$ = 10.0 K (red line) and the DC phase at $T-T_{NDC}$ = −13.0 K (blue line) in the small-angle region.

(a) (b)

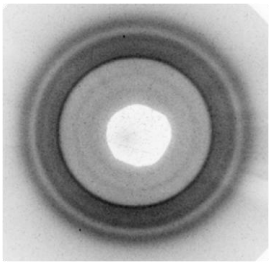

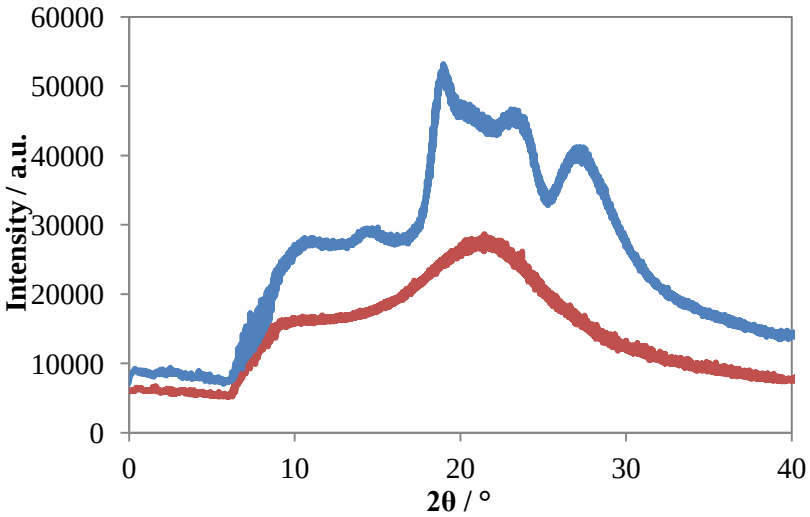

Fig.2– 8 (a) X-ray diffraction pattern of trimer V-(7,7) in the DC phase at $T-T_{NDC}$ = 13.0 K in the wide-angle region. (b) X-ray diffraction profiles of trimer V-(7,7) in the N phase at $T-T_{NDC}$ = 10.0 K (red line) and the DC phase at $T-T_{NDC}$ = 13.0 K (blue line) in the wide-angle region.

Fig.2-9 portrays the temperature dependence of the periodicity length in the DC phase. The layer spacing at T_{NDC} is 56.7 A. The layer spacing decreases with decrease in the temperature in the DC phase. It reaches a value of 56.2 A at $T - T_{NDC} = -28.0$ K. The layer spacing corresponds to the length of the trimer and not to the length of the single mesogenic unit, indicating the segregation of spacers and terminal chains.

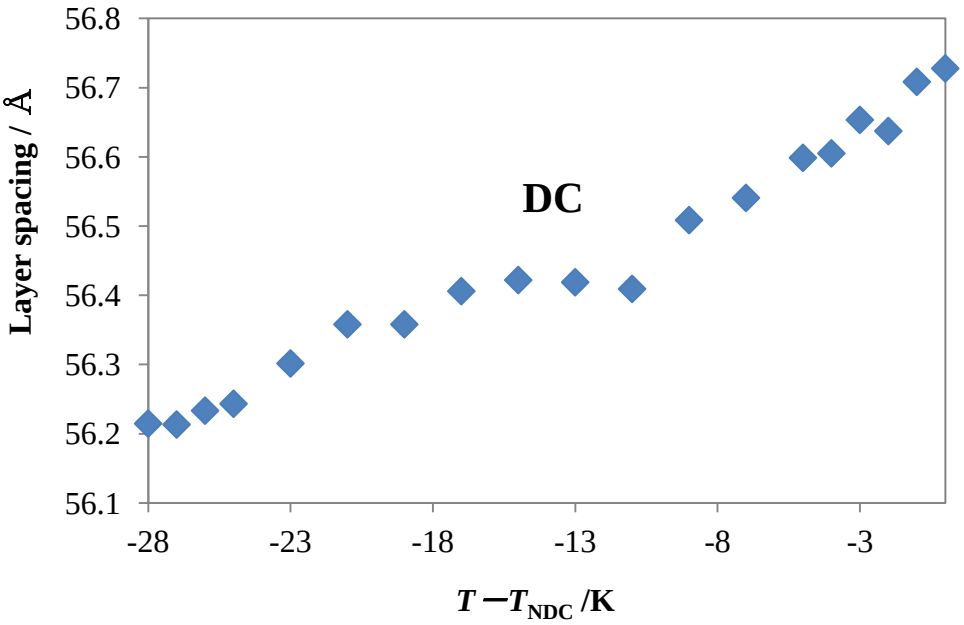

Fig.2– 9 Temperature dependence of the periodicity length in the DC phase of trimer V-(7,7).

Fig.2-10(a) shows that the extended molecular length for trimer **V-(7,7)** with all-trans conformation of the spacers is estimated by semi-empirical calculations using MOPAC-6/PM3 to be 68 A. The layer spacing is shorter than the molecular length. The difference between the layer spacing and molecular length is possible by a molecular tilt with respect to the layer normal, conformational chain disorder, and chain interdigitation. The tilt angle based on the XRD measurements is estimated as 26° if the trimer is tilted with the layer normal. The layer periodicity of 62.3 A in the SmA phase of trimer **VI-(7,7)** described later was used as a basis for the calculation of the tilt angle. On the other hand, this large difference between the layer spacing and molecular length is found similarly for the DC phases of the related 4-iodo and 4-methylresorcinol derivatives.[7,8] The layer spacing in the previously

reported HNF phases is usually close to the molecular length. The shorter layer spacing observed for some resorcinol bent-core LCs is explained in terms of the twisted conformation of the bent-core molecule[8]. The structure– property relations of the resorcinol bent-core mesogens reveal that conformation chirality attributable to the rigid twisted structure plays an important role in the appearance of the DC phase[8]. The molecular length is estimated as 57 Å if compound **V-(7,7)** has a twisted conformation, as portrayed in Fig.2-10(b). The origin for the difference between the layer spacing and molecular length will be discussed later. Trimer **V-(7,7)** exhibited sharp peaks in the wide-angle region and showed no electro-optical switching in the DC phase, suggesting that the DC phase was an HNF phase. It can be swollen in a nematic liquid crystal if the DC phase is an HNF phase[22–24]. However, a binary mixture of **V-(7,7)** (50 wt%) and 6OCB (50 wt%) exhibited the following phase transition: Iso 132 °C Iso + N 118 °C Cry. Phase separation occurred instead of dilution of the DC phase. The molecular length for 6OCB is estimated using MOPAC to be 18 Å. Trimer **V-(7,7)** is 3.8 times the length of 6OCB, and hence efficient packingmight just not be possible; thus a nematic phase is formed. The HNF phases can be swollen up to >90% with a nematic liquid crystal and retain a DC structure. Therefore, the DC phase of trimer **V-(7,7)** is not an HNF phase but more similar to a soft crystalline DC phase[7,8].

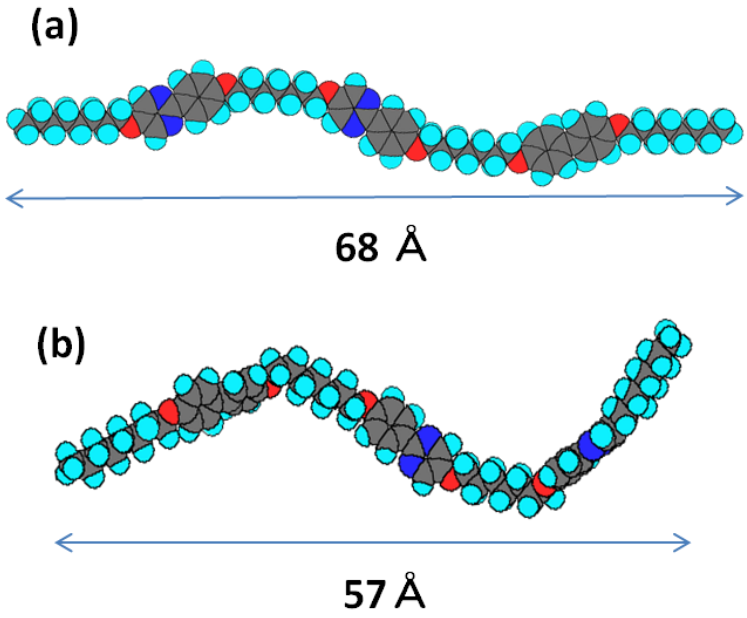

Fig.2– 10 MOPAC models for trimer V-(7,7) with (a) an extended conformation and (b) a twisted conformation.

2.3.2. Effects of the spacer length

I prepared a homologous series of trimers **V-(n,m)** with different spacer lengths and investigated their phase transition behaviour. The results are presented in Fig.2-11. The phase transition temperatures and entropies are listed in Table 2-1. Trimers **V-(7,9)** and **V-(9,9)** exhibited a phase sequence of Iso–N–DC similar to trimer **V-(7,7)**. However, trimer **V-(5,5)** showed no mesogenic phase. Trimer **V-(7,5)** exhibited N and SmC phases. Then, it crystallized without the DC phase. Trimer **V-(6,6)**, possessing even-numbered spacers, exhibited SmC and unidentified smectic phases. If I assume that spacers of these trimers form an all-trans conformation, a trimer with odd-numbered spacers has a zigzag shape in which all three mesogenic units are inclined with respect to each other, whereas a trimer with even-numbered spacers has a linear shape in which the three mesogenic units are co-parallel. Generally, the flexibility of a liquid crystal trimer increases with the increasing spacer length. Therefore, coupling between the zigzag shape and flexibility is thought to play an important role in the appearance of the DC phase.

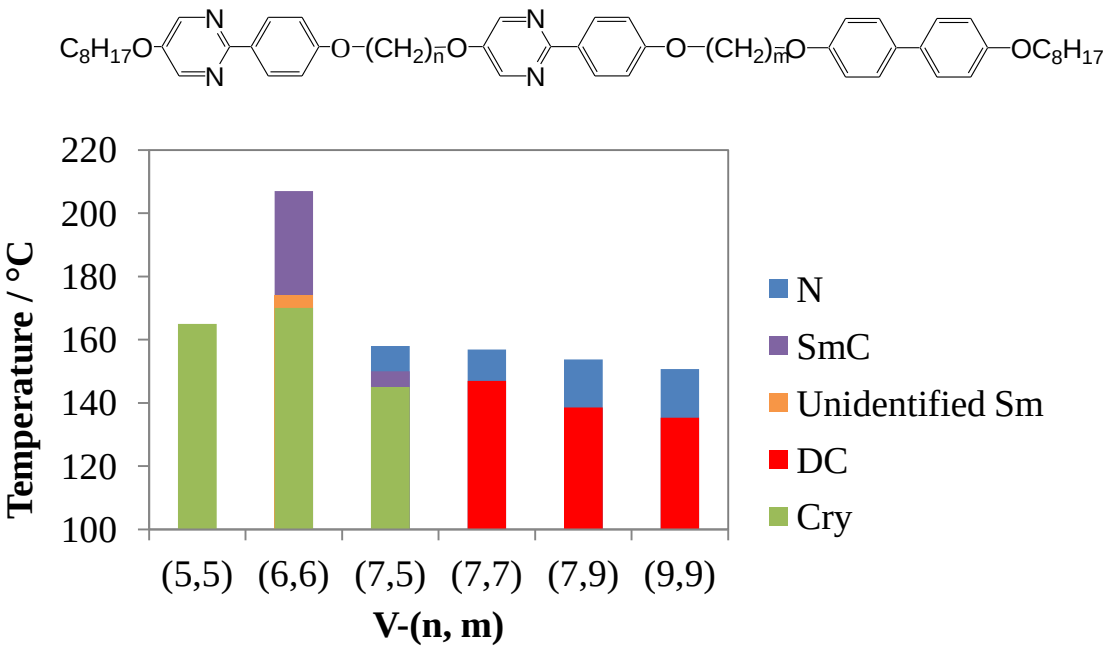

Fig.2– 11 Phase diagram for homologue series of trimers **V-(n,m)**.

Table 2– 1 Phase transition temperatures (°C) and Δ*S*/*R* for **V–(n,m)**.

Compound	Heating	Cooling
V-(5,5)	Cry 168.9 (20.7) Iso	Iso 163.0 (20.4) Cry
V-(6,6)	Cry 178.8 (9.5) SmC 208.1(7.1) Iso	Iso 207.2 (7.5) SmC 174.3 (-)[a] Sm[b] 171.3 (11.3) Cry
V-(7,5)	Cry 151.0 (19.1) N 157.9 (1.3) Iso	Iso 156.8 (1.3) N 150.1 (0.6) SmC 145.7 (7.3) Cry
V-(7,7)	Cry_1 144.0 (5.5) Cry_2 135.2 (8.8) N 156.9 (1.2) Iso	Iso 155.8 (1.2) N 146.4 (10.4) DC
V-(7,9)	Cry_1 130.1 (4.4) Cry_2 138.9 (8.7) N 153.6 (1.3) Iso	Iso 153.1 (1.3) N 137.8 (9.0) DC
V-(9,9)	Cry_1 120.0 (7.7) Cry_2 135.2 (12.7) N 150.4 (3.1) Iso	Iso 149.9 (2.9) N 134.1 (13.4) DC

[a]Entropy change too small to be detected.

[b]Unidentified smectic phase.

2.3.3. Effects of core structures

To elucidate the mechanism by which intermolecular interactions between odd-membered trimers contribute to the appearance of the DC phase, I prepared some derivatives of trimer **V-(7,7)** and investigated their phase transition behaviour. The molecular structures and the phase transition properties are presented in Fig.2-12. Trimer **VII-(7,7)** exhibited N and DC phases similar to trimer **V-(7,7)**. No significant difference is apparent in their mutual transition properties. Both trimers **VI-(7,7)** and **VIII-(7,7)** exhibited a phase sequence of Iso–SmA–SmC–SmX–Y. SmX and Y phases are unidentified phases. They showed neither the N phase nor the DC phase. The polarized optical textures and DSC thermogram of trimer **VI-(7,7)** are shown in Fig.2-13 and 14, respectively. The Schlieren texture in the homeotropically aligned region changed to a mosaic texture at the SmC–SmX transition; however, no enthalpy change was detected. The SmX phase is thought to be one of the smectic C sub-phases. On the other hand, the SmX–Y transition accompanied both a marked texture change and a large transition enthalpy. Further investigation is necessary to identify the Y phase.

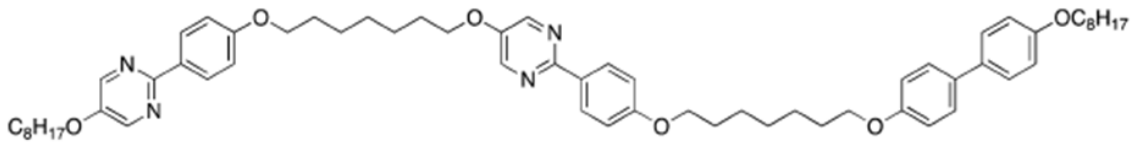

V-(7,7)

Heating: Cry_1 144.0 (5.5) Cry_2 135.2 (8.8) N 156.9 (1.2) Iso
Cooling: Iso 155.8 (1.2) N 146.4 (10.4) DC

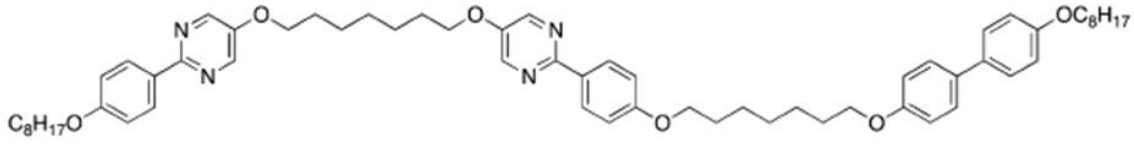

VI-(7,7)

Heating: Cry 120.4 (4.5) Y 137.5 (4.1) SmX 144.8 (–)[a] SmC 157.6 (–)[a] SmA 162.6 (4.2) Iso
Cooling: Iso 160.6 (4.2) SmA 153.7 (–)[a] SmC 143.5 (–)[a] SmX 139.4 (5.4) Y 99.0 (3.3) Cry

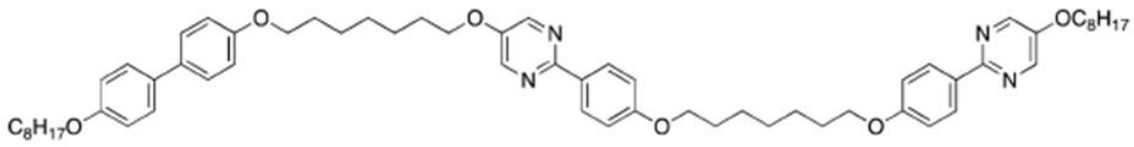

VII-(7,7)

Heating: Cry_1 137.0 (6.2) Cry_2 142.6 (8.3) N 155.6 (1.4) Iso
Cooling: Iso 154.5 (1.4) N 140.8 (8.6) DC 112.7 (2.6) Cry

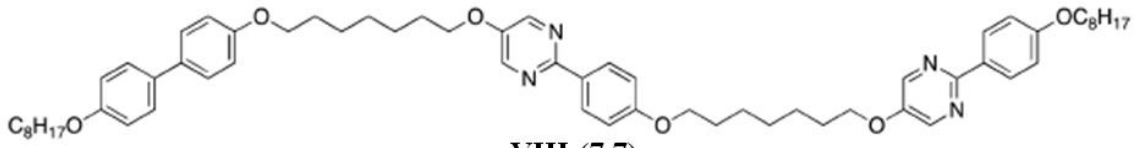

VIII-(7,7)

Heating: Cry 133.8 (4.2) Y 142.9 (5.7) SmX 145.8 (–)[a] SmC 160.8 (–)[a] SmA 164.0 (5.6) Iso

Fig.2– 12 Molecular structures, phase transition temperatures (1C), and DS/R are given in parentheses. SmX and Y phases are unidentified phases. a Entropy changes are too small to be detected.

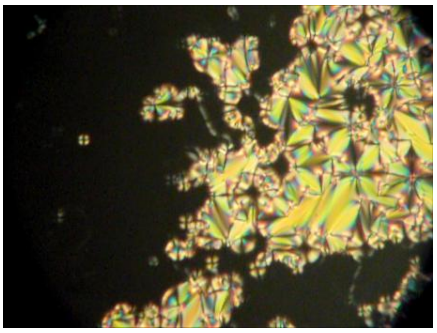

SmA (160 ℃)

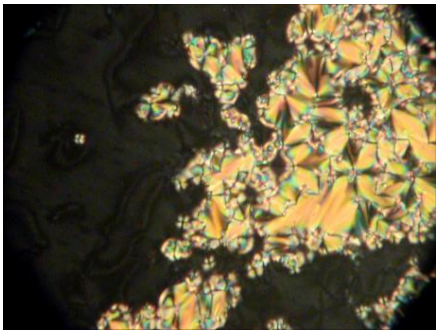

SmC (150 ℃)

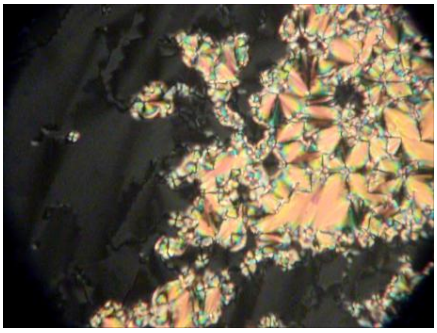

SmX (140 ℃)

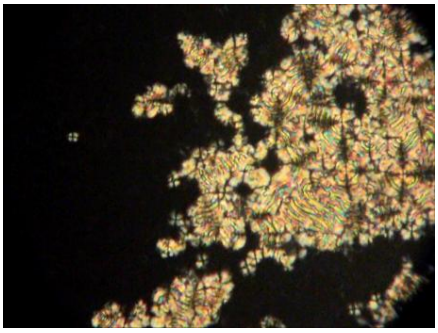

SmX→Y (139 ℃)

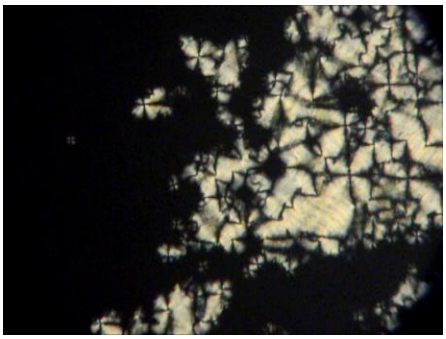

Y (120 ℃)

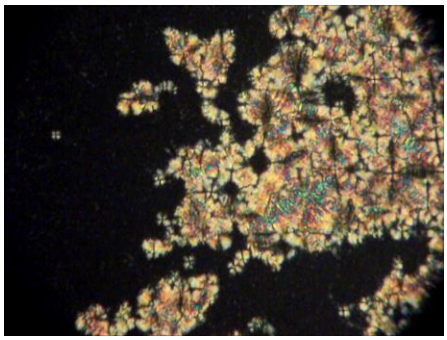

Cr (80 ℃)

Fig.2– 13 Polarized optical textures of trimer **VI–(7,7)** on a glass slide with a cover glass in the SmA, SmC, SmX and Y phases.

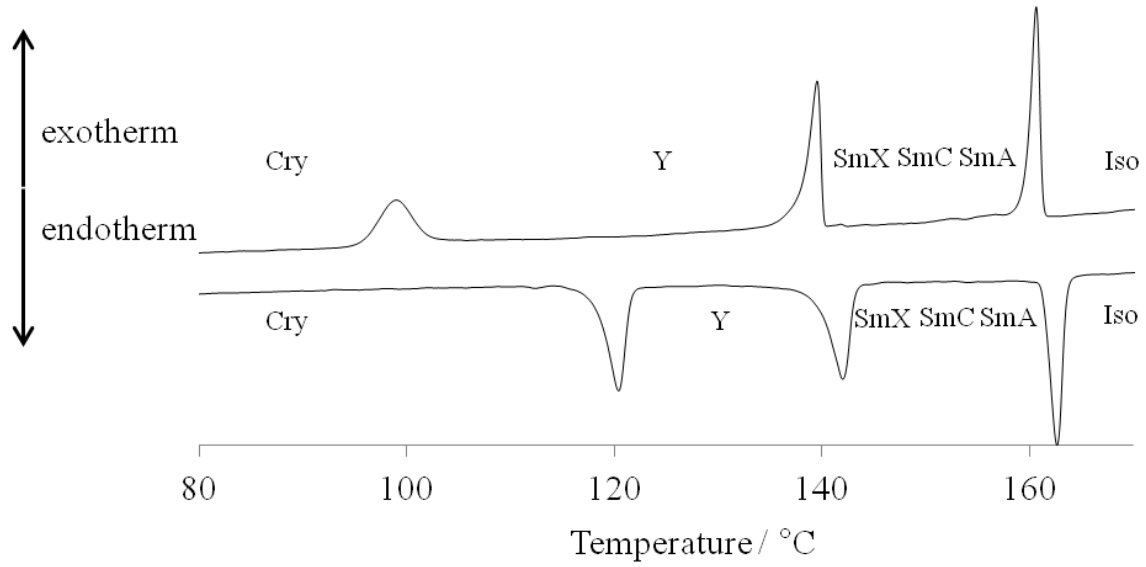

Fig.2– 14 DSC thermogram of trimer **VI–(7,7)**. The rate of cooling and heating was 5 °C $min^{-1.}$

Fig.2-15 shows temperature dependence of the layer periodicity of trimer **VI-(7,7)**. The layer spacing in the SmA phase of **VI-(7,7)** at $T - T_{Iso–SmA} = -5.0$ K is 62.3 Å. It is shorter than the molecular length of 68 Å, suggesting interlayer permeation of terminal tails between adjacent layers. The layer spacing in the SmC phase at $T - T_{Iso–SmA} = -17.0$ K is 61.8 Å. The maximum layer contraction of 0.8% suggests that the biaxiality in the SmC phase is not attributed to the tilt of the long axis but to the zigzag shape of three mesogenic units within the trimer. If the DC phase of trimer **V-(7,7)** has a tilted layer structure, the biaxiality is also attributed to the tilt of each mesogenic unit within the trimer similar to the SmC phase of trimer **VI-(7,7)**. The layer spacings of trimer **V-(7,7)** in the DC phase are much shorter than those of **VI-(7,7)** in the SmC phase. The difference between the layer spacing and molecular length of trimer **V-(7,7)** cannot be explained only by the zigzag shape. Conformational disorder in the spacers might be the most important cause of the difference.

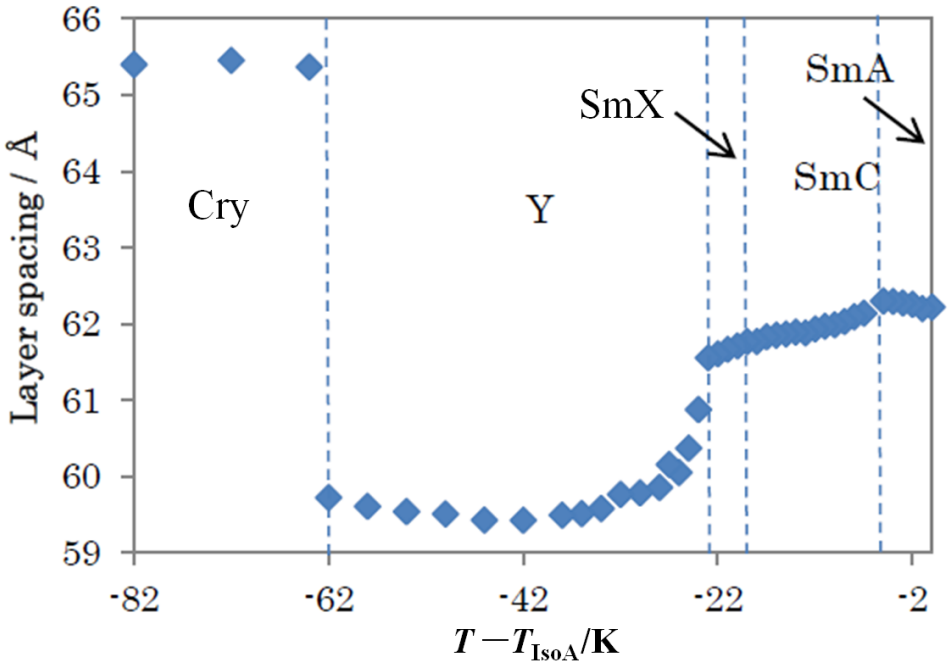

Fig.2– 15 Temperature dependence of the layer periodicity of trimer **VI-(7,7).**

Fig.2-16 portrays models for the molecular organization of these trimers. I assume an antiparallel molecular packing organized by the core–core interaction between central phenylpyrimidine units in adjacent molecules. Core–core interactions of the antiparallel packing for **V-(7,7)** are the same as those for **VII-(7,7)**. Those for **VI-(7,7)** are the same as those for **VIII-(7,7)**. These models can explain that trimers **V-(7,7)** and **VII-(7,7)** have the same transition behaviour, and also that trimers **VI-(7,7)** and **VIII-(7,7)** have the same transition behaviour. The molecular organizationmodels are realistic. Next, I discuss the differences in the transition behaviours of **V-(7,7)** and **VI-(7,7)**. Comparing the organization model between **V-(7,7)** and **VI-(7,7)**, the difference is in the position of pyrimidine in the outer phenylpyrimidine unit. I also consider that trimer **V-(7,9)** possessing different oddnumbered spacers shows the DC phase. I can say that dense molecular packing around the biphenyl unit is not favourable for the appearance of the DC phase.

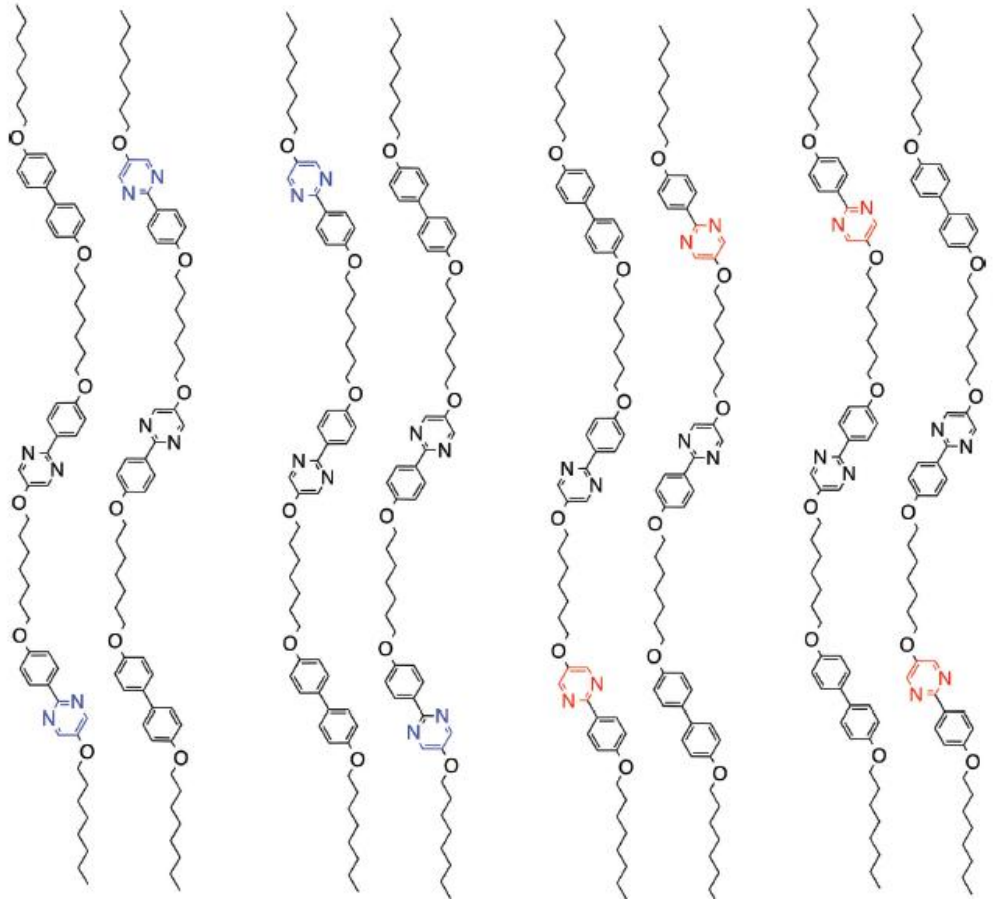

V-(7,7) **VII-(7,7)** **VI-(7,7)** **VIII-(7,7)**

Fig.2– 16 Models for molecular organization of trimers **V-(7,7)**, **VI-(7,7)**, **VII-(7,7)** and **VIII-(7,7)** in their layer structure.

Fig.2-17 shows a possiblemodel for the origin of chirality in the DC phase of trimer **V-(7,7)**. As described above, the trimers have a short-range periodicity of about 62 Å in the N phase, whereas they have a layer periodicity of 56.7 Å at TNDC. Conformational disorder in the spacers of trimer **V-(7,7)** occurs at the N–DC phase transition. The dipole–dipole interaction between the antiparallel central phenylpyrimidine units might drive the layered structure. I surmise that the interaction between the biphenyl unit and the outer phenylpyrimidine unit of **V-(7,7)** is repulsive. The biphenyl unit of **V-(7,7)** can adopt the twisted conformation. The strong core–core interaction between the central phenylpyrimidine units is thought to restrict free rotation of the biphenyl axis of each trimer to produce axial chirality. The attractive interaction between the central cores and the repulsive interactions between outer cores can induce the conformational disorder in the spacers. Coupling between the axial chirality and

the disordered odd-numbered spacers can produce helical conformers. According to an explanation for the formation of soft crystalline DC phases[7,8,25], the packing of helical conformers can produce macroscopic chirality, which induces twisting and bending of the layers to lead to the deformation or fragmentation of these layers.

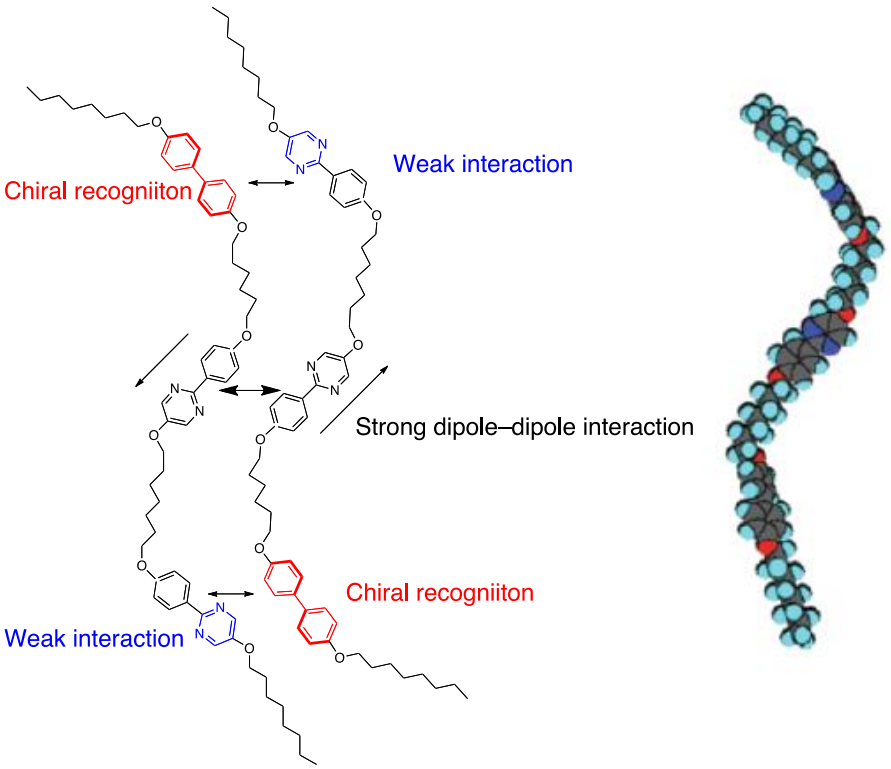

Fig.2– 17 Model for the origin of the chirality of **V-(7,7)** in the DC phase.

2.4. Conclusion

I prepared a homologous series of achiral liquid crystal trimers in which two phenylpyrimidine units and one biphenyl unit were connected via flexible methylene spacers. Some trimers possessing odd-numbered spacers were found to exhibit a crystalline DC phase of domains with opposite handedness. The trimers form an achiral ground-state conformation in the nematic phase, but by intermolecular interactions between cores they adopt a chiral conformation to exhibit the spontaneous mirror symmetry breaking in the low-temperature DC phase.

2.5. Reference

[1] L. E. Hough, M. Spannuth, M. Nakata, D. A. Coleman, C. D. Jones, G. Dantlgraber, C. Tschierske, J. Watanabe, E. Körblova, D. M. Walba, J. E. Maclennan, M. A. Glaser, N. A. Clark, *Science*, 2009, **325**, 452.

[2] L. E. Hough, H. T. Jung, D. Krüerke, M. S. Heberling, M. Nakata, C. D. Jones, D. Chen, D. R. Link, J. Zasadzinski, G. Heppke, J. P. Rabe, W. Stocker, E. Ko¨rblova, D. M. Walba, M. A. Glaser, N. A. Clark, *Science*, 2009, **325**, 456.

[3] D. R. Link, G. Natale, R. Shao, J. E. Maclennan, N. A. Clark, E. Körblova, D. M. Walba, *Science*, 1997, **278**, 1924.

[4] J. Thisayukta, H. Takezoe, J. Watanabe, *Jpn. J. Appl. Phys.* 2001, **40**, 3277.

[5] E. Tsai, J. M. Richardson, E. Körblova, M. Nakata, D. Chen, Y. Shen, R. Shao, N. A. Clark, D. M. Walba, *Angew. Chem., Int. Ed.*, 2013, **52**, 5254.

[6] G. B. Deepa, S. Radhika, B. K. Sadashiva, R. Pratibha, *Phys. Rev. E: Stat., Nonlinear, Soft Matter Phys*., 2013, **87**, 062508.

[7] M. Alaasar, M. Prehm, M. Brautzsch, C. Tschierske, *J. Mater. Chem. C*, 2014, **2**, 5487.

[8] M. Alaasar, M. Prehm, M. Brautzsch, C. Tschierske, *Soft Matter*, 2014, **10**, 7285.

[9] E. Bialecka-Florjanczyk, I. Sledzinska, E. Gorecka, J. Przedmojski, *Liq. Cryst*., 2008, **35**, 401.

[10] T. Ueda, S. Masuko, F. Araoka, K. Ishikawa, H. Takezoe, *Angew. Chem., Int. Ed*., 2013, **52**, 6863.

[11] A. Zep, M. Salamonczyk, N. Vaupotic, D. Pociecha, E. Gorecka, *Chem. Commun*., 2013, **49**, 3119.

[12] A. Zep, K. Sitkowska, D. Pociecha, E. Gorecka, *J. Mater. Chem. C*, 2014, **2**, 2323.

[13] C. Tschierske and G. Ungar, *ChemPhysChem*, 2016, **17**, 9.

[14] Nanoscale Stereochemistry in Liquid Crystals, C. Tschierske, in *Chirality at the Nanoscale*, ed. D. B. Amabilino, Wiley-VCH, Weinheim, 2009, pp. 271–304.

[15] H. Takezoe, *Top. Curr. Chem*., 2012, **318**, 303.

[16] R. A. Reddy and C. Tschierske, *J. Mater. Chem*., 2006, **16**, 907.

[17] D. M. Walba, *US pat.*, 8963140 B2, 2013.

[18] H. Sasaki, Y. Takanishi, J. Yamamoto, A. Yoshizawa, *J. Phys. Chem. B*, 2015, **119**, 4531.

[19] A. Yoshizawa, Y. Kato, H. Sasaki, Y. Takanishi, J. Yamamoto, *Soft Matter*, 2015, **11**, 8827.

[20] E. T. Samulski, *Liq. Cryst*., 2010, **37**, 669.

[21] C. Tschierske and D. J. Photions, *J. Mater. Chem*., 2010, **20,** 4263.

[22] Y. Takanishi, G. J. Shin, J. C. Jung, S.-W. Choi, K. Ishikawa, J. Watanabe, H. Takezoe, P. Toledano, *J. Mater. Chem*., 2005, **15**, 4020.

[23] T. Otani, F. Araoka, K. Ishikawa, H. Takezoe, *J. Am. Chem. Soc.*, 2009, **131**, 12368.

[24] Y. Takanishi, H. Yao, T. Fukasawa, K. Ema, Y. Ohtsuka, Y. Takahashi, J. Yamamoto, H. Takezoe, A. Iida, *J. Phys. Chem. B*, 2014, **118**, 3998.

[25] M. Alaasar, M. Prehm, C. Tschierske, *Chem. Commun*., 2013, **49**, 11062.

CHAPTER 3

Achiral flexible liquid crystal trimers exhibiting gyroid-like surfaces in the chiral conglomerate phases

3.1. Introduction

Not only observations of spontaneous mirror symmetry breaking but also complex hierarchical structure in the DC and HNF phases by formed bent-core liquid crystals are attracting a lot of attention[1,2]. Surfaces of those layered phases exhibit characteristic structures depending on their molecular organization. With respect to the sponge phase, toroidal focal conic domains (TFCDs) self-assemble into a regular closed-packed structure at the free surface of a droplet of the bent-core liquid crystal material[3]. The bulk shows disordered focal conic domains organized in the disordered plumber's nightmare structure[3]. The HNF phase is one of the most complex hierarchical self-assemblies. Layer topology of the HNF phase observed for bent-core molecules has been extensively investigated[4-6]. The diverse topology of the HNF phase on the glass surface was reported by Chen et al. [4] The twisted layer structure of the bulk is suppressed near the glass substrate. Further from the substrate, the layers evolve to the twisted structure and the helical filaments grow with specific handedness. The HNF phases have been reported to form various alignments depending on external fields[7-11]. Furthermore, the helical nanofilaments form a network which acts as a porous nanoconfinement medium of a large internal area, with the guest material confined to nanoscale interstitial volumes between the filaments[2,10,12]. Designed liquid crystals can produce either left or right-handed chiral nanostructures, which are generated on their surfaces and/or in the bulk of the materials in the DC phases. In chapter 3, I reported a homologues series of the achiral liquid crystal trimer **V-(n,m)** exhibiting soft crystalline DC phases[13]. They are neither liquid-crystalline sponge phases nor HNF phases. The driving force of the appearance of the DC phases is the conformation change of the flexible trimer, which differs greatly from that for the bent-core system. Furthermore, a symmetric trimer formed homochiral droplets exhibiting toroidal pits on the surface[14].

In this chapter, in order to understand the molecular organization in the soft crystalline DC phase, I investigated both surface and bulk structures of **V-(n,m)** by atomic force microscopy (AFM) and field-emission scanning electron microscopy (SEM). The results reveal that the DC phase consists of bicontinuous networks, which differ from previously reported nanostructures of the layered phases, i.e., toroidal focal conic domains and helical nanofilaments. I discuss how the trimer molecules organize bicontinuous networks in the soft crystalline DC phase exhibiting optical activity.

3.2. Experimental

3.2.1. Preparation of materials

For use in this study, 5-hydroxy-2-(4-hydroxyphenyl)pyrimidine was purchased from Midori Kagaku Co. Ltd. The purity of each final compound was confirmed using elemental analysis (EA 1110; CE Instruments Ltd). Confirmation of the structures of intermediates and products was obtained by infrared (IR) spectroscopy (BIO RAD FTS-30) and proton nuclear magnetic resonance (^{1}H NMR) spectroscopy (JEOL JNM-ECA500).

In the reporting of IR data, the following abbreviations have been used.

str. stretching

In the reporting of ^{1}H NMR data, the following abbreviations have been used.

s. singlet
d. doublet
t. triplet
q. quartet
m. multiplet

The analyses of the structures of the products by means of spectroscopic methods were found to be consistent with the predicted structures.

Preparation and characterization of trimers **V-(7,7)~V-(9,9)** were reported in chapter 2. Trimer **V-(9,11)** is a new compound. Its Preparation and characterization are listed in below.

3.2.1.1.

2-{4-[11-(4-(4-Octyloxyphenyl)phenyloxy)undecyloxy]phenyl}-5-{9-[4-(5-octyloxy-pyrimidin-2-yl)phenyloxy]nonyloxy}pyrimidine (V-(9,11)).

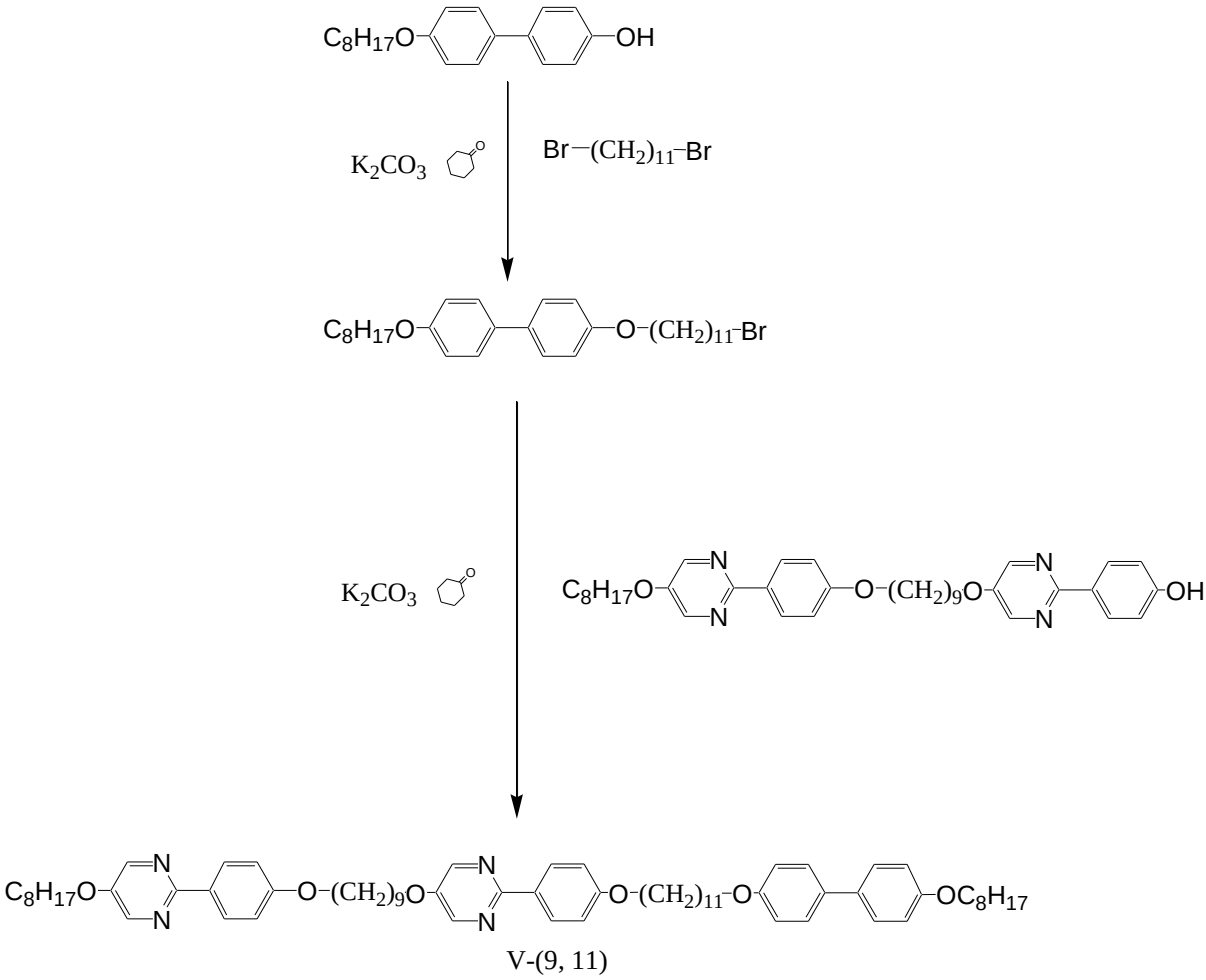

V-(9, 11)

Scheme3– 3 Preparation of **V–(9, 11)**.

Potassium carbonate (2.0 mmol, 276 mg) was added to a solution of 4-(4-octyloxyphenyl)phenol (2.0 mmol, 596 mg) and 1,11-dibromoundecane (2.6 mmol, 817 mg) in cyclohexanone (10 ml). The reaction mixture was stirred at 90 °C for 6 h. After filtration of the precipitate, the solvent was removed by evaporation. Then, the residue was purified using column chromatography on silica gel with a toluene : ethyl acetate (5 : 1) mixture as an eluent. The obtained white solid was recrystallized from ethanol to give 1-(4-octyloxyphenyl)-4-(11-bromoundecyloxy)-benzene. Yield 177 mg (39%).

Potassium carbonate (0.12 mmol, 17 mg) was added to a solution of 1-(4-octyloxyphenyl)-4-(11-bromoundecyloxy)-benzene (0.12 mmol, 64 mg) and 2-(4-Hydroxyphenyl)-5-{7-[4-(5-octyloxypyrimidin-2-yl)heptyloxy]hexyloxy}pyrimidine (0.12 mmol, 74 mg) in cyclohexanone (10 ml). The reaction mixture was stirred at 130 °C for 5 h. After filtration of the precipitate, the solvent was removed by evaporation. Then, the residue was washed with hot ethanol and was recrystallized from toluene to give the desired compound. Yield 75 mg (59%).

1H NMR (500 MHz, $CDCl_3$, TMS): d = 8.40 (s, 4H, Ar–**H**), 8.26 (d, 4H, Ar–**H**, *J* = 9.2 Hz), 7.44 (d, 4H, Ar–**H**, *J* = 6.9 Hz), 6.96 (d, 4H, Ar–**H**, *J* = 8.6 Hz), 6.93 (d, 4H, Ar–**H**, *J* = 8.6 Hz), 4.08 (t, 2H, –OC**H**$_2$–), 4.07 (t, 2H, –OC**H**$_2$–), 4.03 (t, 2H, –OC**H**$_2$–), 4.02 (t, 2H, –OC**H**$_2$–), 3.99 (t, 2H, –OC**H**$_2$–), 3.98 (t, 2H, –OC**H**$_2$–), 1.86–1.76 (m, 12H, aliphatic-**H**), 1.53–1.29 (m, 32H, aliphatic-**H**), 0.89 (t, 6H, –C**H**$_3$, *J* = 6.9 Hz).

IR(KBr): ν cm^{-1}: 2922, 2851 (C–H str), 1608, 1542, 1499, 1434 (C=C, C=N str), 1273 (C–O str).

Elemental analysis calc. for $C_{62}H_{82}N_4O_6$: C, 76.80; H, 8.91; N, 5.27. Found C, 76.50; H, 8.53; N, 5.32.

3.2.2. Liquid-crystalline and physical properties

The optical textures were observed using a polarizing optical microscope (POM, BX-51; Olympus Optical Co. Ltd) equipped with a temperature control unit (LK-600PM; Japan High Tech Co. Ltd). The temperatures and enthalpies of transition were investigated using differential scanning calorimetry (DSC, DSC 6200; Seiko Instruments Inc.). I observed the microstructure of trimer V-(n,m) at the air/liquid crystal interface of a droplet on an untreated glass slide using AFM and SEM. Atomic force microscopy (AFM, NanoNavi2/E-Sweep) was used in tapping mode at room temperature. The sample on the glass slide was heated to produce an isotropic liquid on a hot plate. It was then cooled to room temperature. Field-emission scanning electron micrographs were obtained using a JEOL JSM-7000 FE-SEM with accelerating voltages of 10 keV. The sample was coated with platinum before being analyzed. The X-ray diffraction (XRD) patterns of the samples during the cooling process were obtained using a MicroMax-007HF (Rigaku Corp.). Each sample was put on a convex lens, which was then placed in a custommade temperature stabilized holder (stability within 0.1 °C). Liquid-crystalline molecules tend to align homeotropically at an air/liquid crystal interface. I coated a homeotropically aligning agent on a lens in order to increase the peak intensity. The phase transition of the sample under the X-ray beam was monitored by observing the texture simultaneously, using a polarized light microscope with a charge-coupled device (CCD) camera. The X-ray apparatus was equipped with a platform arrangement and a two-dimensional detector (Image intensifier and CCD C9299-01; Hamamatsu Photonics KK). Then X-rays were generated at 40 kV and 20 mA; a parallel Cu Ka X-ray beam was used to irradiate the sample. The correlation length along the layer normal was determined using the Ornstein–Zernike expression.

3.3. Results and discussion

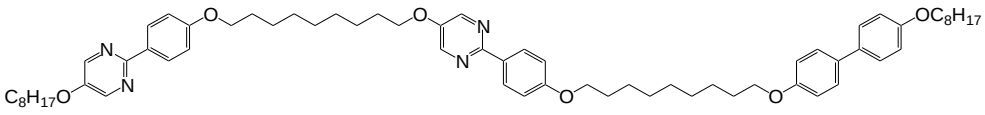

Fig.3– 1 Molecular structure of trimer **V-(9,9)**.

I observed the microstructure of trimer **V-(9,9)** at the air/liquid crystal interface of a droplet on a glass slide by AFM. The molecular structure is shown in Fig.3-1. It exhibits the DC phase with a wide temperature range including room temperature[13]. Fig.3-2 shows the optical textures of trimer **V-(9,9)** on a glass slide without a top cover in the DC phase under uncrossed polarizers. By uncrossing the polarizers in opposite directions by the same angle, the darker and brighter domains were exchanged. The domain brightness did not change by rotation of the sample between the polarizers. These results indicate that they show optical activity with opposite senses. The textures on a glass slide with a cover glass under crossed and uncrossed polarizers are shown in Fig.3-3. The contrast between blight and dark domains for a sample without a top cover was lower than that with a cover glass. Phase transition temperatures and enthalpies of transition for trimer **V-(9,9)** are as follows: Iso 149.9 °C (10.1 kJ mol^{-1}) N 134.1 °C (45.2 kJ mol^{-1}) DC[13]. The N–DC transition accompanied by a large transition enthalpy and no electro-optical switching was observed in the DC phase, revealing that the DC phase is a soft crystalline phase. The DC phase, once formed, does not crystallize even after storage for at least 6 months at room temperature.

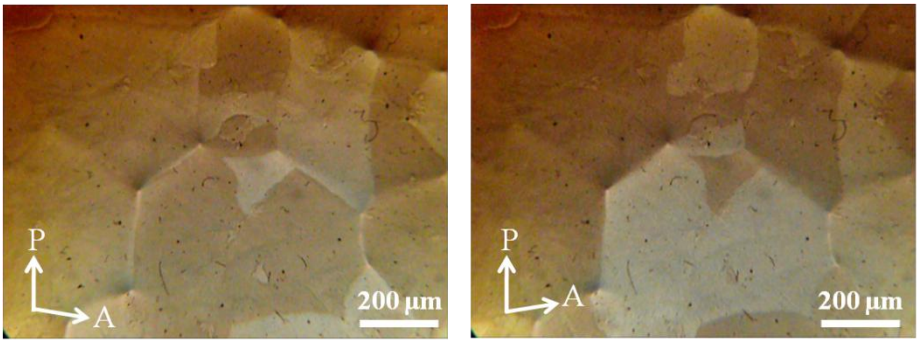

Fig.3– 2 Polarized optical textures of trimer **V-(9,9)** on a glass slide without a top cover in the DC phase at 130 °C under uncrossed polarizers.

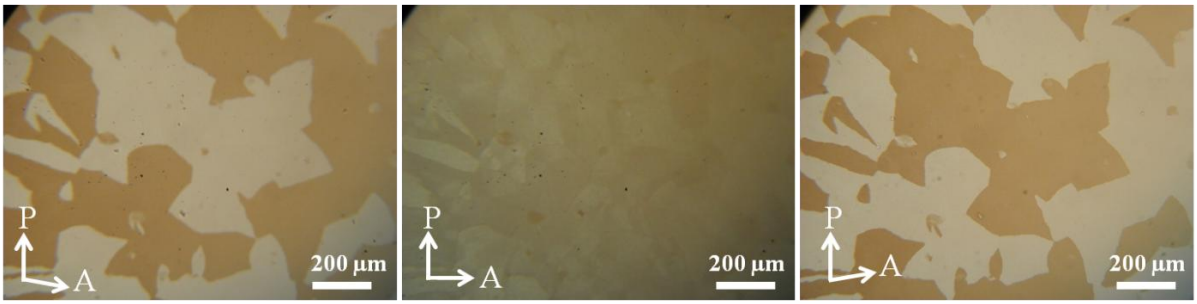

Fig.3– 3 Polarized optical texture of trimer **V–(9,9)** on a glass slide with a cover glass in the DC phase at 120 °C under crossed and uncrossed polarizers**.**

Fig.3-4(a) presents an AFM image of the surface structure of a sample at room temperature. The sample on a glass slide without a top cover was cooled from the isotropic to the DC phase, with the phase being confirmed using a polarized optical microscope. A surface relief with dimples was observed in the whole area. The surface structure was independent of the sample droplet size. Fig.3-4(b) shows higher magnification of the surface structure with the cross section of dimples below the surface. The dimple size, defined as a half-depth diameter, is about 103±11 nm for the dimple indicted in Fig.3-4(b). The distance between centers of neighboring dimples is about 200 nm. Its volume is estimated as $(2.2\pm0.2)\times10^5$ nm^3 based on the assumption that the dimple forms a cone structure.

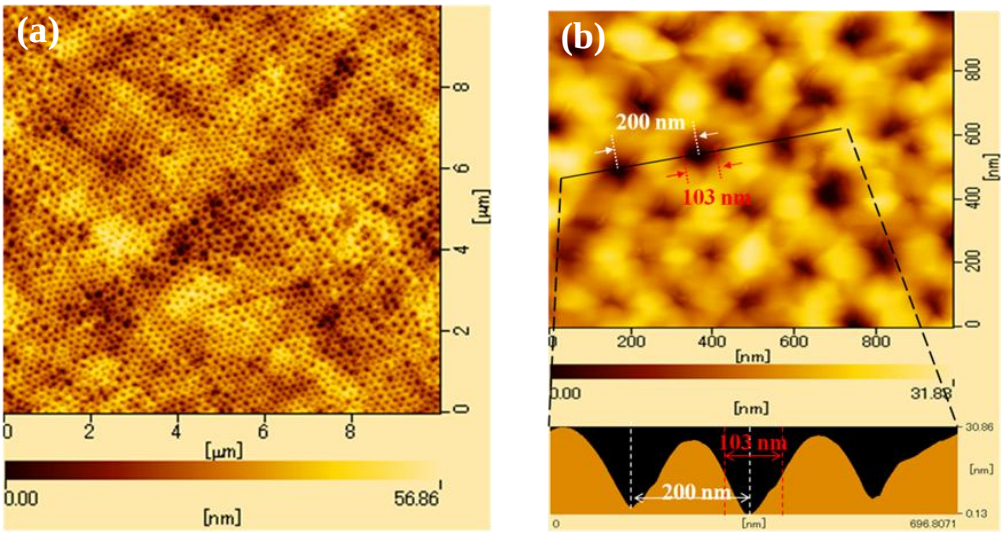

Fig.3– 4 (a) AFM image of the microstructure at the air/liquid crystal interface of a droplet on an untreated glass slide of trimer **V-(9,9)** in the DC phase at room temperature. (b) Higher magnification of the surface structure with the cross section of dimples.

Ordered patterns of toroidal defects were generated by confining a smectic A liquid crystal in microchannels [15,16]. The formation of TFCDs in a smectic A phase is explained in terms of antagonistic anchoring resulting from the competition of planar anchoring on the substrate and homeotropic anchoring at the air/liquid crystal boundary. It is influenced by the width and depth of the microchannels[15,16]. Furthermore, small size TFCDs were observed in HNF phases. [4,6] The periodic pattern of trimer **V-(9,9)** also appeared on the following different substrates: silicon wafer inducing planar alignment, glass coated with a unidirectionally buffed polyimide-aligning agent, and glass coated with a homeotropically aligning agent. Their AFM images are shown in Fig.3-5. The molecular alignment at the bottom substrate, which plays an important role in antagonistic anchoring for the generation of TFCDs, does not affect the pattern formation in the present system. However, when a sample sandwiched between glass layers was heated to an isotropic liquid and then cooled to the DC phase, the periodic pattern did not form (Fig.3-6). These results indicate that self-organization of the molecules at the air/liquid crystal interface plays an important role in the pattern formation.

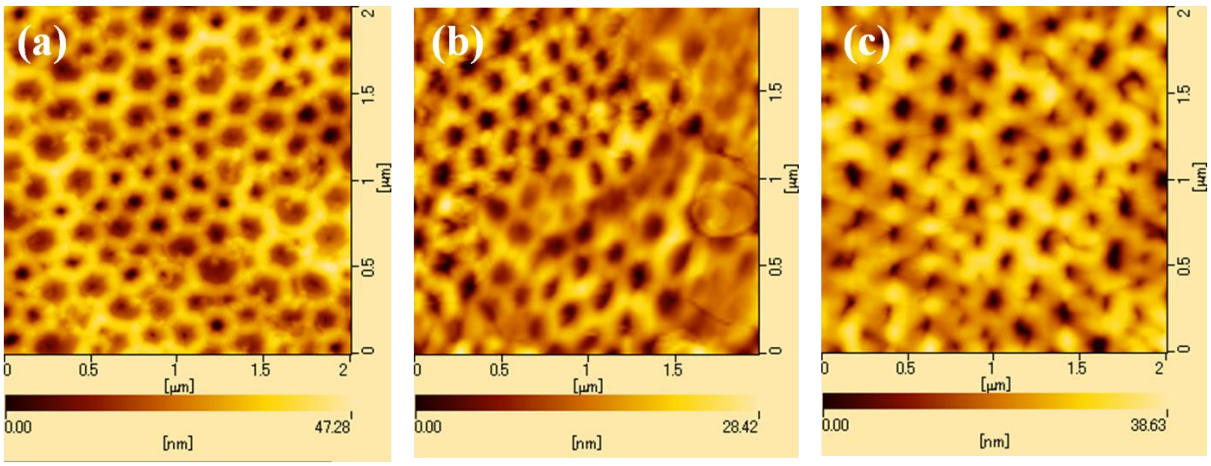

Fig.3– 5 AFM images of the surface structures of **V⁻(9,9)** without a top cover on (a) silicon wafer, (b) glass coated with a homeotropically aligning agent, or (c) glass coated with a unidirectionally buffed polyimide aligning agent at room temperature.

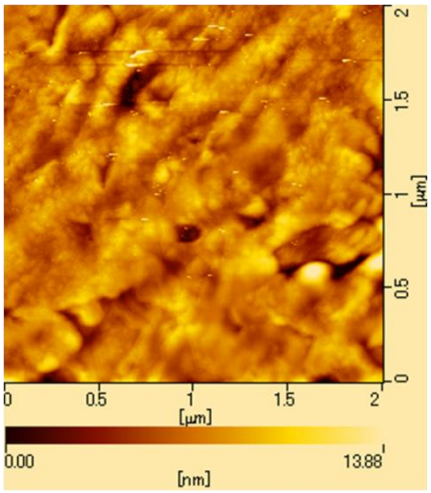

Fig.3– 6 AFM image of the surface structure of **V-(9,9)** in the DC phase formed by cooling a sample with a cover glass at room temperature.

Such a periodic surface pattern of trimer **V-(9,9)** was more clearly observed using SEM. The scanning electron micrographs of trimer **V-(9,9)** at the air/liquid crystal interface of a droplet on a glass substrate are shown in Fig.3-7. Although not only well-ordered regions but also some disordered regions exist, bicontinuous networks accompanying hexagonal voids are organized. A dimple diameter of about 100 nm was ascertained fromthe SEM image in a well-ordered region (Fig.3-7(b)). Furthermore, a smaller dimple can be seen inside. The network consists of bicontinuous triply branchings, which is similar to that for a single gyroid surface observed in lyotropic cubic phases[17,18], in block copolymers [19,20], and in the cuticular structure of butterfly wing [21-23]. Defects exist in the boundaries between adjacent branches. With respect to atriply branching in a well-ordered region, defect lengths for the three boundaries were ascertained to be 57 nm, 70 nm, and 79 nm as shown in Fig.3-7(b).

(a) (b)

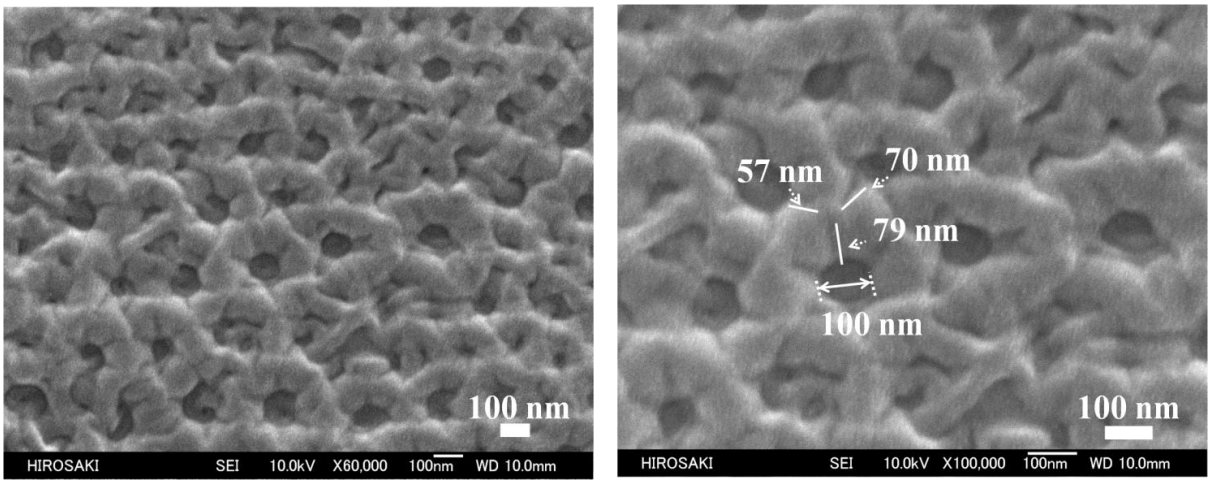

Fig.3– 7 (a) Field-emission scanning electron micrograph of the surface structure of **V-(9,9)**. (b) Higher magnification of the surface structure. The sample on an untreated glass substrate without a top cover was cooled to the DC phase.

To the best of our knowledge, such a gyroid-like cubic surface has never been reported in DC phases. Chen et al. reported that toric focal conic domains self-assemble into a quasi-ordered hexagonal lattice at the air/liquid crystal interface [3]. Recently, unusual phase behaviour was reported for a binary mixture of a bent-core molecule (W624) and 8CB [24]. The DC phase of neat W624 forms disordered focal conics with hexatic ordering within the layers. In mixtures of 8CB, W624 molecules tend to phase separate from 8CB, forming more ordered focal conic structures. A cubic bicontinuous structure was proposed for the phaseseparated DC phase. Although the freeze-fracture transmission electron microscopy image shows an ordered microstructure with the orange surface representing curved smectic layers, it does not seem to be a clear cubic structure.

In order to observe the cross section area, I prepared a thick sample using a sandwich cell in which the cell gap was maintained at 300 mm using spacers. The sample was heated to the isotropic liquid phase and was then filled into the cell. It was cooled down to the DC phase. Then I removed the top cover glass and cut the sample vertically with the glass substrate. I observed the microstructure at the air/liquid crystal interface, near the glass substrate, and that of the cross section area using SEM. Fig.3-8 shows the SEM images. A honeycomb-like pattern is shown at the air/liquid crystal interface (Fig.3-8(a)). The cross section area shows a sponge-like structure accompanying voids (Fig.3-8(c)). Near the glass substrate, the

sponge-like structure is flattened (Fig.3-8(b)). Sponge textures in chiral conglomerates have been observed for the liquid-crystalline sponge phases formed by strongly deformed fluid layers. It should be noted that the crystalline DC phase of trimer **V-(9,9)** forms a sponge texture in the bulk. In analogy to lipid–water systems, a sponge phase is essentially a disordered version of the bicontinuous cubic phases[25]. Both a gyroidlike surface and sponge-like bulk are thought to consist of bicontinuous networks, and they are closely related to each other. The disordered sponge structure of trimer **V-(9,9)** transforms to the gyroid-like periodic pattern from the bulk to the surface. It is analogous to the disorder–order transformation for the bicontinuous cubic phase in the lipid–water systems. Recently, a multi-lamellar sponge–cubic transition was found in thermotropic smectic blue phases[26]. Analysis of the gyroid-like surface structure can provide information of the molecular organization in the DC phase consisting of achiral flexible trimers. Furthermore the network in the DC phase can act as a porous nanoconfinement medium to produce nanocomposites for applications, such as semiconductors and photovoltaics[27-29].

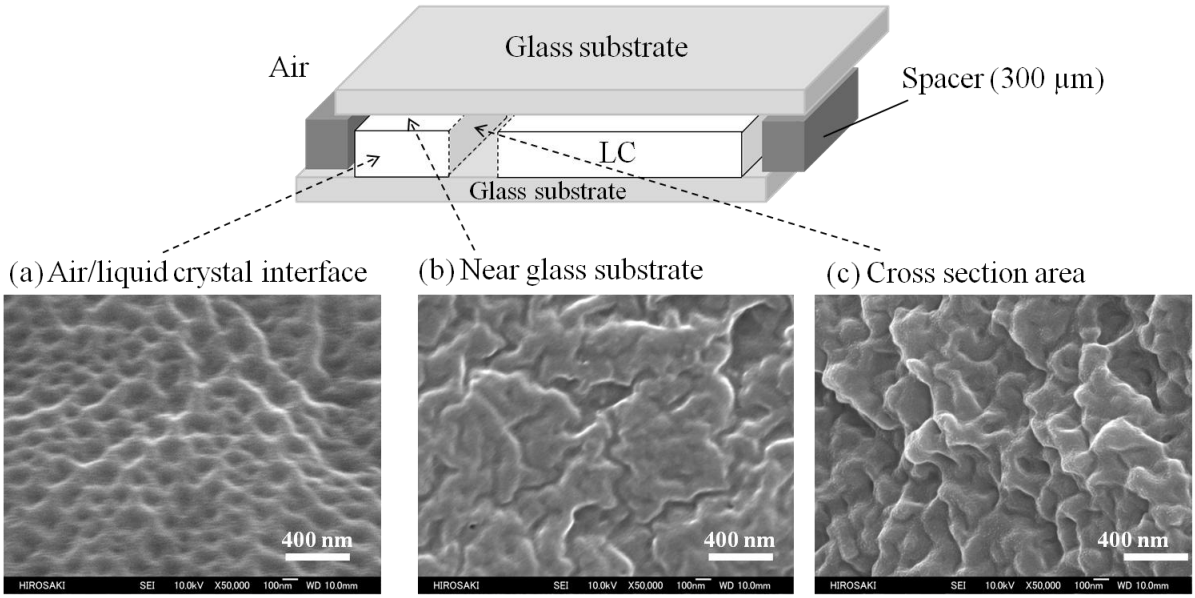

Fig.3– 8 (a) SEM image of the microstructure of trimer **V-(9,9)** at the air/liquid crystal interface, (b) that near the glass substrate, and (c) that of the cross section area.

To elucidate the formation process, I used polarized optical microscopy to observe the texture change near the N–DC phase transition of trimer **V-(9,9)** on a glass without a cover glass. The trimer was found to exhibit a randomly oriented slab-like texture in the N phase above the N–DC transition (Fig.3-9(a)). The slab regions show lower birefringence than the N phase and appear to move on the nematic sea. The coexistence of the N phase and the slab regions is thought to be a phase separation phenomenon. However, no such texture was observed for a sample with a top cover. I prepared two droplets of trimer **V-(9,9)** with different thicknesses on a glass slide and covered them with a glass. The thick droplet was touched with a cover glass, but the thin one was not. The temperature-dependent POM textures are portrayed in Fig.3-9 (b and c). The thin droplet (upper right in each figure) showed a dramatic change from the schlieren texture to the slab-like texture upon cooling toward the N–DC phase transition. No helical signature exists in the slab-like texture. However, the schlieren texture of the thick droplet (lower left in each figure) did not change until the N–DC transition. The slab-like texture is thought to originate from a phase separation induced at the air/liquid crystal interface. Fig.3-10 shows DSC thermograms of trimer **V-(9,9)**. A large enthalpy change at the N–DC phase transition was observed. The appearance of the slab-like texture observed by POM above the N–DC transition did not accompany an enthalpy change.

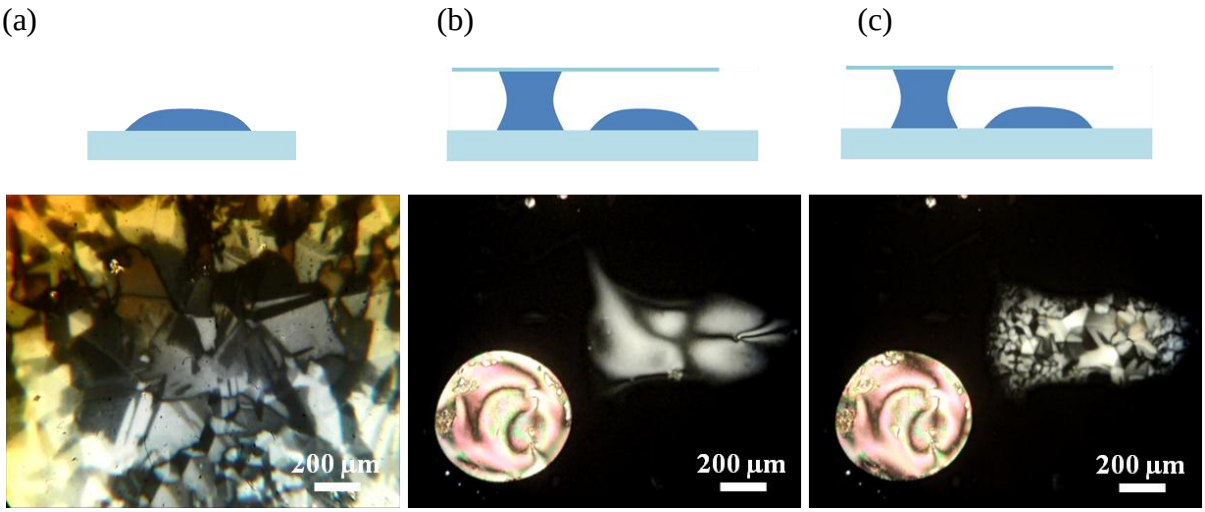

Fig.3– 9 (a) Polarized optical texture of trimer **V-(9,9)** on a glass plate without a cover glass at 135 °C. (b) Textures of two droplets of trimer **V-(9,9)** with different thicknesses sandwiched between glass layers at 146 °C, and (c) those at 134 °C. The lower left textures in (b and c) were those of a thick sample touched with a cover glass. There was no air/liquid crystal surface. The upper right textures were those of a thin sample untouched with a cover glass.

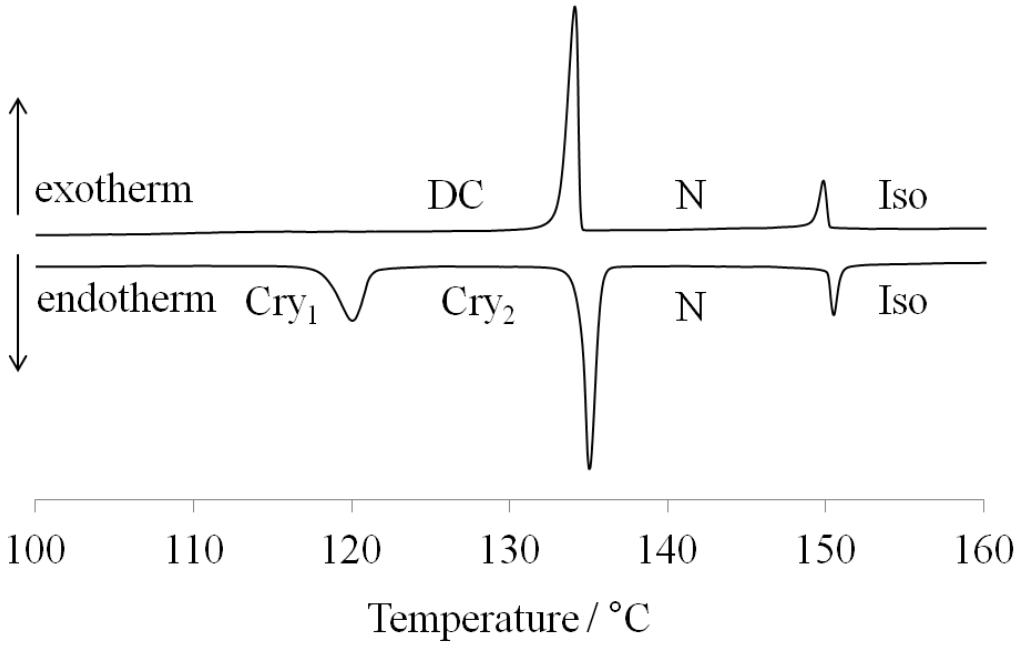

Fig.3– 10 DSC thermograms of trimer **V-(9,9)**. The rate of cooling and heating was 5 °C min^{-1}.

I then investigated the phase transition behavior of trimer **V-(9,9)** using X-ray diffraction. The X-ray diffraction profiles in the N and DC phases of trimer **V-(9,9)** are shown in Fig.3-11. The DC phase has a layer structure with a periodicity length of 63.1 Å. The extended molecular length for trimer **V-(9,9)** with all-trans conformation of the spacers is estimated using semiempirical calculations with MOPAC-6/PM3 as 73 Å. The difference between them is attributed to a twist conformation of the trimer.30 The correlation length along the layer normal is 549±7 Å, which corresponds to about 8–9 layers. Five reflections, 2θ = 13.4°, 17.4°, 18.5°, 20.3°, and 22.8° (the strong intensity), were observed in the wide-angle region, corresponding to the spacings of about 6.6 Å, 5.1 Å, 4.8 Å, 4.4 Å, and 3.9 Å, respectively. With respect to the N phase, a broad reflection around 2θ= 19.31 was observed in the wide-angle region. It corresponds to the spacing of about 4.6 Å. The lateral shortrange order like a smectic A phase exists even in the N phase, however, no layer ordering was detected. No diffraction peak corresponding to the slab-like texture was observed near the N–DC transition. I surmise that the slab-like texture is attributed to a pretransitional state in the N phase above the DC phase, which is caused by surface effects.

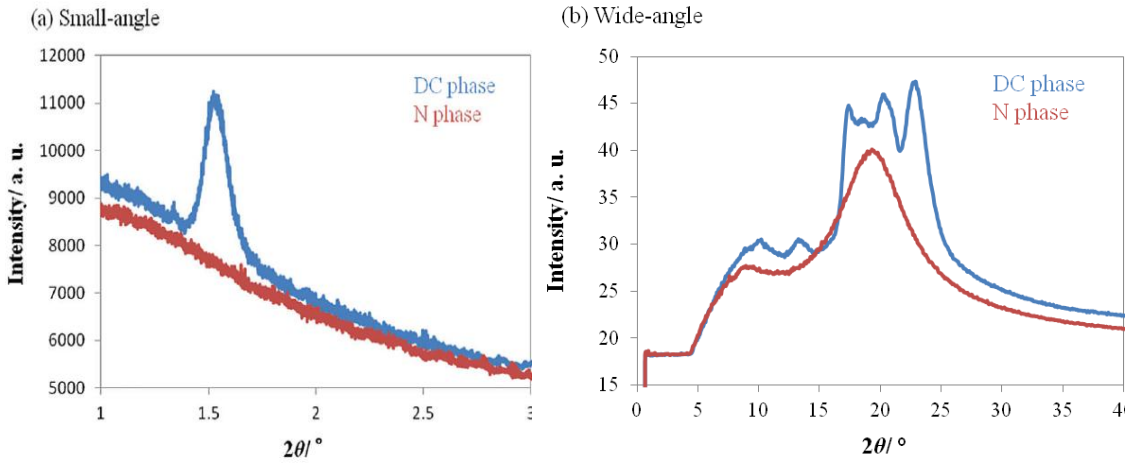

Fig.3– 11 (a) X-ray diffraction profiles of trimer **V-(9,9)** in the N at T_{NDC} = 5 K phase and the DC phase at T_{NDC} =－25 K in the small angle region and (b) those in the wide angle region. Blue lines show diffraction profiles in the DC phase. Red lines show those in the N phase.

I investigated how the spacer length of trimer **V-(n,m)** affects upon the periodic surface formation. Phase transition temperatures of the trimers under investigation are shown in Fig.3-12 Trimers **V-(7,7)**, **V-(7,9)**, and **V-(9,9)** showed N and DC phases, whereas trimer **V-(9,11)** exhibited another chiral conglomerate phase denoted as DC0 below the DC phase. The DC–DC0 phase transition was detected clearly as the discontinuous increase of the layer spacing by X-ray diffraction. Polarized optical textures of trimer **V-(9,11)** in the DC and DC' phases are shown in Fig.3-13.

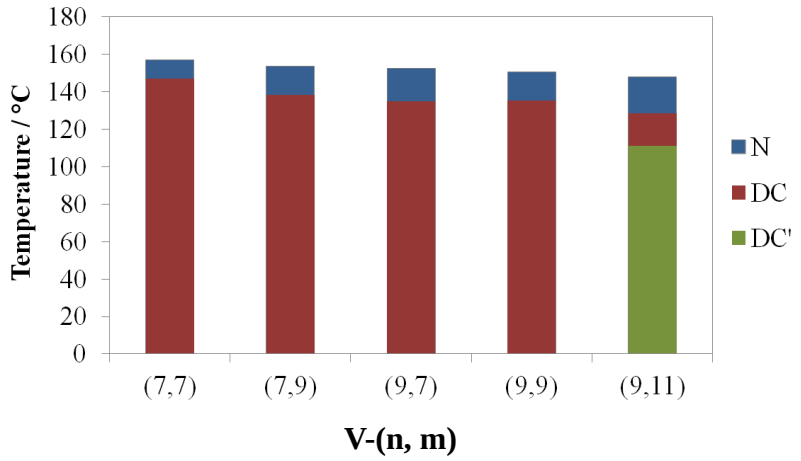

Fig.3– 12 Phase transition temperatures on cooling of trimers **V–(7,7)**, **V–(7,9)**, **V–(9,9)**, and **V–(9,11)**.

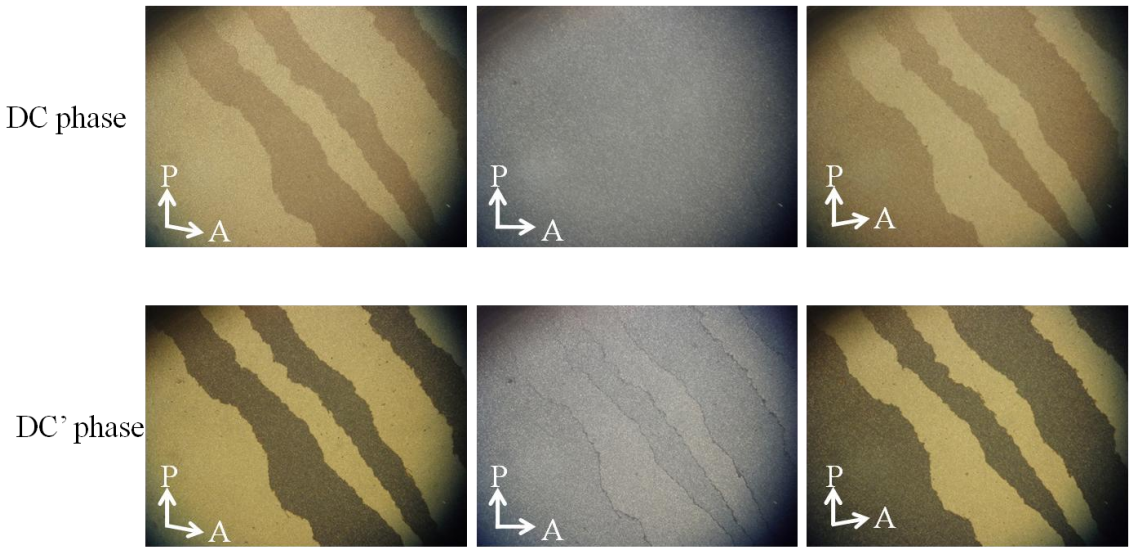

Fig.3– 13 Polarized optical textures of trimer **V–(9,11)** in the DC phase at 124 °C and those in the DC' phase at 90 °C.

Fig.3-14 presents AFM images of the surface structures of those trimers at room temperature. According to the POM observation, the AFM image for **V-(9,11)** is probably the surface structure of the supercooled DC phase. Dimple sizes, layer spacings, and the correlation lengths are presented in Table 1. Trimer **V-(7,7)** showed a disordered surface relief exhibiting dimples with 40±20 nm diameter, whereas trimer **V-(9,11)** showed a well-ordered surface relief exhibiting dimples with 140 ± 10 nm diameter. The dimple-size distribution becomes narrow and the distribution periodicity of the dimples becomes higher with increasing spacer length. The sample thickness strongly influences the formation of the TFCDs in the SmA phase[15,16]. With respect to the present system, the pattern formation did not depend on the sample thickness. No significant difference exists between the pattern formation at the centre of the LC droplet and that in the thinner part (Fig.3-15). In the AFM image of **V-(7,9)**, both disordered regions with small dimples as observed for **V-(7,7)** and ordered regions with large dimples as observed for **V-(9,9)** coexist. With respect to their layer structures in the DC phases, the layer spacing increases from 56.4 Å for **V-(7,7)** to 66.2 Å for **V-(9,11)** with increasing spacer length. The increase in layer spacing is attributed to the increase in molecular length. The correlation length also increases from 323 Å for **V-(7,7)** to 1055 Å for **V-(9,11)**. Larger layer blocks form larger dimples. The texture changes corresponding to the appearance of the intermediate state were seen for those trimers near the N–DC transition. However, the textures differed among the trimers. The texture changes will be investigated in detail.

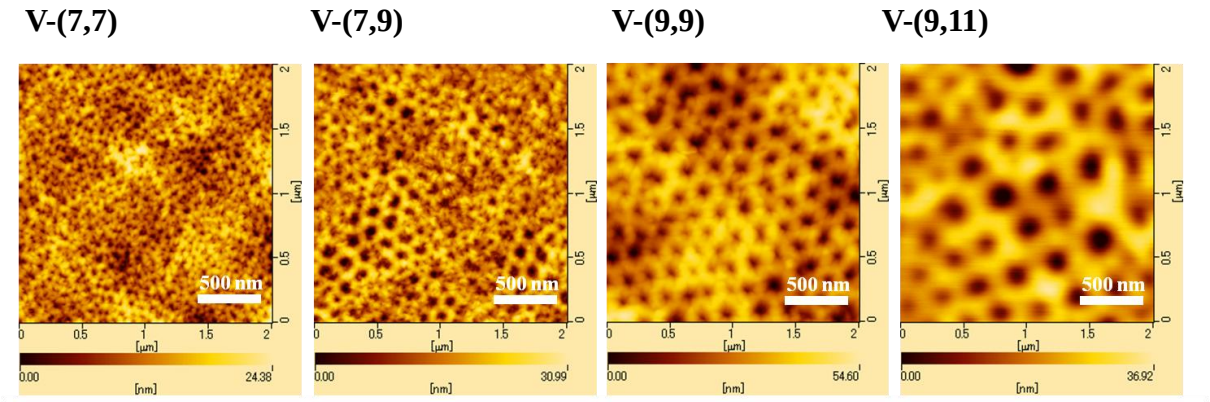

Fig.3– 14 AFM images of trimers **V-(7,7)**, **V-(7,9)**, **V-(9,9)**, and **V-(9,11)** in their chiral conglomerate phases at room temperature. Each image shows a microstructure at the air/liquid crystal interface of a droplet sample on an untreated glass substrate.

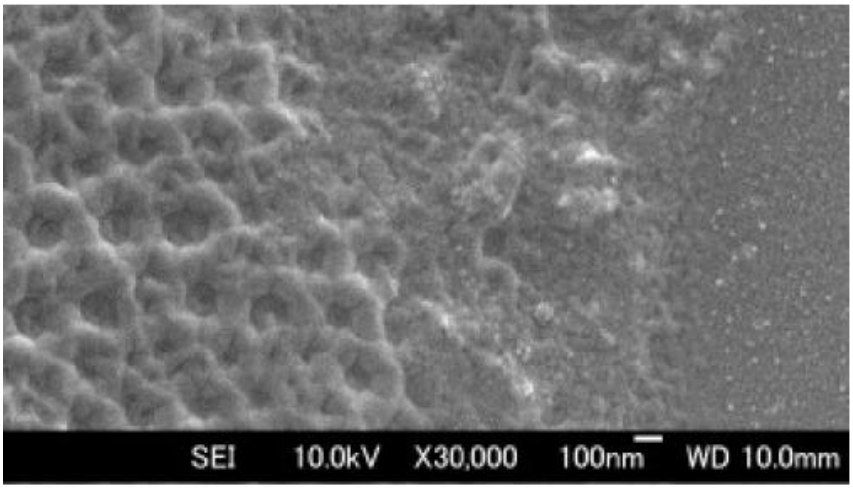

Fig.3– 15 SEM image of the surface pattern of trimer **V-(9,9)** in the thinner part of the LC droplet. The sample on an untreated glass substrate without a top cover was cooled to the DC phase.

Table 4– 1 Dimple sizes, layer spacings and correlation lengths of trimers **V-(7,7)**, **V-(7,9)**, **V-(9,9)**, and **V-(9,11)** in their DC phases

Compounds	Molecular length[a]/ Å	Dimple size[b]/nm	Layer spacing[c] / Å	Correlation length[c] / Å
V–(7,7)	68	40±20	56.4	323±4
V–(7,9)	71	65±35	60.7	377±22
V-(9,9)	73	95±15	63.1	549±17
V–(9,11)	76	140±10	66.2	1055±45

[a] Extended molecular length for each trimer with all-trans conformation of the spacers was estimated using semi-empirical calculations with MOPAC-6/PM3.

[b] Dimple sizes defined as half-depth diameter were ascertained from the AFM images.

[c] Layer spacings and correlation lengths for trimers **V-(7,7)**, **V-(9,9)** and **V-(9,11)** were obtained at $T - T_{NDC} = -5$ K, and those for trimer **V-(7,9)** at $T - T_{NDC} = -16$ K.

A marked difference exists between the AFM images of trimers **V-(7,7)** and **V-(9,9)**. I investigated the microstructures of trimer **V-(7,7)** using SEM. I also tried to observe those of trimer **V-(9,11)**, however, I could not get a clear SEM image because the sample was not stable against irradiation of the electron beams. Fig.3-16 shows SEM images of trimer **V-(7,7)** in the DC phase. Networks consisting of tangled tubes can be seen and they accompany small dimples. The surface structure seems to be a version of the disordered bicontinuous cubic phase. I observed the cross section area of trimer **V-(7,7)** in a similar method to that for trimer **V-(9,9)**. The SEM image is shown in Fig.3-17. The bulk structure of trimer **V-(7,7)** shows the networks consisting of tangled tubes accompanying small dimples, which resemble the surface structure as shown in Fig.3-16. The bulk structure is more disordered than the surface. A texture change also appeared in the N phase above the DC phase of trimer **V-(7,7)**, however, it was slight as shown in Fig.3-18. Dimple sizes at the surface for trimer **V-(7,7)** are much smaller than those for trimer **V-(9,9)**. Typical tube diameters are about 40–47 nm (Fig.3-16(a)). Those are close to the correlation length of the layer structures for trimer **V-(7,7)**.

(a) (b)

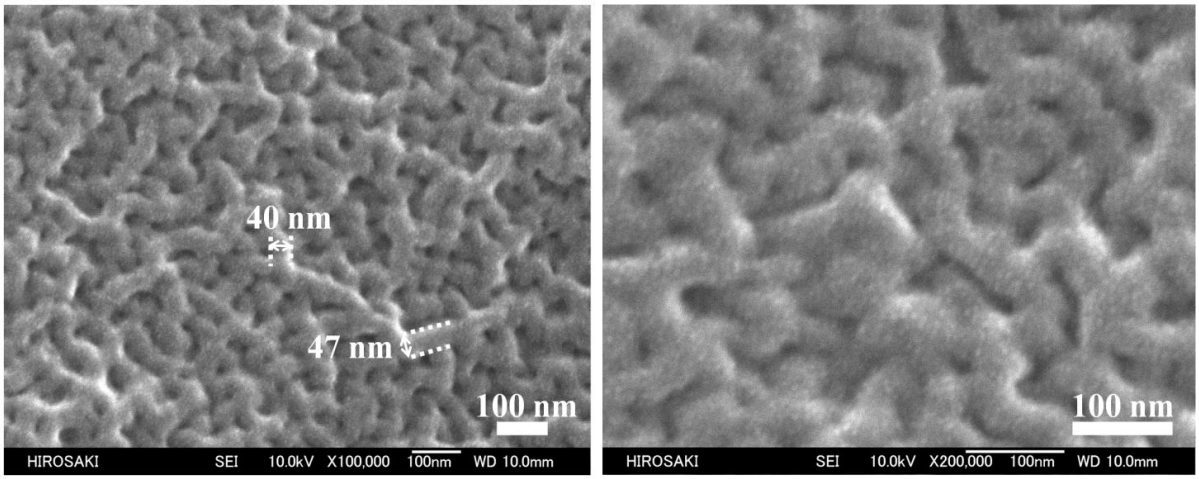

Fig.3– 16 (a) SEM image of the microstructure of trimer **V-(7,7)** at the air/liquid crystal interface of a droplet in the DC phase. (b) Higher magnification of the surface structure. The sample on an untreated glass substrate without a top cover was cooled to the DC phase.

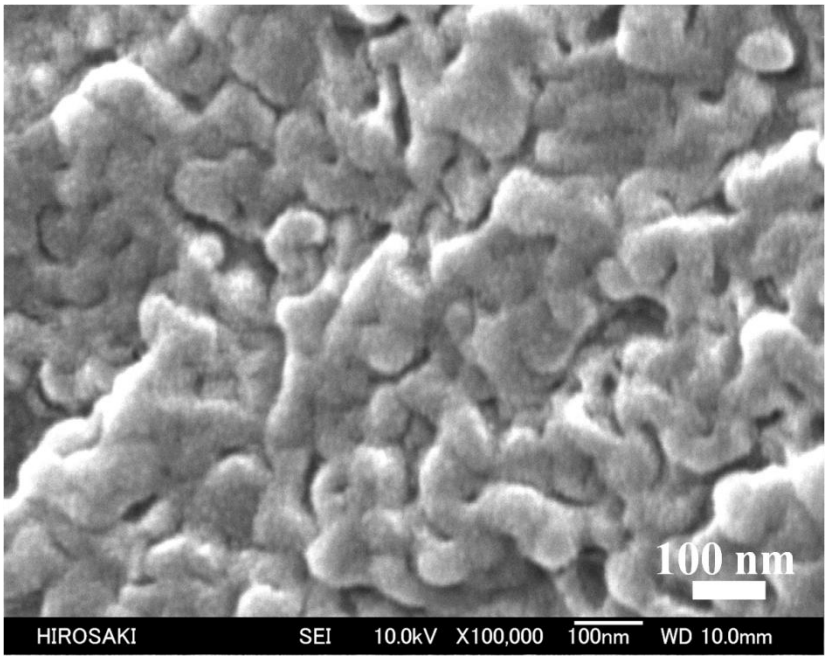

Fig.3– 17 SEM image of the cross section area of trimer **V-(7,7)**. The image for trimer **V-(7,7)** was obtained using a similar method to that for trimer **V-(9,9)**.

(a) (b)

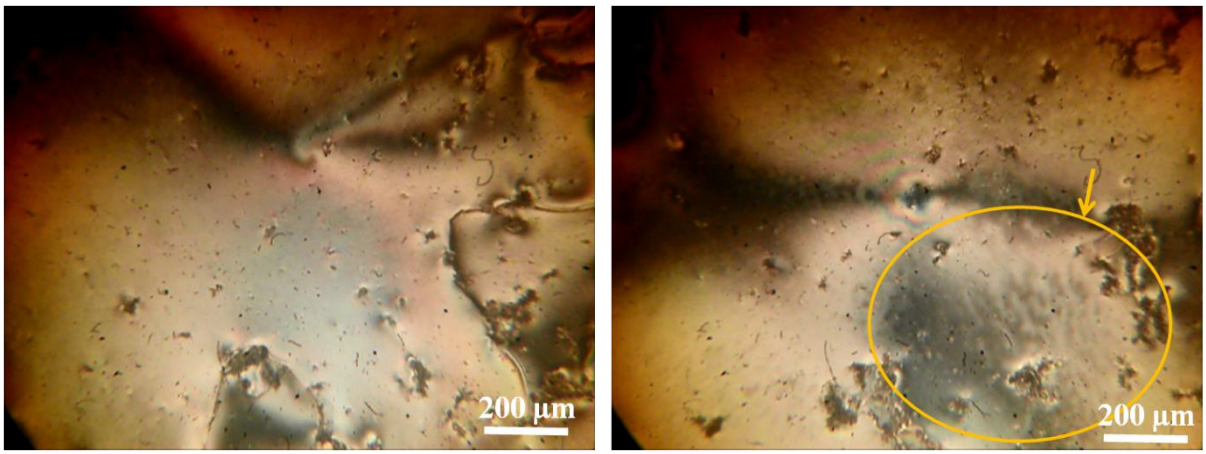

Fig.3– 18 (a) Polarized optical texture of **V–(7,7)** on a glass plate without a cover glass in the N phase. (b) Polarized optical texture in the N phase just above the DC phase. The circle indicates the appearance of the transient state.

I compare physical properties between trimers **V-(9,9)** and **V-(7,7)** to understand the molecular organization producing bicontinuous networks in this achiral trimer system. I reported that the conformation change of trimer **V-(7,7)** plays an important role in the appearance of the DC phase in our previous paper as follows. The trimer forms an achiral ground-state conformer in the nematic phase, but by intermolecular interactions between cores it adopts a twisted chiral conformer. The packing of helical conformers can produce macroscopic chirality in the DC phase. The twist conformation degree of the trimer can be described as a ratio of layer spacing (d) divided by molecular length (L). The d/L ratios for **V-(7,7)** and **V-(9,9)** are 0.83 and 0.86, respectively. With respect to XRD in the wide-angle region of trimer **V-(7,7)** in the DC phase, five reflections, 2θ = 14.8°, 19.4° (the strongest intensity), 20.0°, 23.5° and 27.5°, were observed, corresponding to the spacings of 6.0 Å, 4.6 Å, 4.4 Å, 3.8 Å, and 3.2 Å, respectively[13]. The intralayer spacings for trimer **V-(9,9)** are significantly longer than those for trimer **V-(7,7)**, suggesting that the packing of molecules in each layer for trimer **V-(9,9)** is looser than that for trimer **V-(7,7)**. With respect to the N phase of trimer **V-(7,7)**, a broad reflection around 2θ = 21.4° was observed in the wide-angle region. It corresponds to the spacing of about 4.2 Å, which is shorter than that for trimer **V-(9,9)**. Trimer **V-(7,7)** shows the smaller d/L and shorter intralayer spacings than trimer **V-(9,9)**, indicating that trimer **V-(7,7)** has stronger twisting power than trimer **V-(9,9)**. The correlation length of layer periodicity for trimer **V-(7,7)** is shorter than that for trimer **V-(9,9)**, indicating that trimer **V-(7,7)** has weaker desire for layer ordering than **V-(9,9)**. Therefore, tubes consisting of layer ordering might be twisted and might get entangled with each other on the surface of trimer **V-(7,7)**.

Although trimer **V-(9,9)** exhibited some disordered regions as described above, I focus on the surface exhibiting wellordered voids and discuss the surface pattern formation. The bulk shows a sponge-like structure. The interfacial tension at the air/liquid crystal interface induces slab-like regions in the N phase just above the N–DC transition of trimer **V-(9,9)**. As discussed above, a bicontinuous cubic structure was proposed for the DC phase separated from the nematic 8CB in mixtures of W624[24]. In a droplet of trimer **V-(9,9)**, I surmise that interfacial tension induces phase separation, which results in a gyroid-like bicontinuous cubic structure in the surface as follows. Smectic liquid-crystalline molecules tend to align homeotropically at an air/liquid crystal interface[15,16]. The schlieren texture as shown in Fig.

9(b) reveals that the trimermolecules form a planar alignment in the N phase. Near the N–DC transition, the interfacial tension can enhance the desire for the trimer molecules to align homeotropically to induce slab-like regions. The slab-like regions have higher molecular density than the other regions in the N phase. However, they exhibit neither layer ordering nor optical activity. Upon cooling to the DC phase, layer ordering occurs and then the layers are helically deformed at the surface, which produce an ordered cubic structure. On the other hand, both layer formation and helical ordering of the trimermolecules occur simultaneously in the bulk. The competition between those ordering induces frustration in the system, which can be released by layer deformation to the sponge-like structure in the bulk. Fig.3-19 shows a model for the bicontinuous triply branching of the gyroid-like surface for trimer **V-(9,9)**. The lengths of the connected regions between adjacent branchings are 57–79 nm (Fig. 5(b)). The correlation length for **V-(9,9)** is 55 nm. I assume that two helically deformed layer structures consisting of about 8–9 layers coexist in each unit block. The branch periodicity of the biscontinuous network in the DC phase for trimer **V-(9,9)** is much longer than that in cubic phases for lyoropic and thermotropic liquid crystals [25,30]. The helical interpenetration of each layer structure might occur between adjacent branchings, which grows to the bicontinuous network possessing well-ordered voids. On the other hand, trimer **V-(7,7)** has the shorter layer correlation length and the stronger twisting power than trimer **V-(9,9)**. Therefore, tubes consisting of layer ordering are twisted and tangled with each other to form disordered bicontinuous networks. A comparison of structure–property relationships between trimers **V-(7,7)** and **V-(9,9)** suggests that the stronger twisting power of trimer **V-(7,7)** causes the larger layer deformation to produce a more disordered cubic network than trimer **V-(9,9)**. The twist conformation of flexible trimer **V-(n,m)** can cause helical layer deformation, which produces a bicontinuous cubic network exhibiting optical activity.

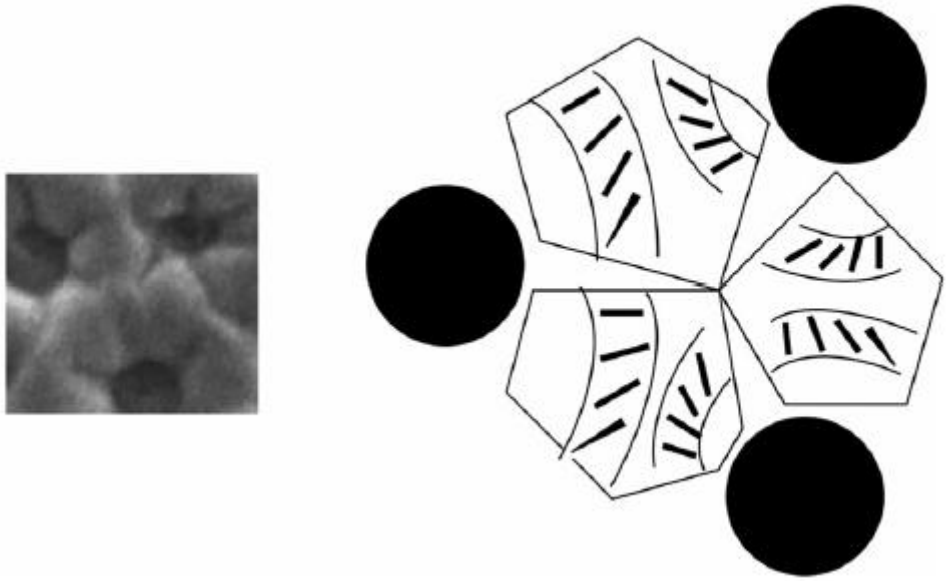

Fig.3– 19 Model for the bicontinuous triple branching of the gyroid-like surface of trimer **V-(9,9)**.

3.4. Conclusion

I investigated both surface and bulk structures of achiral flexible trimers possessing odd-numbered spacers in the soft crystalline DC phase. The trimers were found to formbicontinuous networks in the DC phase. In particular, trimer **V-(9,9)** exhibits a single gyroid-like surface accompanying periodic distribution of dimples with a size of about 100 nm. The DC phase is apparently a solid phase, however, it shows a sponge-like structure in the bulk of the material. The phase separation induced at the air/liquid crystal interface produces the ordered cubic surface. The dimple size on the surface changes from 40 nm to 140 nm relative to the spacer length. The twist conformation of flexible trimer **V-(n,m)** can cause layer deformation, which produces a bicontinuous network exhibiting optical activity. Furthermore, the soft crystalline chiral conglomerate phase forming porous structures is a promising new candidate for producing nanostructured composites.

3.5. Reference

[1] C. Tschierske and G. Ungar, *ChemPhysChem*, 2016, **17**, 9.

[2] V. L. Khoa, H. Takezoe, F. Araoka, *Adv. Mater*., 2017, **29**, 1602737.

[3] D. Chen, Y. Shen, C. Zhu, L. E. Hough, N. Gimeno, M. A. Glaser, J. E. Maclennan, M. B. Ros, N. A. Clark, *Soft Matter*, 2011, **7**, 1879.

[4] D. Chen, M.-S. Heberling, N. Nakata, L. E. Hough, J. E. Maclennan, M. A. Glaser, E. Körblova, D. M. Walba, J. Watanabe, N. A. Clark, *ChemPhysChem*, 2012, **13**, 155.

[5] H. Kim. S. Lee, T. J. Shin, Y. J. Cha, E. Körblova, D. M. Walba, N. A. Clark, S. B. Lee, N. A. Clark, D. K. Yoon, *Soft Matter*, 2013, **9**, 6185.

[6] S. H. Ryu, H. Kim, S. Lee, Y. J. Cha, T. J. Shin, H. Ahn, E. E. Körblova, D. M. Walba, N. A. Clark, S. B. Lee, D. K. Yoon, *Soft Matter*, 2015, **11**, 7778.

[7] D. K. Yoon, Y. Yi, Y. Shen, E. Körblova, D. M. Walba, I. I. Smalyukh, N. A. Clark, *Adv. Mater*., 2011, **23**, 1962.

[8] F. Araoka, G. Sugiyama, K. Ishikawa, H. Takezoe, *Adv. Funct. Mater.*, 2013, **23**, 2701.

[9] T. Ueda, S. Masuko, F. Araoka, K. Ishikawa, H. Takezoe, *Angew. Chem., Int. Ed.*, 2013, **52**, 6863.

[10] H. Kim, S. Lee, T. J. Shin, E. Körblova, D. M. Walba, N. A. Clark, S. B. Lee, D. K. Yoon, Proc. *Natl. Acad. Sci. U. S. A.*, 2014, **111**, 14342.

[11] J. Matraszek, N. Topnani, N. Vaupotič, H. Takezoe, J. Mieczkowski, D. Pociecha, E. Gorecka, *Angew. Chem., Int. Ed.*, 2016, **55**, 3468.

[12] D. Chen, C. Zhu, H. Wang, J. E. Maclennan, M. A. Glaser, E. Körblova, D. M. Walba, J. A. Rego, E. A. Soto-Bustamante, N. A. Clark, *Soft Matter*, 2013, **9**, 462.

[13] H. Sasaki, Y. Takanishi, J. Yamamoto, A. Yoshizawa, *Soft Matter*, 2016, **12**, 3331.

[14] A. Yoshizawa, Y. Kato, H. Sasaki, Y. Takanishi, J. Yamamoto, *J. Phys. Chem. B*, 2016, **120**, 4843.

[15] M. C. Choi, T. Pfohl, Z.Wen, Y. Li, M. W. Kim, J. N. Israelachvili, C. R. Safinya,

Proc. *Natl. Acad. Sci. U. S. A.*, 2004, **101**, 17340.

[16] Y. H. Kim, D. K. Yoon, M. C. Choi, H. S. Leong, M. W. Kim, O. D. Lavrentovich, H.-T. Jung, *Langmuir*, 2009, **25**, 1685.

[17] V. Luzzati and P. A. Spegt, *Nature*, 1967, **215**, 701.

[18] V. Luzzati, A. Tardieu, T. Gulik-Krzywicki, E. Rivas, F. Reiss-Husson, *Nature*, 1968, **220**, 485.

[19] T. S. Bailey, C. M. Hardy, T. H. Epps, III, F. S. Bates, *Macromolecules*, 2002, **35**, 7007.

[20] M. Takenaka, T. Wakada, S. Akasaka, S. Nishitsuji, K. Saijo, H. Shimizu, M. I. Kim, H. Hasegawa, *Macromolecules*, 2007, **40**, 4399.

[21] K. Michielsen and D. Stavenga, *J. R. Soc., Interface*, 2008, **5**, 85.

[22] P. Vukusic and J. R. Sambles, *Nature*, 2003, **424**, 852.

[23] M. R. J. Scherer, Double-Gyroid-Structural Functinal Materials, Synthesis and Applications, *Springer, Switzerland*, 2013, pp. 7–19.

[24] D. Chen, Y. Shen, J. Aguero, E. Körblova, D. M. Walba, N. Kapernaum, F. Giesselmann, J. Watanabe, J. E. Maclennan, M. A. Glaser, N. A. Clark, *ChemPhysChem r* , 2014, **15**, 1502.

[25] J. M. Seddon and R. H. Templer, in Handbook of Biological Physics, ed. R. Lipowsky and E. Sackmann, *Elsevier,* 1995, pp. 97–160.

[26] J. Yamamoto, I. Nishiyama, M. Inoue, H. Yokoyama, *Nature*, 2005, **437**, 525.

[27] Y. Matsuo, Y. Sato, T. Niinomi, I. Soga, H. Tanaka, E. Nakamura, *J. Am. Chem. Soc.*, 2009, **131**, 16048.

[28] D. M. Walba, *US Pat.*, 8963140 B2, 2013.

[29] R. A. Callahan, D. C. Coffey, D. Chen, N. A. Clark, G. Rumbles, D. M. Walba, *ACS Appl. Mater. Interfaces*, 2014, **6**, 4823.

[30] G. Ungar, F. Liu and X. Zeng, in *Handbook of Liquid Crystals*, ed. J. W. Goodby, P. J. Collings, H. Gleeson, P. Raynes, C. Tschierske and T. Kato, Wiley-VCH Verlag, Weinheim, 2014, vol. 5, ch. 7, pp. 363–436.

CHAPTER 4

Photo-driven chirality switching in a dark conglomerate phase of an achiral liquid crystal trimer

4.1. Introduction

Much research has focused on the chiral conglomerate phases not only for the spontaneous mirror symmetry breaking but also for their nanostructures[1,2]. The network in DC phases can act as a porous nanoconfinement medium to produce nanocomposites for applications, such as semiconductors and photovoltaics[3,4]. Results of earlier studies have demonstrated that the smectic layers of both the sponge and HNF phases of bent-core liquid crystals tend to have saddle splay curvature[5,6]. The optical activity in both phases is attributable to the layer chirality[7] or the coupling of molecular conformational chirality to the layer chirality[8]. The tilt organization of bent-core molecules in the layers drives the twisting of those layers to produce the saddle splay curvature which can relieve the stress in the layer structures. We reported a homologous series of achiral liquid crystal trimers exhibiting soft crystalline DC phases in chapter 2[9]. The driving force of the appearance of the DC phases is a conformation change of the flexible trimer, which differs greatly from that of bent-core systems. Furthermore, with respect to trimer with nonylmethylene spacers, a gyroid-like surface and a sponge-like structure inside of the material were observed as denoted in the chapter 3[10]. The appearance of the gyroid-like surface at the air/liquid crystal interface is explained in terms of the stepwise formation, i.e., layer ordering is induced by the surface tension and then the layers are helically deformed to form a saddle splay curvature. On the other hand, both occur simultaneously inside of the material to produce the sponge-like structure. If layer formation and layer twisting in the bulk material could be separated by an external field, it may control a nanostructure in DC phases consisting of saddle splay layer structures. I applied photo-irradiation as the external field.

Photo-induced isomerization of an azobenzene unit is well known to cause a remarkable change in the physical properties of liquid crystals[11–13]. For example, the *trans* isomer of a liquid crystal possessing an azobenzene unit forms a rod-like shape to stabilize the nematic phase, while the *cis* isomer forms to a bent shape to destabilize the phase structure, as shown in Fig.4-1. Thus, the nematic-isotropic liquid transition temperature a nematic liquid crystal with *cis* form is much lower than that with the *trans* form.

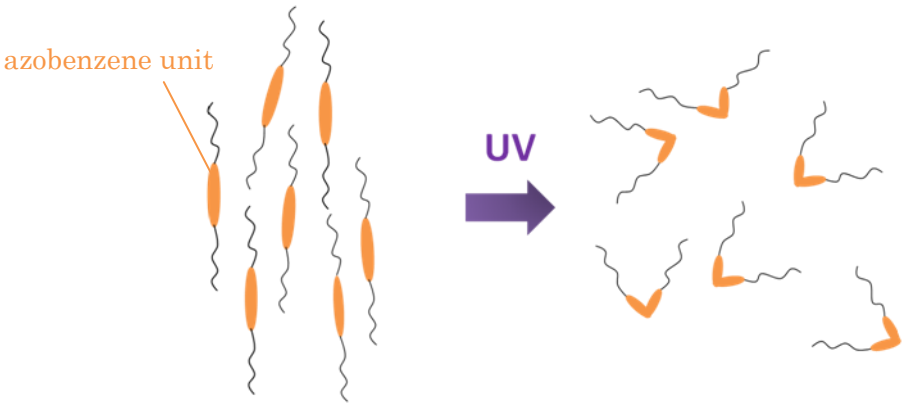

Fig.4– 1 Process of photoinduced phase transition of an azobenzene-based compound.

Recently, the HNF phase to Iso phase transition was reported to be observed for azobenzene-based dimers with an odd-numbered spacer by irradiation with UV light (λ = 365 nm)[14]. If UV light is switch off, the dimer returns from isotropic phase to the HNF phase directly, although the dimer exhibits N and SmC phases in the temperature sequence. The HNF phase formed directly from the isotropic liquid has its fibers oriented differently than when it is formed from the SmC phase. Thus, formation of the HNF phase by azobenzene-based dimers gives the possibility for obtaining a new type of nano-system controlled by light. Azobenzene-based achiral liquid crystal dimer CB6OABOBu was found to show an isothermal N_{TB}-N phase transition when illuminated by UV light. It is driven by the photoisomerization of the azo linkage generating the *cis* isomer[15]. This photoinduced phase transition increases symmetry order of the system. Alaasar et al. reported that the SmA phase to chiral isotropic liquid transition is induced by photoisomerization of achiral polycatenar compounds involving an azobenzene group[16]. In this case mirror-symmetry breaking takes place at the transition by UV irradiation from a higher order phase (SmA phase) to a lower order phase (chiral isotropic liquid ; Iso[*]). It is contrary to common knowledge, where symmetry breaking occurs at the transition from lower to higher order, for example, crystallization from solutions or melts.

Achiral trimer **V-(9,9)** shows a phase sequence of Iso-N-DC as described in chapter 2[9]. I replaced the biphenyl unit of the trimer by a photoisomerizable azobenzene unit as shown in Fig.4-2. I report in this chapter that the soft crystalline DC phase of a newly designed trimer changes to an achiral liquid crystalline phase consisting of layer structures with short

correlation length with the introduction of UV irradiation. I discuss how this photo-driven chirality switching occurs. Furthermore, I applied the reversible chirality switching to control the nanostructure of the DC phase.

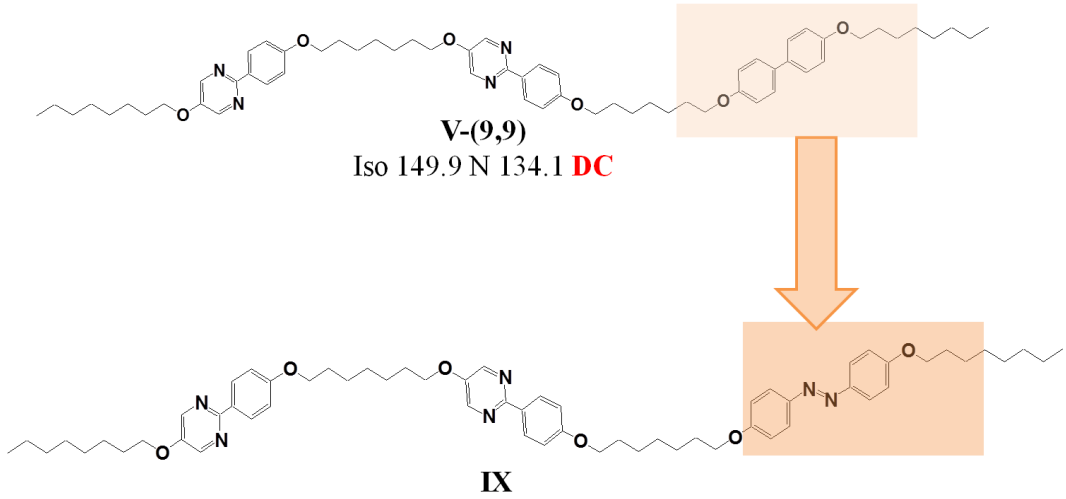

Fig.4– 2 Molecular design of photosensitive trimer **IX.**

4.2. Experimental

4.2.1. Preparation of materials

For use in this study, 5-hydroxy-2-(4-hydroxyphenyl) pyrimidine was purchased from Midori Kagaku Co. Ltd. The purity of the trimer **IX** was checked by elemental analysis (EA 1110; CE Instruments Ltd). Confirmation of the structures of intermediates and products was obtained by infrared (IR) spectroscopy (BIO RAD FTS-30) and proton nuclear magnetic resonance (^{1}H NMR) spectroscopy (JEOL JNM-ECA500).

In the reporting of IR data, the following abbreviations have been used.

str. stretching

In the reporting of ^{1}H NMR data, the following abbreviations have been used.

s. singlet

d. doublet

t. triplet

m. multiplet

The analyses of the structure of the product by means of spectroscopic methods were found to be consistent with the predicted structure.

4.2.1.1.

2-{4-[9-(4-(4-octyloxyazobenzene-4'-yloxy)nonyloxy)phenyl]-5-{9-[4-(5-octyloxypyrimidin-2-yl)phenyloxy]nonyloxy}pyrimidine (IX)

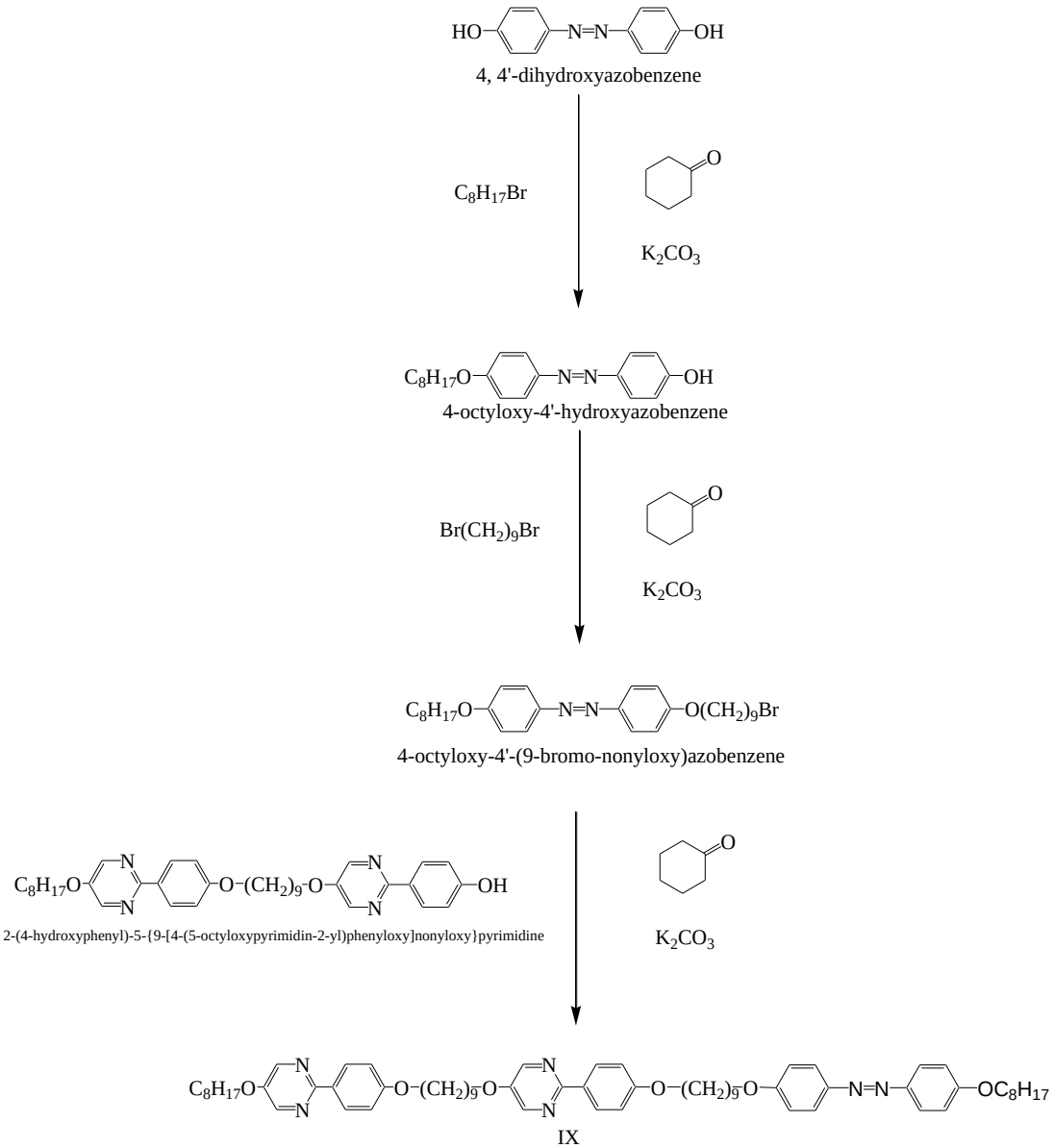

Scheme4– 1 Preparation of trimer **IX**

4-Aminophenol (37.4 mmol, 4.08g) was dissolved in hydrochloric acid (6 mol/L, 10.3 mL) and water (10.3 ml). Aqueous sodium nitrate ($NaNO_2$: 42.5 mmol, 2.85g and H_2O : 8.75ml) was added dropwise to the aminophenol solution while stirring at 0 ºC. Phenol (37.5 mmol, 3.41g) was dissolved in a sodium hydroxide solution (9.38 mmol, 3.75g in 3.5mL water), and cooled to 0°C. The aminophenol/sodium nitrate solution was added dropwise to the phenolate. Concentrated hydrochloric acid was added until the pH reached 1, and the mixture was allowed to stir at 0 ºC for 2 h. The blackish-brown precipitate was then filtered off and dried overnight. Then, the residue was purified using column chromatography on silica gel with a toluene : ethyl acetate (1 : 1) mixture as an eluent. Yield 1.49 g (18.6 %)

Potassium carbonate (3.00 mmol, 415 mg) was added to a solution of 4, 4'-dihydroxyazobenzene (3.75 mmol, 803 mg) and 1-bromooctane (3.00 mmol, 579 mg) in cyclohexanone (20 ml). The reaction mixture was stirred at 95 °C for 10 h. After filtration of the precipitate, the solvent was removed by evaporation. Then, the residue was purified using column chromatography on silica gel with a toluene : ethyl acetate (20 : 1) mixture as an eluent. The obtained solid was recrystallized from hexane to give 4-octyloxy-4'-hydroxyazobenzene. Yield 449 mg (46 %).

Potassium carbonate (1.25 mmol, 180 mg) was added to a solution of 4-octyloxy-4'-hydroxyazobenzene (1.25 mmol, 424 mg) and 1,9-dibromononane (1.63 mmol, 465 mg) in cyclohexanone (20 ml). The reaction mixture was stirred at 95 °C for 5 h. After filtration of the precipitate, the solvent was removed by evaporation. Then, the residue was purified using column chromatography on silica gel with a toluene : hexane (10 : 1) mixture as an eluent. The obtained white solid was recrystallized from ethanol to give 4-octyloxy-4'-(9-bromononyloxy)azobenzene. Yield 383 mg (56 %).

Potassium carbonate (0.15 mmol, 21 mg) was added to a solution of 4-octyloxy-4'-(9-bromo-nonyloxy)azobenzene (0.15 mmol, 80 mg) and 2-(4-hydroxyphenyl)-5-{9-[4-(5-octyloxypyrimidin-2-yl)phenyloxy]nonyloxy}pyrimidine (0.15 mmol, 92 mg) in cyclohexanone (10 ml). The reaction mixture was stirred at 130 °C for 10 h. After filtration of the precipitate, the solvent was removed by evaporation. Then, the residue was washed with hot ethanol and was recrystallized from toluene to give the desired compound. Yield 116 mg (73 %).

^{1}H NMR (500 MHz, $CDCl_3$, TMS): δ= 8.39 (s, 4H, Ar–**H**), 8.25 (d, 4H, Ar–**H**, *J* = 8.6 Hz), 7.85 (d, 4H, Ar–**H**, *J* = 8.6 Hz), 6.98 (d, 4H, Ar–**H**, *J* = 8.0 Hz), 6.96 (d, 4H, Ar–**H**, *J* = 7.5 Hz), 4.06 (t, 4H, –OC**H**$_2$–, *J* = 6.3 Hz), 4.02 (t, 4H, –OC**H**$_2$–, *J* = 6.3 Hz), 4.01 (t, 4H, –OC**H**$_2$–, *J* = 6.3 Hz), 1.84–1.78 (m, 12H, aliphatic-**H**), 1.49–1.29 (m, 40H, aliphatic-**H**), 0.89 (t, 6H, –C**H**$_3$, *J* = 6.3 Hz).

IR(KBr): ν cm^{-1}: 2934, 2852 (C–H str), 1606, 1581, 1544, 1500, 1434 (C=C, C=N str), 1249 (C–O str).

Elemental analysis calc. for $C_{66}H_{90}N_6O_6$: C,74.54; H, 8.53 ; N, 7.90. Found C, 74.55; H, 8.53; N, 7.86.

4.2.2. Liquid-crystalline and physical properties

The initial phase assignments and corresponding transition temperatures for the final compound was determined by thermal optical microscopy using a polarizing microscope (BX-51; Olympus Optical Co. Ltd.) equipped with a temperature control unit (LK-600PM; Japan High Tech). The temperatures and enthalpies of transition for trimer **IX** were investigated using differential scanning calorimetry (DSC, DSC 6200 Seiko Instruments Inc.). The material was studied at a scattering rate of 5 °C min^{-1} for both cooling and heating after being encapsulated in aluminium pans. Homogeneous configuration cells with different cell gaps were purchased from E H C Co., Ltd. The inner surfaces was coated with a polyimide aligning agent and buffed unidirectionally. The XRD patterns of the homeotropically aligned sample during a cooling process were obtained using a real-time X-ray diffractometer (MicroMax−007HF; Rigaku Corp.) equipped with a hot stage and a temperature-control processor. A sample was put on a convex lens, which was then placed in a custom-made temperature-stabilized holder (stability within ±0.1 °C). A sample was irradiated using a UV light source of wavelength 365 nm. The UV-Vis absorption spectra of a chloroform solution of trimer **IX** (2.5 x 10^{-5} M) were measured using UV-vis spectrometer (V-670; JASCO Co. Ltd.) in transmission mode at room temperature. Field-emission scanning electron micrographs were obtained using a JEOL JSM-7000 FE-SEM with accelerating voltages of 5 or 10 keV. The sample was coated with platinum before being analyzed.

4.3. Results and discussion

4.3.1. Liquid crystalline properties of liquid crystal trimers

Fig.4-3 shows molecular structure, transition temperatures and associated enthalpies of transition for trimer **IX**. Trimer **IX** exhibited the N and DC phases on cooling. When heated the crystal melted to the N phase at 140 °C.

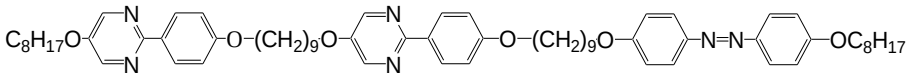

Trimer **IX**

Iso 160.7 (7.3) N 137.4 (36.5) DC 122.2 (23.0) Cr m.p. 140.0~140.7 °C

Fig.4– 3 Molecular structure, phase transition temperatures/°C and ΔH/kJmol^{-1} of trimer **IX**.

Fig.4-4 portrays the optical textures of trimer **IX** on a glass slide with a cover glass. The N phase with the schlieren texture was observed at 155 °C. Further cooling, the DC phase with a nearly dark texture appears under crossed polarizers. When observing the sample in the DC phase under slightly uncrossed polarizers (10°), the texture was split into darker and brighter domains (Fig.4-5, left). When uncrossing the polarizers in opposite directions at the same angle, the darker and brighter domains were switched (Fig.4-5 right). The domain brightness did not change by rotation of the sample between the polarizers. These results indicate that they have optical activity with opposite senses. Neither the N phase nor the Cry phase showed a chiral nature.

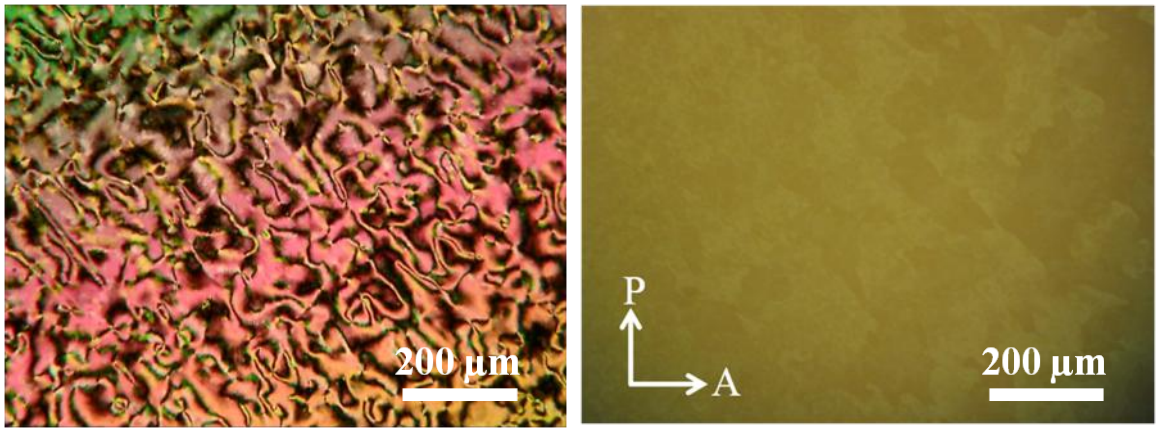

(a) N phase (155 °C) (b) DC phase (135 °C)

Fig.4– 4 Optical textures of trimer **IX** on cooling.

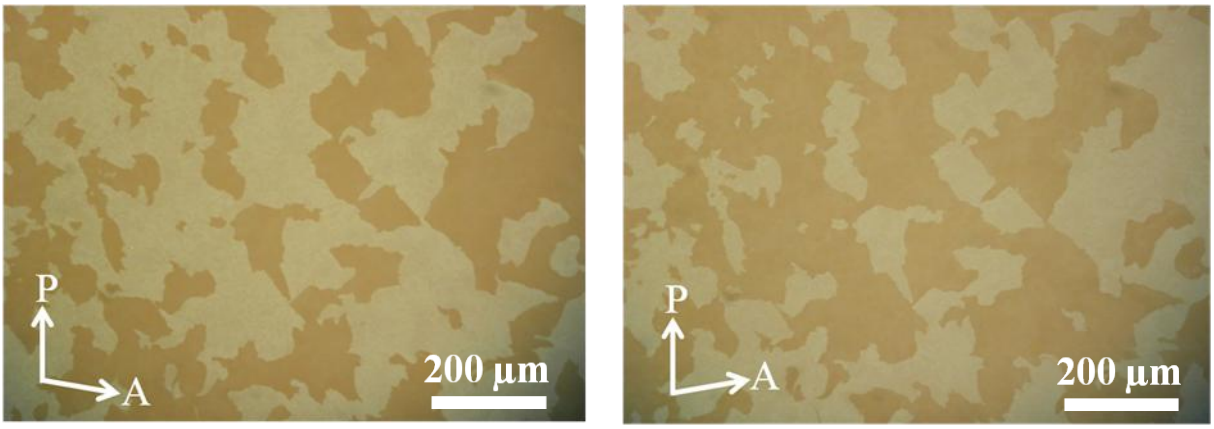

Fig.4– 5 Optical textures of trimer **IX** in the DC phase at 135 °C with uncrossed polarizers.

DSC measurements were carried out at a scanning rate of 5 °C/min for both cooling and heating cycles, and the results are shown in Fig.4-6. Enthalpy changes of the N-Iso, N-DC, DC-Cr transition were observed. They are coincident with transition behavior by observation of optical microscopy. The enthalpy change at the N-DC phase transition is larger than that at the DC-Cr transition, indicating the DC phase is a soft crystal phase.

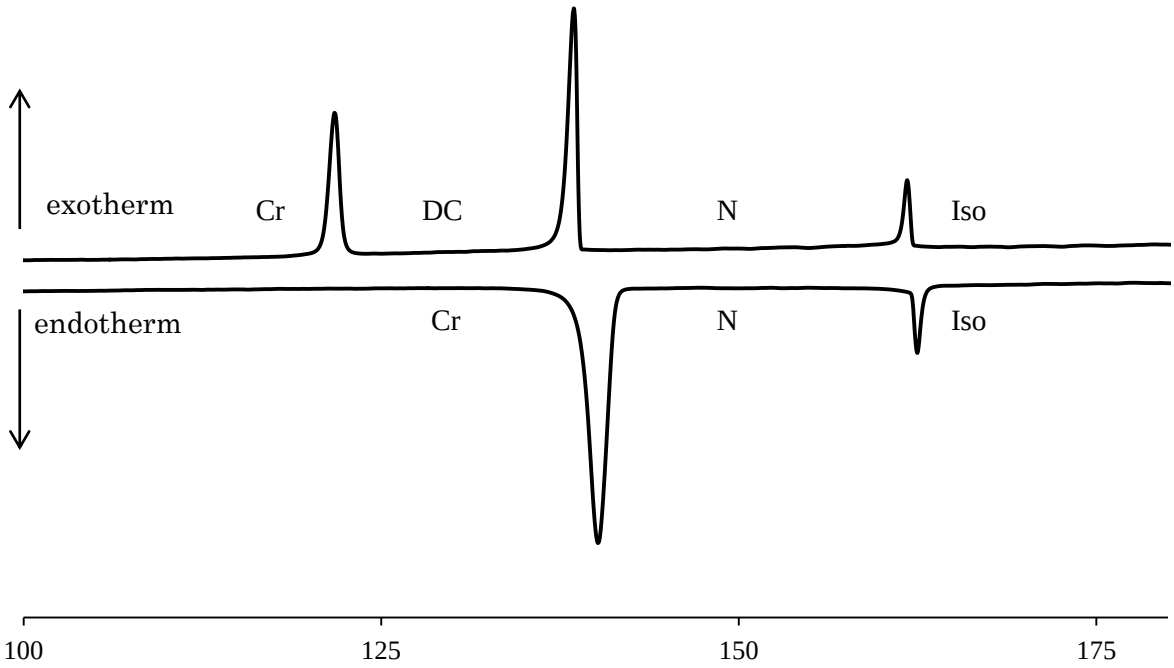

Fig.4– 6 DSC thermograms of trimer **IX**. The rate of cooling and heating was 5 °C min^{-1}.

Fig.4-7 (a) portrays an X-ray diffraction pattern in a small angle region of trimer **IX** in the DC phase. The weak and broad scattering was found as a circle. Fig.4-7 (b) shows the X-ray diffraction profiles in a small angle region of trimer **IX** in the N and DC phases. No diffraction peak was detected in the N phase. A peak at 2θ = 1.34° was observed in the DC phase, revealing that it has a layer structure with a periodicity length of 66.1 Å. Fig.4-8 depicts temperature dependence of the periodicity length in the DC phase and the crystal state of trimer **IX**. The layer spacing is independent of temperature in the DC phase, which shows a discontinuous increase at the DC-Cr phase transition at $T–T_{NDC}$= –12K. The layer spacing in the crystal was about 71 Å.

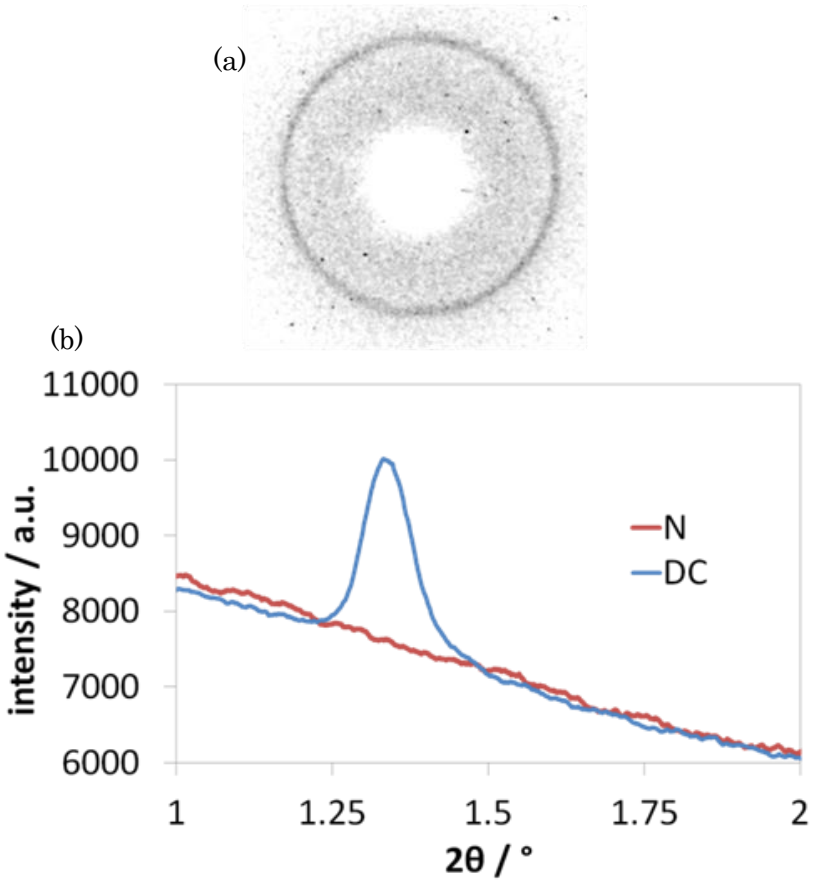

Fig.4– 7 (a) X-ray diffraction pattern of trimer **IX** in the DC phase. (b) X-ray diffraction profiles of trimer **IX** in the N phase (red line) and the DC phase (blue line) in the small-angle region.

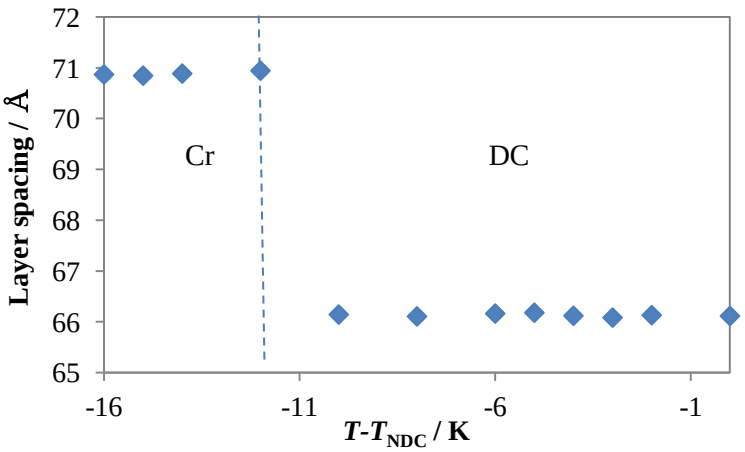

Fig.4– 8 Temperature dependence of the periodicity length in the DC and Cr phases of trimer **IX**.

The extended molecular length for all the spacers' *trans* conformation in trimer **IX** was estimated through semi-empirical calculations with MOPAC-6/PM3 to be 75 Å (Fig. 4-9(a)). The layer spacing in the DC phase is shorter than the molecular length. According to our previous report[9], the difference between them can be explained as follows. The DC phase has a monolayer structure. The *trans* azobenzene trimer **IX** forms a twisted shape in which some of the methylene units in the spacers adopt a gauche conformation in the DC phase (Fig. 4-9(b)). Intermolecular interactions are thought to induce the twisted shape, which is one origin of chirality in the trimer system. During the DC–Cry transition, the trimer is thought to change from the twist conformation to the extended one resulting in the Cry phase not showing a chiral nature.

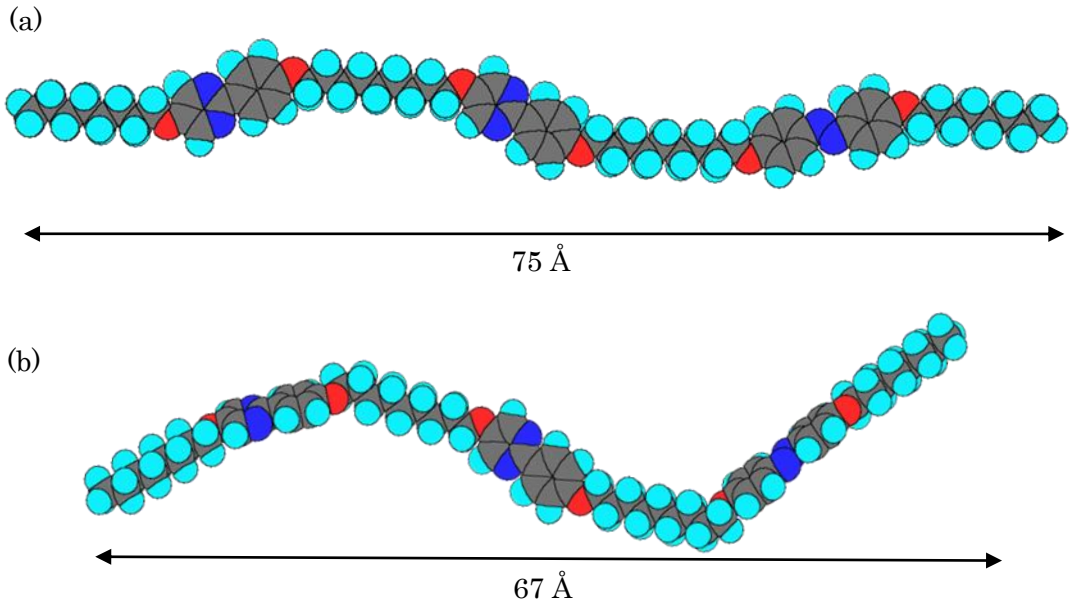

Fig.4– 9 (a) MOPAC model for an extended *trans*-azobenzene trimer, (b) that for a twisted *trans*-azobenzene trimer.

4.3.2. UV irradiation in the DC phase

The confined sample was exposed to UV irradiation in a 2.4 μm cell without surface treatment in the DC phase. Fig.4-10 depicts dependence of the optical texture of trimer **IX** with UV light (365 nm) at 135 °C as a function of irradiation intensity. Fig.4-10(a) shows the optical texture of the DC phase without UV irradiation. When UV irradiation intensity was 2.50 mW cm^{-2}, it changed to a fan shaped texture similar to that observed in smectic phases (Fig. 4-10(b)) for about 1 s. The smectic-like texture did not change during the UV irradiation. The light was switched off, and for about 1 s, the DC phase reappeared. Due to the high temperature (135 °C), the reversion time was short. With increasing the light intensity, the color of the texture changed from light green to brown (Figs. 4-10(b), 4-10(c) 4-10(d) and 4-10(f)), indicating that the optical anisotropy increases. Although some of the darker and brighter domains were switched when uncrossing the polarizers in opposite directions at the same angle (Fig. 4-11), the domain switch was also observed when rotating the sample between the crossed polarizers (Fig. 4-12). These results reveal that the photo-induced smectic-like phase does not have optical activity. It should be noted that trimer **IX** did not exhibit a smectic phase in the thermal phase transition. When the UV light intensity was 12.5 mW cm^{-2}, the color of the texture showed a slight blue shift and fluctuation appeared in the texture (Fig. 4-10(g)). This might reflect the pretransition to the N phase. When the sample was irradiated with UV light with an intensity of 16.3 mW cm^{-2}, the DC phase changed to the N phase showing the schlieren texture after going the smectic-like phase for a few ms (Fig. 4-10(h)). A few ms after the light was switched off the DC phase reappeared after passing through the smectic-like phase. Therefore, the photo-induced DC to N transition was also reversible. Furthermore, the sample changed to the isotropic liquid through the smectic-like and N phases when it was irradiated with UV light with an intensity of 25 mW cm^{-2} (Fig. 4-10(i)).

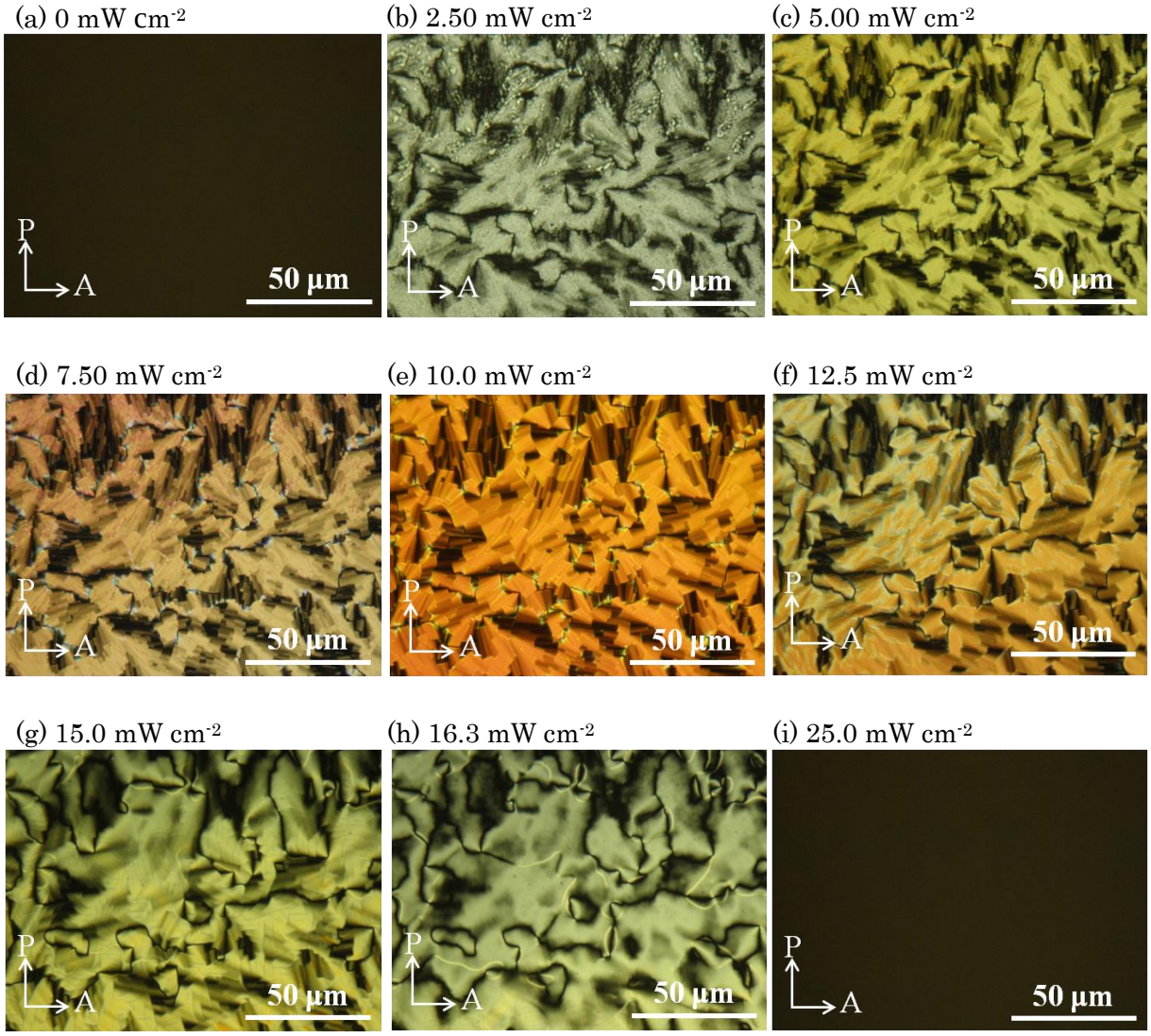

Fig.4– 10 Polarized optical textures of trimer **IX** confined in a 2.4 µm cell without surface treatment at 135 °C under exposed to UV light of different irradiation intensities.

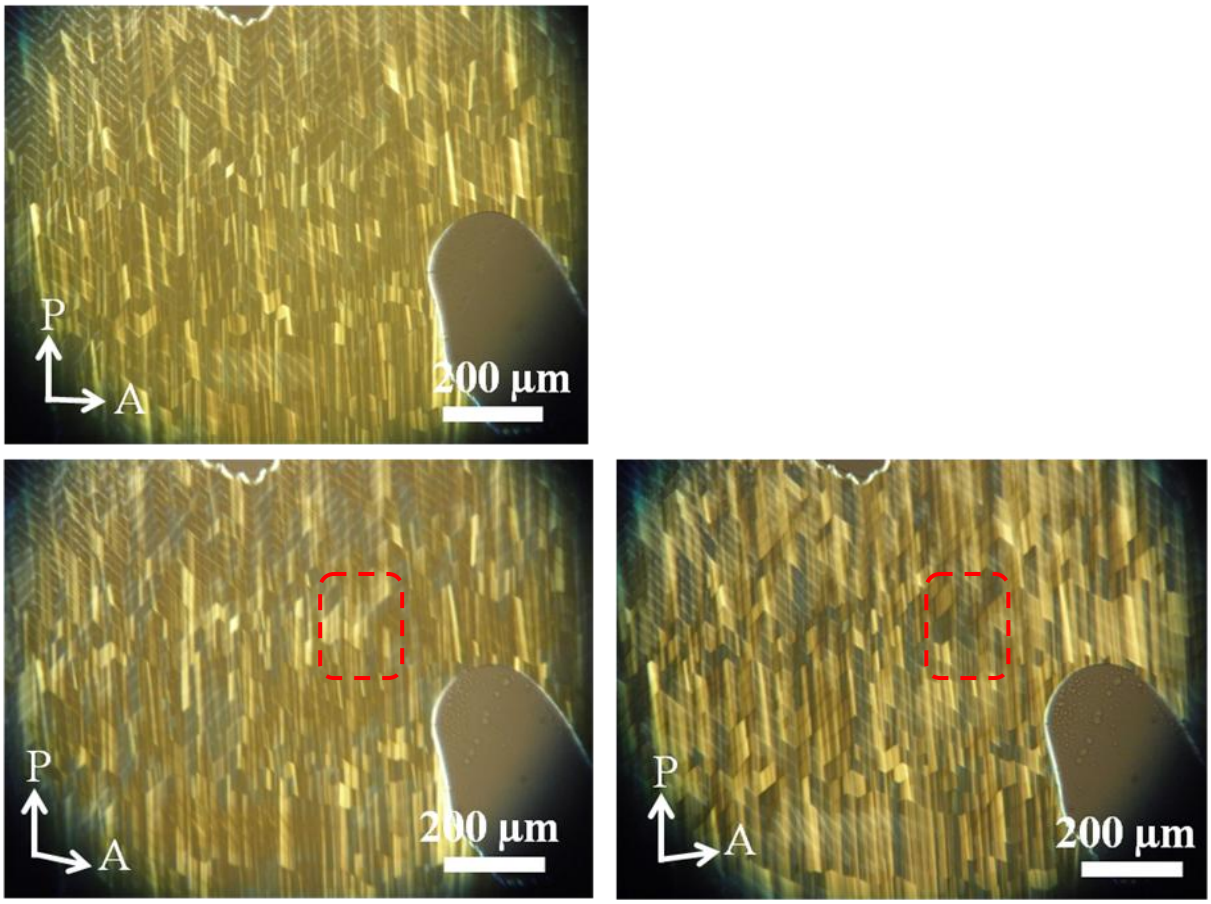

Fig.4– 11 Polarized optical textures of trimer **IX** confined in a 2 µm homogeneous cell in the photoinduced phase with UV (λ = 365 nm) at an intensity of 3 mW cm^{-2} at 135 °C under crossed and uncrossed polarizers.

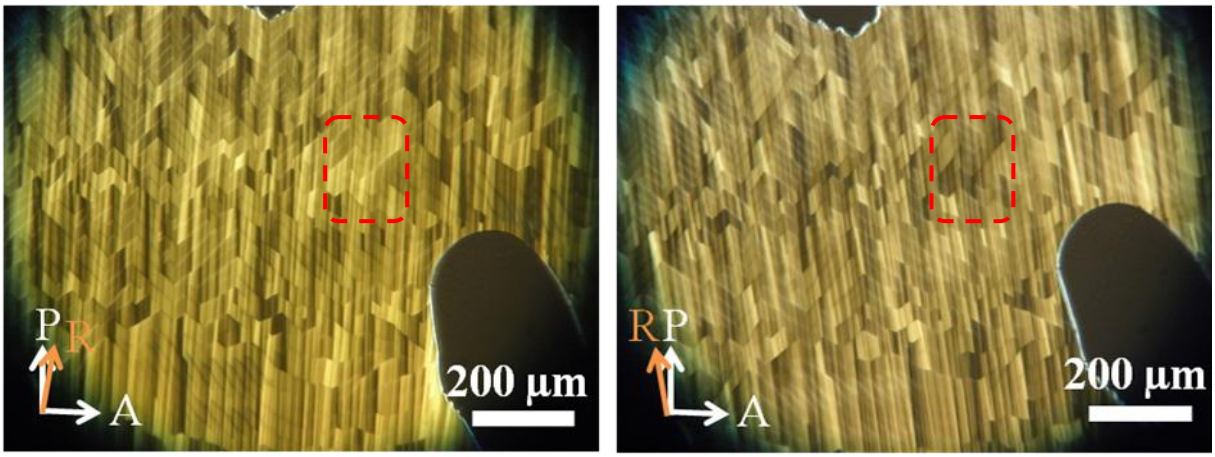

Fig.4– 12 Polarized optical textures of trimer **IX** confined in a 2 µm homogeneous cell in the photoinduced phase with UV (λ = 365 nm) at an intensity of 3 mW cm^{-2} at 135 °C when the sample was rotated clockwise and anticlockwise. R indicates the rubbing direction.

I measured the X-ray diffraction for the sample with UV irradiation. Fig.4-13 depicts the X-ray diffraction profiles in the small angle region of trimer **IX** as a function of UV irradiation intensity at 135 °C. Their XRD patterns are presented in Fig. 4-14. Obtained layer spacing and correlation lengths are listed in Table 4-1. The layer spacing does not change as the irradiation intensity increases but the correlation length decreases. With respect to the two dimensional XRD patterns in the smectic-like phase, weak and broad scattering appeared as a circle. Interestingly, they were the same as scattering from the optically isotropic DC phase. The phase structure of the photo-induced liquid crystalline phase is likely identical to that of the DC phase except chirality.

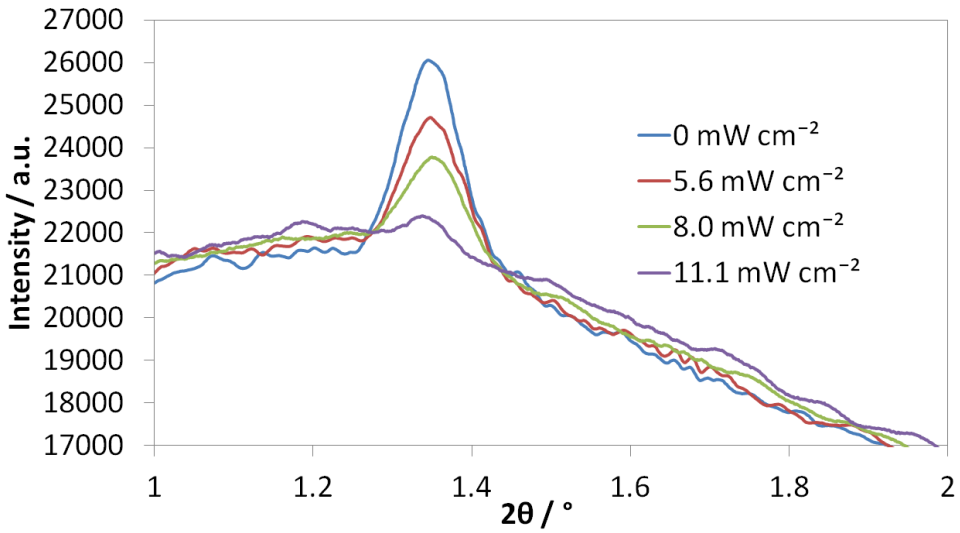

Fig.4– 13 X-ray diffraction during irrasiation by UV light pattern and intensity profile in the small-angle region in the the DC phase of trimer **IX**.

Table 4– 1 Effect of UV irradiation intensity on the layer spacing and correlation length.

Exposure intensity (mW cm^{-2})	Layer spacing (Å)	Correlation length (Å)
0	65.7	908
5.6	65.7	774
8.0	65.6	532
11.1	66.4	368

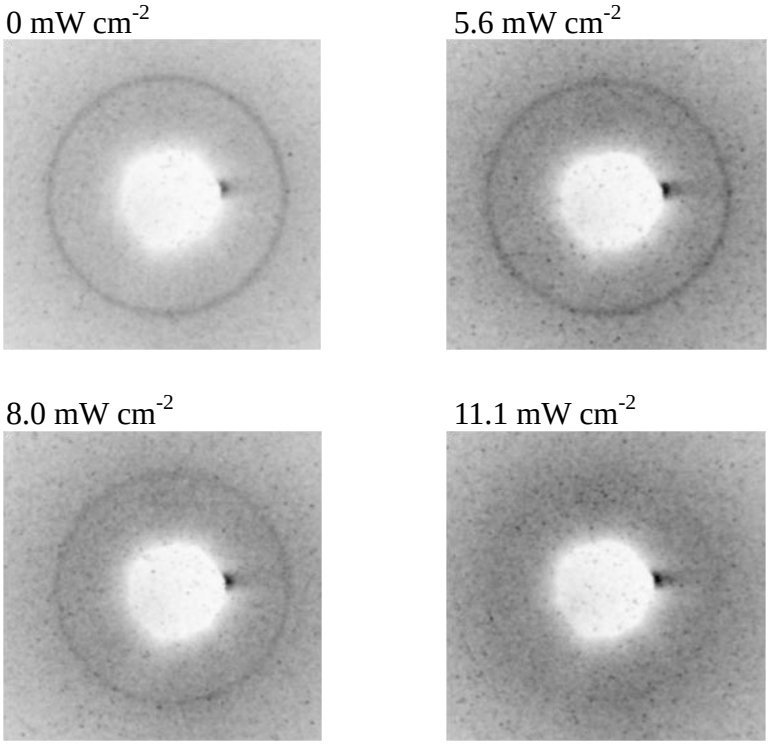

Fig.4– 14 X-ray diffraction patterns in the small-angle region of trimer **IX** as a function of UV irradiation intensity at 135 °C.

POM and XRD measurements of trimer **IX** with UV irradiation revealed the following. The soft crystalline DC phase changed to the liquid crystalline phase which possessed short-range layer ordering following irradiation with UV light (λ=365 nm). The liquid crystalline phase did not show a chiral nature. It did not appear in the thermal phase transition of trimer **IX** either. Although short correlation length layer structures have been observed in cybotactic nematic (Ncyb) phases[17], the present photo-induced phase is not a Ncyb phase judging from the optical texture. The smectic blocks with short-range layer ordering can be seen in the twist grain boundary (TGB) phases of chiral rod-like molecules, where the layers are twisted discontinuously[18]. On the other hand, the continuous layer twisting produces the saddle splay curvature in typical DC phases. The layer twisting in the DC phase of trimer **IX** is unwound by the UV irradiation to produce the achiral liquid crystalline phase which consists of layer structures with a short correlation length.

In order to clear how the photo-irradiation affects the azobezene unit of trimer **IX**, I measured the UV-vis spectra of the chloroform solution with trimer **IX** (2.5 x 10^{-5} M) during UV light with a wavelength of 365 nm as a function of the irradiation intensity (Fig. 4-15). Before UV irradiation, the UV-vis spectrum shows a strong peak at around 365 nm associated with the π-π* transition of *trans* form and a broad peak at around 450 nm assoiated with the weak symmetry forbidden n-π* transition of *cis* form. Under UV irradiation, an absorbance at 365 nm peak decreased whereas an absorbance at 450 nm peak increased, revealing that the *trans-cis* photoisomerization of the azobenzene unit occurs. Furthermore, the *trans* over *cis* ratio depends on the exposure intensity. I assume that all the trimer molecules form the *trans* isomer without UV irradiation whereas they form the *cis* isomer at an irradiation intensity of 20 mW cm^{-2}. The content of the *cis* isomer in the molecular at 2 mW cm^{-2} is 47.5%. The content of the *cis* isomer in the molecular at 5 mW cm^{-2} is 88.9%.

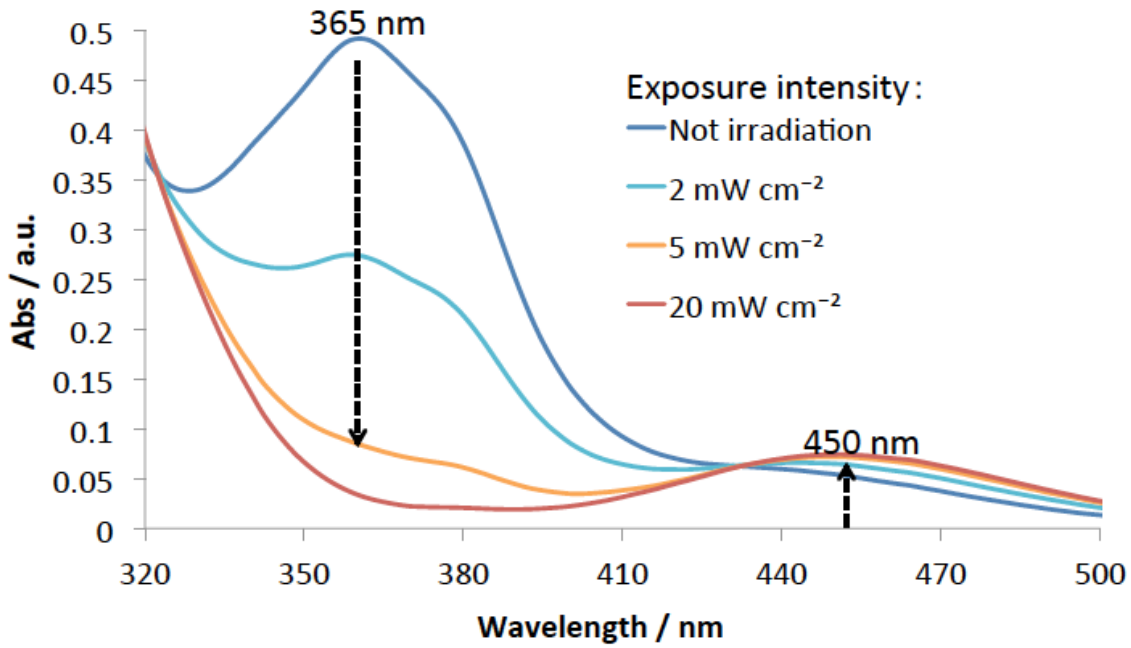

Fig.4– 15 UV-vis spectra of trimer **IX** in chloroform (2.5 x 10^{-5} M) during UV light of wavelength 365 nm as a function of the irradiation intensity. After the sample was exposed to UV light for 10 s, UV-vis spectra were recorded. Each spectrum was confirmed not to change for at least 5 min after the UV irradiation.

4.3.3. Molecular organization models

Fig 4-16 shows a molecular organization model of the photo-induced phase transition. The *trans-cis* isomerization of the azobenzene unit of trimer **IX** induces a bent shape in the terminal of trimer **IX** as shown for the indicated molecule in the middle of Fig 4-16. This conformation change increases intermolecular distances between the *cis* trimer and the surrounding *trans* trimers, reducing the intermolecular core-core interactions between them. Therefore, the spacers of the *cis* trimer adopt all *trans* conformation to form an L-shaped molecule as indicated on the right side of Fig 4-16. As shown in Fig.4-17, the molecular length for the L-shaped molecule with a *cis* azobenzene unit is estimated to be 67 Å, which is as same as the molecular length for the twisted molecule with a *trans* azobenzene unit. The lateral twist interaction in each layer cannot synchronize, which causes the layer to unwind. The achiral layered phase appears, where the splay layer deformation can produce the saddle splay curvature without layer twisting. As the irradiation intensity increases, the content of the L-shaped *cis* trimer increases, which destabilizes the layer structure and leads to the N phase.

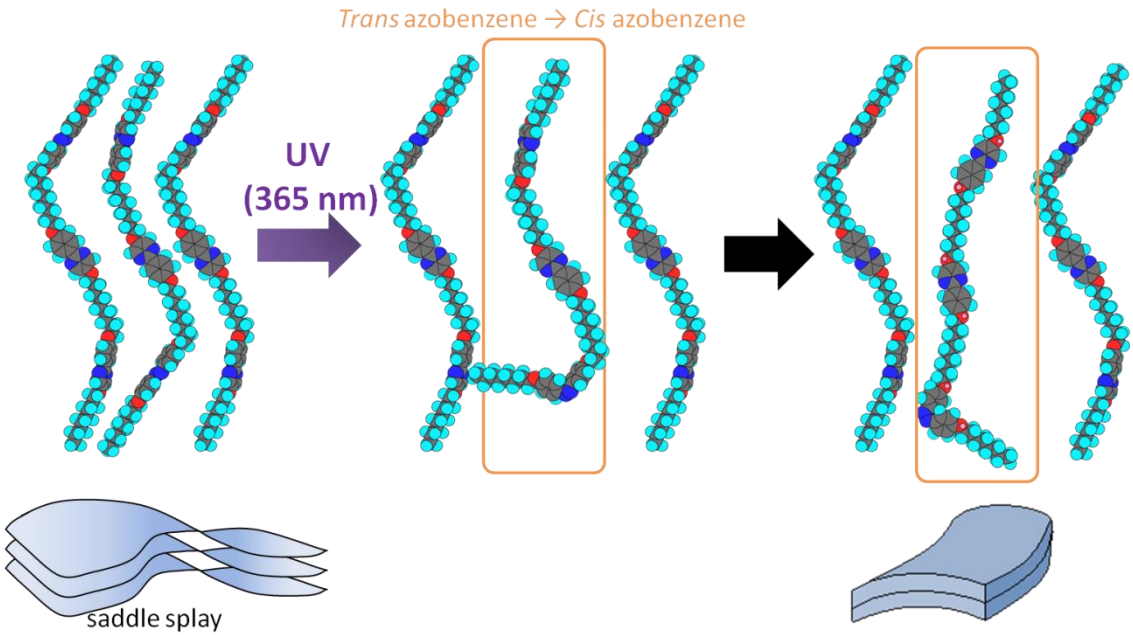

Fig.4– 16 Molecular organization model for the photo-induced phase transition form the chiral DC phase to the layer ordered phase.

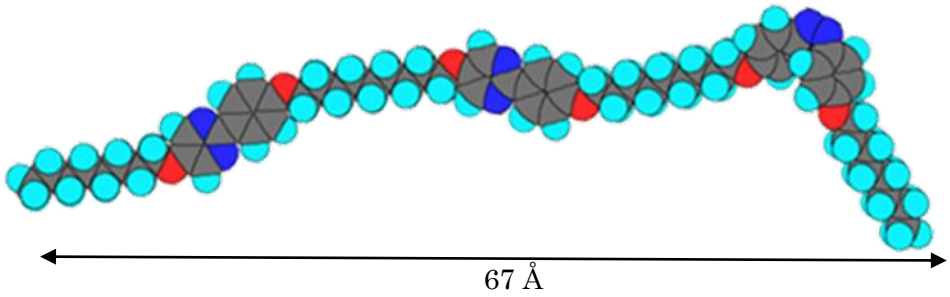

Fig.4– 17 MOPAC model for an L-shape *cis*-azobenzene trimer.

4.3.4. Observation of microstructures in DC phases

The photo-induced phase transition of the DC to the achiral smectic-like phase is reversible. Therefore, the stepwise formation of the DC phase could be achieved by photo-irradiation as follows. After cooling to the DC phase from the isotropic liquid, the sample is exposed to UV light of an appropriate intensity to change the achiral layered phase. Then, the light is switched off, and the DC phase reappears accompanied by layer twisting. The previously reported trimer **V-(9,9)** (Fig. 4-18) exhibited an ordered cubic structure in the surface and a sponge structure inside of the material[10]. I made a mixture of trimer **V-(9,9)** (75 mol%) and the photosensitive trimer **IX** (25 mol%). The phase transition temperatures were as follows: Iso 153.1 °C N 134.3 °C DC. The mixture did not crystalise at room temperature. I observed how the photo-driven chirality switching changes the microstructure of the mixture using field-emission scanning electron microscopy (SEM). Fig. 4-19 shows the SEM images at room temperature. Without UV irradiation, a honeycomb-like pattern was observed at the air/liquid crystal interface (Fig. 4-19(a)) and a sponge-like structure accompanying disordered voids in the cross section area (Fig. 4-19(b)). They are likely identical to those observed for trimer **V-(9,9)** itself. Then the mixture was irradiated with UV light (365 nm) with an intensity of 24 mW cm^{-2} at 134 °C in the DC phase. After the DC phase changed to the smectic-like phase, the UV light was switched off. The sample was cooled to room temperature. The honeycomb-like pattern was also shown at the air/liquid crystal interface (Fig. 4-19(c)), whereas a relatively ordered porous structure was observed in the cross section area (Fig. 4-19(d)).

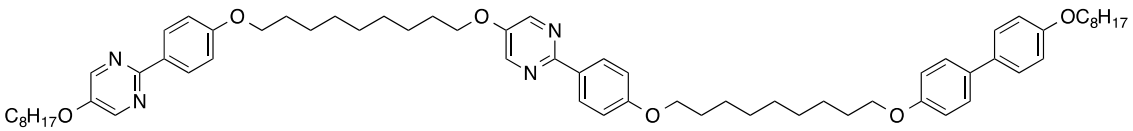

Fig.4– 18 Molecular structure of **V-(9,9)**

(a)

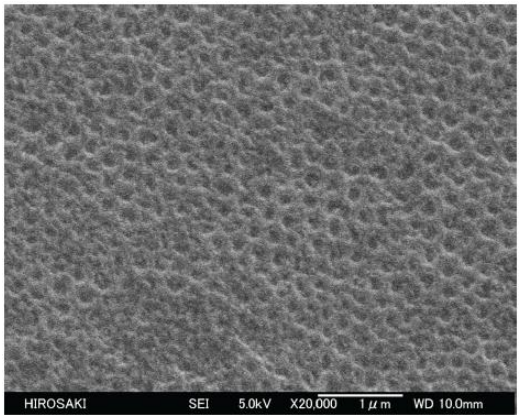

(b)

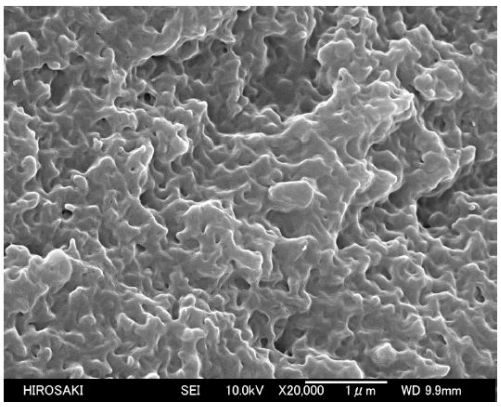

(c)

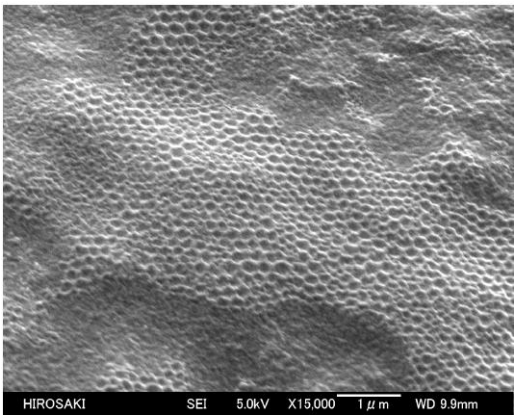

(d)

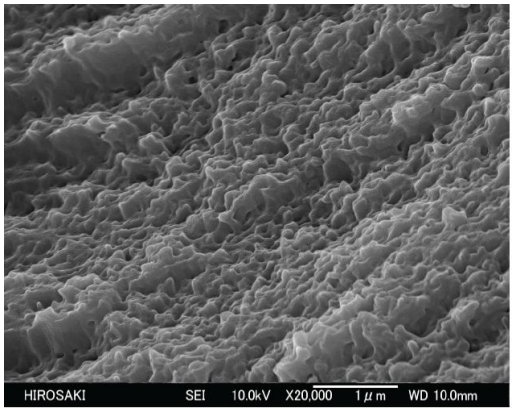

Fig.4– 19 SEM images of the microstructures of a mixture of trimer **V-(9,9)** (75 mol%) and trimer **IX** (25 mol%) in the DC phase at room temperature. (a) The air/liquid crystal interface before UV irradiation, (b) the cross-section area before UV irradiation, (c) the air/liquid crystal interface after UV irradiation, and (d) the cross-section area after UV irradiation.

The formation of the ordered cubic structure was explained in chaper 3 as follows. Upon cooling to the DC phase from the isotropic liquid, layer ordering occurs and then the layers are helically deformed at the surface, which produce an ordered cubic structure. On the other hand, both layer formation and helical ordering of the trimer molecules occur simultaneously in the inside of material. The competition between those ordering induces frustration in the system, which can be released by layer deformation to the sponge-like structure in the inside of material[10]. Therefore, the stepwise formation of the DC phase by photo-irradiation is same as the formation of DC phase at the air/liquid crystal interface surface upon cooling to the DC phase from the isotropic liquid. As a result, the ordered porous structure was observed not only at the air/liquid crystal interface surface but also in the inside of material.

4.4. Conclusion

I designed a photosensitive achiral liquid crystal trimer exhibiting N and DC phases. The UV irradiation induced a phase transition from the soft crystalline chiral conglomerate phase to the achiral liquid crystalline phase consisting of short correlation length layer structures via the *trans-cis* photo-isomerization of the azobenzene unit. The photo-driven reversible chirality switching transforms the sponge structure in the DC phase to a more ordered porous structure. Not only an unusual layered phase but also a porous material is demonstrated.

4.5. Reference

[1] D. K. Yoon, Y. Yi, Y. Shen, E. Körblova, D. M. Walba, I. I. Smalyukh, N. A. Clark, *Adv. Mater.*, 2011, **23**, 1962.

[2] E. Gorecka, N. Vaupotic, A. Zep, D. Pociecha, *Angew. Chem. Int. Ed.*, 2016, **55**, 12238.

[3] D. Chen, C. Zhu, H. Wang, J. E. Maclennan, M. A. Glaser, E. Körblova, D. M. Walba, J. A. Rego, E. A. Soto-Bustamante, N. A. Clark, *Soft Matter*, 2013, **9**, 462.

[4] R. A. Callahan, D. C. Coffey, D. Chen, N. A. Clark, G. Rumbles, D. M. Walba, *ACS Appl. Mater. Interfaces*, 2014, **6**, 4823.

[5] L. E. Hough, M. Spannuth, M. Nakata, D. A. Coleman, C. D. Jones, G. Dantlgraber, C. Tschierske, J. Watanabe, E. Körblova, D. M. Walba, J. E. Maclennan, M. A. Glaser, N. A.

Clark, *Science*, 2009, **325**, 452.

[6] E. Hough, H. T. Jung, D. Kruerke, M. S. Heberling, M. Nakata, C. D. Jones, D. Chen, D. R. Link, J. Zasadzinski, G. Heppke, J. P. Rabe, W. Stocker, E. Korblova, D. M. Walba, M. A. Glaser, N. A. Clark, *Science*, 2009, **325**, 456.

[7] D. R. Link, G. Natale, R. Shao, J. E. Maclennan, N. A. Clark, E. Körblova, D. M. Walba, *Science*, 1997, **278**, 1924.

[8] J. Thisayukta, H. Takezoe, J. Watanabe, *Jpn. J. Appl. Phys.*, 2001, **40**, 3277.

[9] H. Sasaki, Y. Takanishi, J. Yamamoto, A. Yoshizawa, *Soft Matter*, 2016, **12**, 3331.

[10] H. Sasaki, Y. Takanishi, J. Yamamoto, A. Yoshizawa, *Soft Matter*, 2017, **13**, 6521.

[11] S. Tazuke, S. Kurihara and T. Ikeda, *Chem. Lett.*, 1987, 911.

[12] T. Ikeda, O. Tsustumi and *Science*, 1995, **268**, 1873.

[13] T. Ikeda, *J. Mater. Chem.*, 2003, **13**, 2037.

[14] A. Zep, K. Sitkowska, D. Pociecha, E. Gorecka, *J. Mater. Chem. C*, 2014, **2**, 2323.

[15] D. A. Paterson, J. Xiang, G.Singh, R. Walker, D. M. Agra-Kooijman, A. Martíez-Felipe, M. Gao, J. M. D. Storey, S. Kumar, O. D. Lavrentovich, C. T. Imrie, *J. Am. Chem. Soc*., 2016, **138**, 5283.

[16] M. Alaasar, S. Poppe, Q. Dong, F. Liu, C. Tschierske, *Angew. Chem*. *Int. Ed*., 2017, **56**, 10801.

[17] E. T. Samulski, *Liq. Cryst.*, 2010, **37**, 669.

[18] J. W. Goodby, *Struc. Bond*., 1999, **95**, 83.

CONCLUSIONS

In this thesis, novel achiral flexible liquid crystal trimers were designed and their mesogenic properties investigated. The results obtained from this study are summarized as follows.

1. An equimolecular mixture of a trimer with an N phase **(II-(7,7))** and that with SmA, SmC and SmB **(IV-(7,7))** was found to exhibit N, SmC and DC phases. This is the first report of a trimer system forming chiral conglomerates. The interdigitation of the zigzag trimers driven by the dipole−dipole interaction might form a supermolecular bent configuration, which induces a local preference for the saddle splay curvature to drive the DC phase.

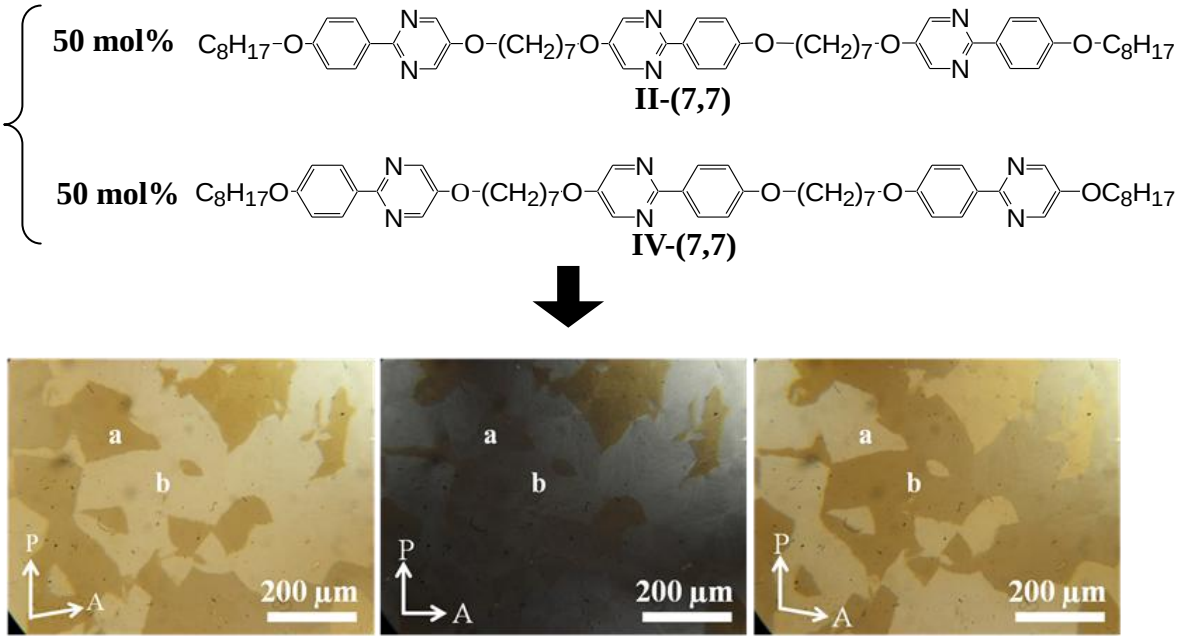

herical nanofilament phase

Fig.C− 1 A trimer system forming chiral conglomerates.

2. The following liquid crystal trimer **V-(7,7)** was found to exhibit the DC phase possessing chiral domains with opposite senses. The trimer forms an achiral ground-state conformation in the nematic phase, however, by intermolecular interactions between cores they adopt a twisted chiral conformation to exhibit the spontaneous mirror symmetry breaking in the low-temperature DC phase.

.

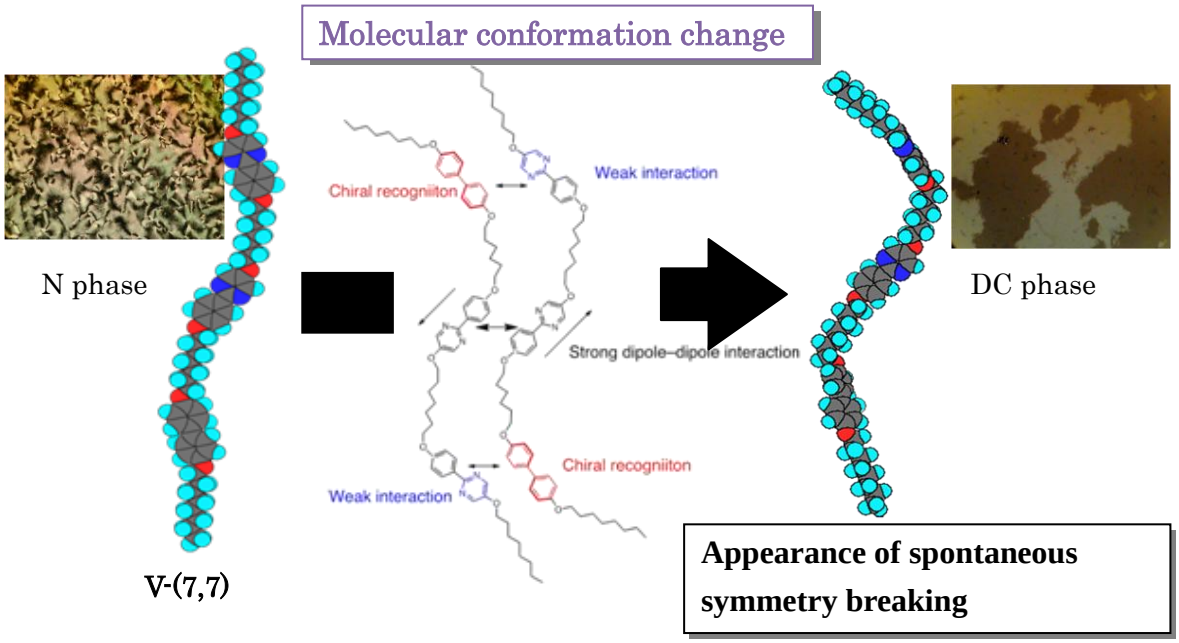

Fig.C− 2 Model for the origin of the chirality of timers in the DC phase.

3. The produced dark conglomerate phase of trimer **V-(9,9)** was found to exhibits a single gyroid-like surface and a sponge like bulk structure. The microstructures in the DC phase of the flexible trimer are quite different from those in DC phases of bent-core molecules. The soft crystalline chiral conglomerate phase forming porous structures is a promising new candidate for producing nanostructured composites.

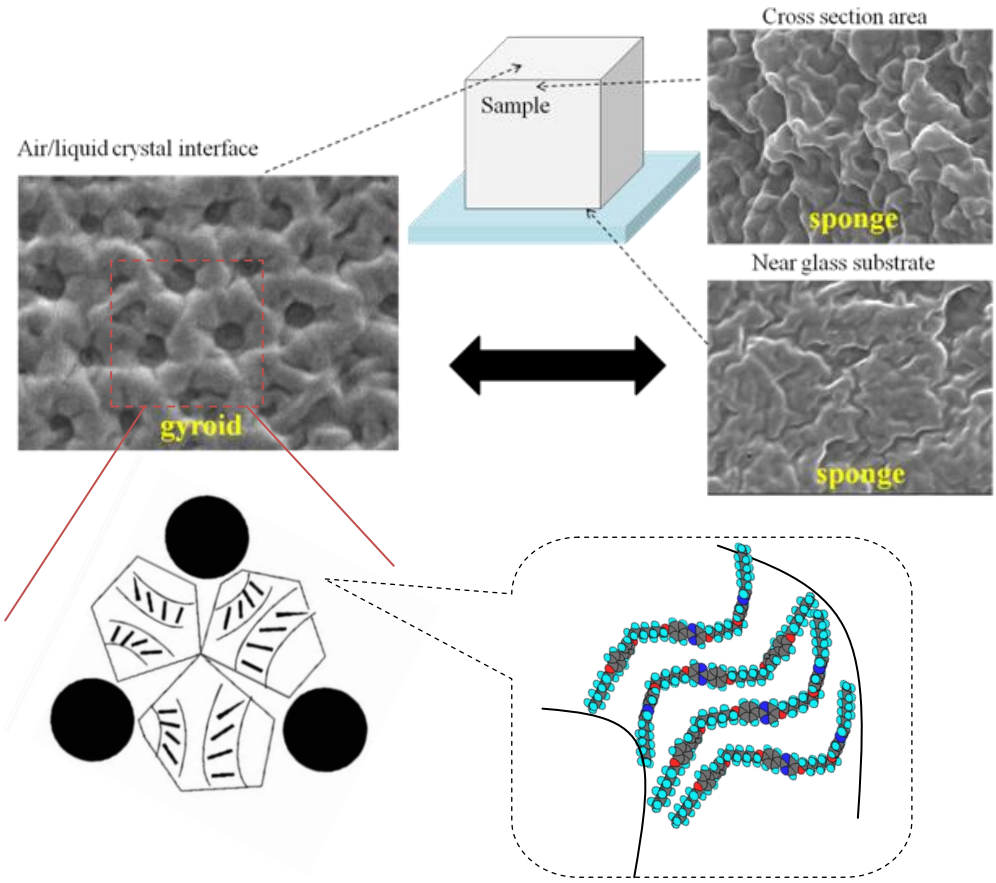

Fig.C− 3 SEM image of the surface and the bulk structure in the DC phase with a possilbe model for the molecular organization.

4. I designed a photosensitive achiral liquid crystal trimer exhibiting N and DC phases. The UV irradiation induced a phase transition from the soft crystalline chiral conglomerate phase to the achiral liquid crystalline phase consisting of short correlation length layer structures via the *trans-cis* photo-isomerization of the azobenzene unit. The photo-driven reversible chirality switching transforms the sponge structure in the DC phase to a more ordered porous structure. Not only an unusual layered phase but also a porous material is demonstrated.

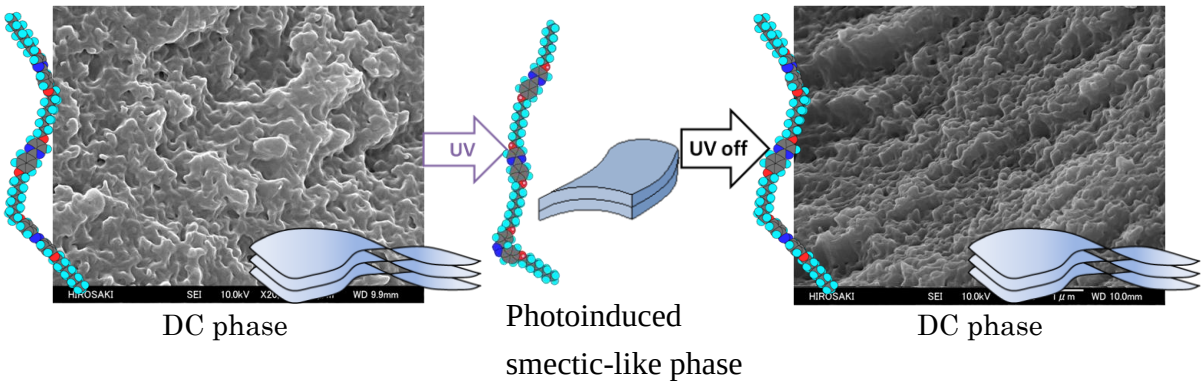

Fig.C−4 Model for the origin of the chirality and chiral switching of azobenzene-based timers in the DC phase and SEM image of inside of material in DC phases.

An achiral flexible liquid crystal trimer was found to exhibit a DC phase possessing chiral domains with opposite senses. Intermolecular core–core interactions induce a twisted conformation in the trimer, resulting in the spontaneous mirror symmetry breaking. The DC phase of the trimer shows unusual nanostructures, i.e., a gyroid-like cubic structure at the air/liquid crystal interface and a sponge structure inside of the material. Furthermore, the photo-driven reversible chirality switching transforms the sponge structure to a more ordered porous structure. Not only a mirror symmetry breaking driven by conformational change but also a novel porous structure is demonstrated.

PUBLICATIONS

(1) Haruna Sasaki, Yoichi Takanishi, Jun Yamamoto and Atsushi Yoshizawa, “Supermolecular bent configuration composed of achiral flexible liquid crystal trimers exhibiting chiral domains with opposite handedness”, *J. Phys. Chem. B*, 2015, 119, 4531.

(2) Haruna Sasaki, Yoichi Takanishi, Jun Yamamoto and Atsushi Yoshizawa, “Achiral flexible liquid crystal trimers exhibiting chiral conglomerates ”, *Soft Matter,* 2016, 12, 3331.

(3) Haruna Sasaki, Yoichi Takanishi, Jun Yamamoto and Atsushi Yoshizawa, “Achiral flexible liquid crystal trimers exhibiting gyroid-like surfaces in chiral conglomerate phases”, *Soft Matter,* 2017, 13, 6521.

(4) Haruna Sasaki, Yoichi Takanishi, Jun Yamamoto and Atsushi Yoshizawa, “Photo-Driven Chirality Switching in a Dark Conglomerate Phase of an Achiral Liquid Crystal Trimer”, accepted for publication in *ChemistrySelect*.

Following papers are not contained in this thesis.

(1) Atsushi Yoshizawa, Yusuke Kato, Haruna Sasaki, Yoichi Takanishi, Jun Yamamoto, “Chiral conglomerates observed for a binary mixture of a nematic liquid crystal trimer and 6OCB”, *Soft matter.*, 2015, 11, 8827.

(2) Atsushi Yoshizawa, Yusuke Kato, Haruna Sasaki, Yoichi Takanishi, Jun Yamamoto, “Optically isotropic homochiral structure produced by intercalation of achiral liquid crystal trimers”, *J. Phys. Chem. B*, 2016, 120, 4843.

(3) Atsushi Yoshizawa, Yukiko Kondo Haruna Sasaki, “Crystal–nematic phase separation in an asymmetric liquid crystal dimer possessing a terminal hydroxyl group”, *Liq. Cryst*., 2016, 43, 680.

ACKNOWLEDGEMENTS

I would like to express his sincerest gratitude to Professor Atsushi Yoshizawa for his inspired supervision and valuable discussions.

I also wish to thank Professor Toshiyuki Abe, Professor Hideo Sawada, Professor Masaaki Okazaki and Associate Professor Masanobu Sagisaka for their kind advice and discussions.

I would like to thank Dr. Isa Nishiyama and Mr. Koichi Endo of DIC Corporation for valuable and powerful discussions.

I also wish to thank Professor Jun Yamamoto and Associate Professor Yoichi Takanishi of Kyoto University, for valuable, powerful discussions and XRD measurements.

I would like to thank Mr. Natsuki Ujiie for elemental analysis measurements, and Mr. Kazuto Yamada for IR measurements.

I would like to thank Dr. Tsuyoshi Narumi and Dr. Tetsu Hirose for valuable and powerful discussions.

I am grateful to all members in Yoshizawa and Sagisaka Lab., Dr. Tsuyoshi Narumi, Ms. Michiko Yamaguchi, Mr. Kenji Shimizu, Mr. Masahiro Chiba, Mr. Ryuji Oikawa, Ms. Hirona Kato, Mr. Syomi Sayama, Ms. Misaki Kurata, Mr. Tatsuma Nagai, Mr. Kodai Abe, Mr. Tatsuya Saito, Mr. Koki Takahashi, Mr. Kazuki Fuzjita, Mr. Yasushi Umetsu, Mr. Takahiro Kawaki, Mr. Tsubasa Kondo, Mr. Toma Yagihashi, Mr. Takumi Suto, Mr. Syota Suhara and undergraduate students.

I would like to thank my parents for their support and understanding.